KALMAN FILTER DESIGN FOR AN INERTIAL NAVIGATION SYSTEM AIDED BY NON-SYNCHRONOUS NAVIGATION SATELLITE CONSTELLATIONS

Ronald Ray Butler, et al

Air Force Institute of Technology
Wright-Patterson Air Force Base, Ohio

March 1974

UNCLASSIFIED

SECURITY CLASSIFICATION OF THIS PAGE (When Data Entered)

REPORT DOCUMENTATION PAGE		READ INSTRUCTIONS BEFORE COMPLETING FORM
1. REPORT NUMBER GA/EE/74M-1	2. GOVT ACCESSION NO.	3. RECIPIENT'S CATALOG NUMBER AD 779 724
4. TITLE (and Subtitle) Kalman Filter Design for an Inertial Navigation System Aided by Non-Synchronous Navigation Satellite Constellations		5. TYPE OF REPORT & PERIOD COVERED M.S. Thesis 6. PERFORMING ORG. REPORT NUMBER
7. AUTHOR(s) Ronald R. Butler 2/Lt USAF George T. Rhue 2/Lt USAF		8. CONTRACT OR GRANT NUMBER(s)
9. PERFORMING ORGANIZATION NAME AND ADDRESS AF Institute of Technology (AU) Wright-Patterson AFB, Ohio 45433		10. PROGRAM ELEMENT, PROJECT, TASK AREA & WORK UNIT NUMBERS
11. CONTROLLING OFFICE NAME AND ADDRESS AF Avionics Labcratory Wright-Patterson AFB, Ohio 45433		12. REPORT DATE March 1974 13. NUMBER OF PAGES 174
14. MONITORING AGENCY NAME & ADDRESS(if different from Controlling Office)		15. SECURITY CLASS. (of this report) UNCLASSIFIED 15a. DECLASSIFICATION/DOWNGRADING SCHEDULE

16. DISTRIBUTION STATEMENT (of this Report)

Approved for public release; di stribution unlimited.

17. DISTRIBUTION STATEMENT (of the abstract entered in Block 20, if different from Report)

18. SUPPLEMENTARY NOTES

Approved for public release; IAW AFR 190-17

JERRY C. HIX, Captain, USAF
Director of Information

19. KEY WORDS (Continue on reverse side if necessary and identify by block number)

Kalman Filter
Inertial Navigation System
Navigation Satellite
Optimally Aided Inertial System
Optimal Estimation

20. ABSTRACT (Continue on reverse side if necessary and identify by block number)

This report is a Kalman filter design study for the proposed Integrated Navigation Satellite/Inertial System. Primary emphasis is placed upon determination of the "best" filter observable vector and investigation of various measurement rates using external range measurements from a set of 27 non-synchronous satellites. The INI system errors are assumed to be represented by a 44 state linear state model, and the filter operated without

DD FORM 1 JAN 73 1473 EDITION OF 1 NOV 65 IS OBSOLETE

UNCLASSIFIED

20. (cont'd)

benefit of an altimeter. A one-hour INI flight at constant speed and altitude over a great circle path is simulated on the digital computer and filter designs are compared by plotting the system position, velocity, and attitude error covariance versus time. A 15 state filter with weak coupling terms removed is determined to provide the best tradeoff between accuracy and computational burden. Filter performance is compared at 5, 15, 30, 60 and 90 second measurement update rates. Additionally, "Optimal" sequencing of satellite observables is shown to provide improved performance.

KALMAN FILTER DESIGN FOR AN INERTIAL NAVIGATION SYSTEM AIDED BY NON-SYNCHRONOUS NAVIGATION SATELLITE CONSTELLATIONS

THESIS

GA/EE/74M-1

Ronald R. Butler
2/Lt USAF
George T. Rhue
2/Lt USAF

GA/EE/74M-1

KALMAN FILTER DESIGN FOR AN INERTIAL NAVIGATION SYSTEM AIDED BY NON-SYNCHRONOUS NAVIGATION SATELLITE CONSTELLATIONS

THESIS

Presented to the Faculty of the School of Engineering

of the Air Force Institute of Technology

Air University

in Partial Fulfillment of the

Requirements for the Degree of

Master of Science

by

Ronald R. Butler, B.A.E.

2Lt USAF

Graduate Astronautics

George T. Rhue, B.S.A.A.E.

2Lt USAF

Graduate Astronautics

March 1974

iv

Preface

It is interesting to note that only a short decade or so ago, neither the theory nor the computational capability (let alone the requirement) for attacking the problem of this thesis topic existed. In the early 1960's, R. E. Kalman presented his theories on optimal control and filtering techniques. The advent of that electronic marvel of our age, the digital computer, provided the tool for applying Kalman's filtering theory. Many Saturday and Sunday mornings as well as weeknights were spent with our dear friend, the CDC 6600 computer, in order to bring to you, the reader, the meticulous CALCOMP plots of the system state variable covariances presented throughout this report.

Although there were many individuals from both the Air Force Avionics Laboratory and the School of Engineering faculty who rendered us assistance from time to time during the preparation of this thesis, there are two people to whom we are especially indebted. We would like to express our most sincere appreciation to Lt Peter S. Maybeck, faculty advisor for this thesis topic. Even though he was enduring the trials and tribulations of an expectant father and also attending the Academic Instructor School (in addition to his everyday faculty duties) during the time period of this study, he somehow always managed to find time to talk with us. For his patient guidance and instruction we are indeed grateful. We also gratefully acknowledge the assistance of Mr. Richard M. Reeves of the Avionics Laboratory in providing us with computer programs and other documents related to our study. We especially thank him for sharing with us his experience and expertise in the application of Kalman filter design theory.

Finally, as we emerge from the dark "Caves of Knowledge" blinking our eyes in response to the bright sunlight, we would like to express appreciation to our wives, Dottie and Carolyn, who are patiently waiting to welcome us home.

Ronald R. Butler

George T. Rhue

Table of Contents

Table of Contents

List of Figures

List of Figures

List of Figures

List of Figures

List of Tables

List of Symbols

Symbol	Defined or first used	Symbol	Defined or first used
A	Equation 43	G_e	Equation 51
A_x	Equation 14	G_f	Page 30
A_y	Equation 13	G_s	Page 29
C	Equation 51	H_f	Page 31
C_o	Table V	H_s	Page 29
C_1	Table V	h	Equation 35
C_2	Table V	I	Page 20
C_i^e	Equation 1	I_x	Figure 2
C_e^n	Equation 2	I_y	Figure 2
C_i^n	Equation 3	I_z	Figure 2
C_e^i	Page 9	i	Page 20
c	Page 16	$\underline{i}_r$	Equation 39
D	Equation 39	$\underline{i}_r^*$	Equation 28
D_{max}	Equation 34	$\underline{i}_{rn}$	Equation 58
E_{min}	Equation 34	$\underline{i}_{rx}$	Equation 58
E_x	Figure 2	$\underline{i}_{ry}$	Equation 58
E_y	Figure 2	$\underline{i}_{rz}$	Page 18
E_z	Figure 2	J	Page 20
$E[x]$	Equation 76	J'	Page 20
$\hat{e}_x$	Page 10	J''	Page 20
$\hat{e}_y$	Page 10	j	Page 20
F_f	Page 30	K	Page 20
F_s	Page 29	K'	Page 20
$f(x)$	Page 32	K_f	Page 31

List of Symbols

Symbol	Defined or first used	Symbol	Defined or first used
k	Page 20	$\underline{r}_s^*$	Equation 23
M	Page 22	r_s^e	Page 24
N_x	Figure 2	r_x	Equation 56
N_y	Figure 2	r_y	Equation 56
N_z	Figure 2	r_z	Equation 56
η	Page 24	r^n	Equation 36
P_f	Equation 70	$u(t)$	Figure 8
$\dot{P}_f$	Equation 70	u_f	Page 30
P_o	Equation 75	u_s	Page 29
Q'	Equation 78	V^n	Page 111
Q_f	Equation 66	V_x	Equation 7
Q_s	Equation 61	V_y	Equation 6
q	Page 43	v	Page 16
q_1^*	Page 56	$\underline{v}_f$	Page 31
R	Equation 6	$\underline{v}_s$	Page 29
R_f	Equation 68	$\underline{x}_f$	Page 30
R_s	Equation 63	$\hat{\underline{x}}_f$	Page 30
$\underline{r}$	Page 13	$\dot{\underline{x}}_f$	Equation 69
r'	Equation 20	$\hat{x}_o$	Equation 34
r^*	Equation 21	x_s	Page 29
$\underline{r}_s$	Page 13	$\dot{x}_s$	Equation 60
$\underline{r}_s^*$	Equation 24	Z_f	Page 31
$\underline{r}_s^n$	Equation 35	Z_s	Page 29
$\underline{r}_s$	Page 13	α_{bx}	Table IV

List of Symbols

Symbol	Defined or first used	Symbol	Defined or first used
α_{by}	Table IV	δT_{s2}	Table IV
α_{bz}	Table IV	δT_{s3}	Table IV
α_{rx}	Table IV	δT_{s4}	Table IV
α_{ry}	Table IV	δT_u	Page 16
α_{rz}	Table IV	$\dot{\varepsilon}$	Table V
β	Equation 80	$\ddot{\varepsilon}$	Equation 97
β_a	Page 44	ε_{bx}	Table IV
β_g	Page 45	ε_{by}	Table IV
Δy	Table IV	ε_{bz}	Table IV
$\Delta \dot{y}$	Table IV	ε_{rx}	Table IV
Δz	Table IV	ε_{ry}	Table IV
$\Delta \dot{z}$	Table IV	ε_{rz}	Table IV
Δr	Equation 22	ε_b	Page 45
δb	Page 16	ε_r	Page 45
δb_1	Table IV	ζ	Page 20
δb_2	Table IV	η	Page 20
δb_3	Table IV	θ	Page 6
δb_4	Table IV	$\dot{\theta}$	Equation 7
$\delta r'$	Equation 20	Λ	Page 6
δr^*	Equation 21	$\dot{\Lambda}$	Equation 6
δr_a^*	Equation 24	μ	Page 32
δr_s^*	Equation 23	ξ	Page 20
δT_s	Page 16	ρ	Equation 9
δT_{s1}	Table IV	$\dot{\rho}_x$	Equation 13

List of Symbols

Symbol	Defined or first used	Symbol	Defined or first used
ρ_y	Equation 10		
$\dot{\delta}_y$	Equation 14		
ρ_z	Equation 11		
$\dot{\rho}_z$	Equation 15		
σ_r	Page 54		
τ	Page 43		
ϕ_x	Table IV		
ϕ_y	Table IV		
ψ_z	Table IV		
Ω	Equation 16		
Ω_x	Equation 4		
Ω_y	Equation 4		
Ω_z	Equation 4		
ω_{ie}^e	Equation 4		
ω_{en}	Equation 5		
ω_{ie}^e	Equation 4		
ω_{en}^n	Equation 8		
ω_{in}^n	Equation 16		
$\dot{\omega}_{en}^n$	Equation 12		
ω_s	Page 72		
ω_x	Equation 16		
ω_y	Equation 16		
ω_z	Equation 16		

Abstract

This report is a Kalman filter design study for the proposed Integrated Navigation Satellite/Inertial System (INI). Primary emphasis is placed upon determination of the "best" filter state variable vector and investigation of various measurement rates using external range measurements from a set of 27 non-synchronous satellites. The INI system errors are assumed to be represented by a 44 state linear system model, and the filter operates without benefit of an altimeter. A one-hour INI flight at constant speed and altitude over a great circle path is simulated on the digital computer and filter designs are compared by plotting the system position, velocity, and attitude error covariances versus time. A 15 state filter with weak coupling terms removed is determined to provide the best tradeoff between accuracy and computational burden. Filter performance is compared at 5, 15, 30, 60 and 90 second measurement update rates. Additionally, "optimal" sequencing of satellite observables is shown to provide improved performance.

KALMAN FILTER DESIGN FOR AN INERTIAL NAVIGATION SYSTEM AIDED BY NON-SYNCHRONOUS NAVIGATION SATELLITE CONSTELLATIONS

I. Introduction

This report is a Kalman filter design study for the proposed Integrated Navigation Satellite/Inertial System (INI). This design is a subproblem of the proposed INI system which is a current research and development topic of interest to the Navigation Division of the Air Force Avionics Laboratory at Wright-Patterson Air Force Base as well as other government and private agencies.

The development of this study is presented by chapters in the following sequence. The preliminaries such as reference frames and their angular rates are presented in the second chapter. Chapter III discusses theory which is peculiar to the use of navigation satellites as an updating aid to inertial navigation systems. Chapter IV is a development of the Kalman filter equations required to solve the navigation problem. The forty-four state system model selected for this study is presented next in Chapter V. The intent of Chapter VI is to determine the "best" state variable vector, both in terms of dimension and selection of components for implementation in the filter. Chapter VII investigates the effects of varying the measurement update rate of this design. A description of the computer program used in simulating the INI flight is given in Chapter VIII. The results and conclusions compose the final chapter of this design study.

Integrated NAVSAT/Inertial System

The basic idea of the INI is to combine external navigation

information (such as range, range rate, and attitude) received from orbiting constellations of satellites with the inertial navigation system (INS) of an aircraft or missile to provide highly accurate position and velocity information, such as would be required for instrument landing or weapon delivery. The Navigation Satellite (NAVSAT) portion of the system consists of a total of 27 orbiting satellites. The number of satellites and their orbits are arbitrary and the particular configuration selected for this study will be discussed in detail in Chapter III. A filter design study utilizing a cluster of four satellites in a Y-configuration with the central satellite in synchronous orbit and the remaining satellites orbiting about it is detailed in Reference 1 of the bibliography. There are several existing satellites under consideration for adaptation, one of which, the Timation III, will be used as a baseline. Each satellite contains a transmitter, receiver, and a clock (i.e., quartz crystal oscillator). A ground tracking network periodically measures and updates the ephemeris and satellite clock phase and frequency so as to maintain synchronization of all satellite clocks. The satellites in turn continually transmit this information together with identifiable range codes to the user. The signals from each satellite are modulated by orthogonal codes so that they may be distinguished from each other by the user. By means of a correlation detector the time shift between each satellite signal and the user's unsynchronized clock is measured in the user's receiver (Ref 1:1-2 & 1-3). The portion of the system on board the aircraft consists of a computer, receiver, and an inertial measurement unit (IMU). The receiver is required for acquisition of the satellite signal. The IMU consists basically of a set of accelerometers and gyros which provide internal or

on-board navigation information using specific force and angular rates along three mutually orthogonal axes. The computer is used to apply the Kalman filter equations, i.e., to compute the Kalman gains or weighting coefficients, to estimate the state variables, and to apply the control to the INS.

Kalman Filter

The Kalman filter is simply an optimal recursive data processing algorithm which resides in the central processor or on-board computer. This filter, or computer program, combines all available measurement data, plus prior knowledge of the system and measuring devices to produce an estimate of the desired variables in such a manner that the resulting error is minimized statistically. Stated in simpler terms, it provides the best estimate possible subject to certain modeling assumptions.

The filter will enhance the attitude and position information accuracy by weighting each data source heavily in the frequency regime where it provides good information, and suppressing it in the region where it is in error. The inertial system provides good high frequency information, but it drifts slowly and therefore exhibits poor low frequency performance. On the other hand, the NAVSAT data is good on the average, but subject to high frequency noise. Thus the filter will use the good low frequency NAVSAT information to damp out the slowly growing errors inherent in the inertial system.

Basic Assumptions. Under the three restrictions of system linearity, noise whiteness, and Gaussian noises, the Kalman filter can be shown to be the best filter of any conceivable form. Although the

system itself is actually nonlinear, the formulation of an approximate linear error model makes linear analysis possible. The justifications for the linear system model are that (1) the use of linear models in engineering studies has proved fruitful and (2) the techniques of linear systems analysis are well developed, whereas those for nonlinear systems are not, in general. "Whiteness" implies that the noise value is not correlated in time and also has equal power at all frequencies. Gaussianness pertains to the amplitude of the noise; at any single point in time, the probability density of a Gaussian noise amplitude takes on the shape of a normal bell-shaped curve. These three assumptions greatly simplify the mathematics of the problem and, in fact, render them tractable (Ref 2:3-11 & Ref 3:132).

Type of Filter Employed in the INI. An indirect filter estimates the errors in the navigation information using the difference between INS and external NAVSAT data as the measurements to drive the filter. This is in contrast to the direct Kalman filter which utilizes the total state space formulation. The filter is mechanized in a feedback configuration (as opposed to feedforward) which keeps the INS errors small by continually feeding back a correcting signal (see Figure 1). Since the INS is corrected after each measurement sample, the predicted error states and measurement differences at the next sample time will be zero. Consequently, there is no need to propagate the error state variable estimates.

A discussion of the relative merits of both direct versus indirect and feedforward versus feedback configurations is found in Reference 4 pages 1-10. It is not the intent of this report to dwell on the development of Kalman filter theory, rather the purpose here is to apply this

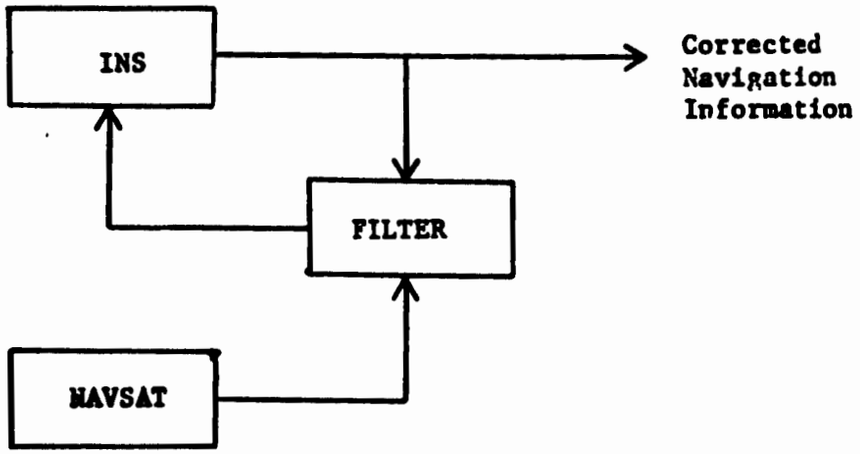

Fig. 1. Block Diagram of Filter in Feedback Configuration

theory to a practical engineering problem. Therefore, the reader who is either unfamiliar with Kalman filter theory and its applications to inertial navigation systems or else seeks more detailed information on this subject is referred to References 2 through 5 in the bibliography.

Limitations of the Study

It is realized that no matter what system reference model or "truth model" is selected it will only be an approximation since the complex real world dynamics defy exact mathematical description. The validity of the filter design is sensitive to erroneous reference system models and statistics; thus great care must be taken to model the reference system as accurately as possible in the computer simulation to yield meaningful results.

II. Coordinate Systems, Transformation Matrices, and Angular Rates

Coordinate Frame Definitions

Three different coordinate frames are defined for use in the computer simulation. These are the inertial reference frame, the Earth-fixed frame, and the navigation frame. The following paragraphs will summarize the definitions of these coordinate systems.

Inertial Reference Frame. The inertial coordinate system is fixed at the center of the Earth and maintains a constant orientation with respect to inertial space. The coordinate system thus defined is not truly an inertially-fixed frame, but for the error analysis of a vehicle moving near the Earth, the errors introduced by this definition of inertial space are negligible. The axes of the coordinate system form an orthogonal right-handed triad with the x-axis pointing from the center of the Earth through the North Pole in alignment with the Earth's spin axis.

Earth-fixed Frame. This coordinate system is identical to the inertial reference system with the exception that it is allowed to rotate with the Earth. The axes of this coordinate system are oriented with the x-axis directed outward through the North Pole, the y-axis directed outward through the intersection of the 90 degree West meridian and the equator (0,-90), and the z-axis directed through the intersection of the Greenwich meridian and the equator (0,0). Since this frame rotates with the Earth, any point on the Earth's surface can be specified in terms of a set of Euler angle rotations in the Earth-fixed frame, Λ about the x-axis (longitude) and θ about the y-axis (latitude).

Navigation Frame. The navigation frame is the coordinate system in

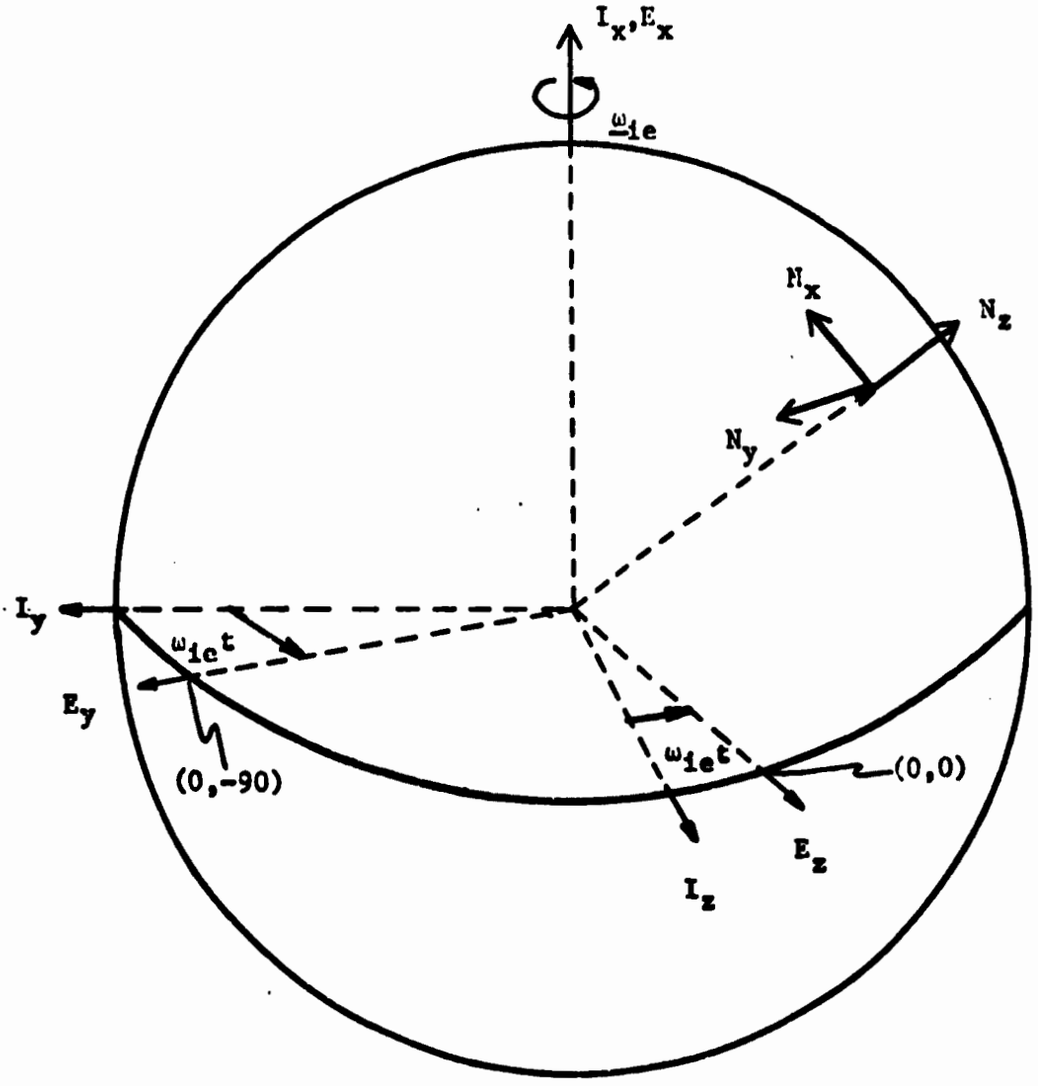

Fig. 2. Coordinate Frame Definition

which the navigation problem is solved. The position, velocity, and attitude errors are expressed in navigation coordinates. Since the problem involves a gimballed platform (as opposed to strapdown) which remains essentially locally level at all times, the z-axis of the navigation frame remains perpendicular to the Earth (positive upward). There are several choices available for mechanization of the locally level system in terms of the azimuth angular rate. Among these are azimuth wander, constant azimuth, unipolar, and free azimuth. There are certain advantages to each, for example, azimuth wander would be used in navigation near the polar regions. For this simulation, however, constant azimuth mechanization with the x-axis of the system always pointing North was selected. The y-axis is then chosen as pointing West to complete the right-handed orthogonal set.

Transformation Matrices

In order to transform vector quantities such as positions and velocities from one of the above coordinate frames to another it is convenient to first derive a set of time varying transformation matrices which will be used in subsequent development of the simulation equations.

Inertial to Earth Transformation. The transformation from the inertial reference frame to the Earth fixed frame involves simply a rotation about the x-axis through an angle equal to the Earth angular rate (which is constant) multiplied by the time. Projecting vector components of the inertial frame along the axes of the Earth frame and installing these as columns of the transformation matrix yields

$$C_i^e = \begin{bmatrix} 1 & 0 & 0 \\ 0 & \cos(\omega_{ie}t) & \sin(\omega_{ie}t) \\ 0 & -\sin(\omega_{ie}t) & \cos(\omega_{ie}t) \end{bmatrix} \qquad (1)$$

Earth to Navigation Transformation. This transformation matrix is derived similarly to the previous one only this time involving two rotations. The first one through an angle Λ about the x-axis, and the second a rotation about the y-axis through an angle θ.

$$C_e^n = \begin{bmatrix} \cos\theta & 0 & -\sin\theta \\ 0 & 1 & 0 \\ \sin\theta & 0 & \cos\theta \end{bmatrix} \begin{bmatrix} 1 & 0 & 0 \\ 0 & \cos\Lambda & \sin\Lambda \\ 0 & -\sin\Lambda & \cos\Lambda \end{bmatrix} = \left[\begin{array}{c|c|c} \cos\theta & \sin\theta \sin\Lambda & -\cos\Lambda \sin\theta \\ \hline 0 & \cos\Lambda & \sin\Lambda \\ \hline \sin\theta & -\sin\Lambda \cos\theta & \cos\theta \cos\Lambda \end{array}\right] \quad (2)$$

Inertial to Navigation Transformation. This transformation is simply a product of the above two.

$$C_i^n = C_e^n C_i^e \quad (3)$$

Also note that $C_e^i = (C_i^e)^{-1} = (C_i^e)^T$ and similarly for C_n^i, C_n^e.

Angular Rates

The angular rates are now obtained and coordinatized in the navigation frame, since this is the frame in which the computations will be performed. A profile generating computer program which will be discussed in detail in Chapter VIII is used to calculate and store values related to the dynamics of the aircraft and satellites at each time increment of numerical integration. The velocity and acceleration components (as well as other pertinent values) are stored and available in navigation coordinates and are thus used in the following development of angular rates. These angular rates and accelerations will be required in the propagation of the Pinson inertial system error model plant states. Also note that the aircraft's distance from the Earth's center is approximated as being equal to the radius of the Earth. This is justified by the fact that the altitude of the aircraft is on the order of two miles as compared to approximately 4000 miles for the

radius of the Earth.

The angular rate of the Earth with respect to the inertial frame and coordinatized in the navigation frame is

$$\underline{\omega}_{ie}^{n} = C_e^{n}\omega_{ie}^{e} = C_e^{n}\begin{bmatrix}\omega_{ie}\\0\\0\end{bmatrix} = \begin{bmatrix}\omega_{ie}\cos\theta\\0\\\omega_{ie}\sin\theta\end{bmatrix} \equiv \begin{bmatrix}\Omega_x\\\Omega_y\\\Omega_z\end{bmatrix} \tag{4}$$

To get the angular rate of the navigation frame with respect to the Earth-fixed frame using the stored values of aircraft velocity coordinatized in the navigation frame

(1) rotate through an angle A about E_x

(2) rotate through an angle θ about E_y

where E_x and E_y are defined in Figure 2. Then

$$\underline{\omega}_{en} = \dot{A}\,\hat{e}_x + \dot{\theta}\,\hat{e}_{y'} \tag{5}$$

and

$$\dot{A} = \frac{-V_y}{R\cos\theta} \tag{6}$$

and

$$\dot{\theta} = \frac{V_x}{R} \tag{7}$$

where $\hat{e}_x$ and $\hat{e}_{y'}$ are unit vectors along the axes about which rotation occurs. The angular rate of the navigation frame with respect to the Earth in navigation coordinates becomes

$$\underline{\omega}_{en}^{n} \triangleq \begin{bmatrix}\rho_x\\\rho_y\\\rho_z\end{bmatrix} \tag{8}$$

$$\rho_x = \dot{A}\cos\theta = -V_y/R \tag{9}$$

$$\rho_y = \dot{\theta} = V_x/R \tag{10}$$

$$\rho_z = \dot{A}\sin\theta = -V_y/R\tan\theta \tag{11}$$

where R is the radius of the Earth. The angular accelerations are now obtained by taking the time derivatives of the angular rates.

$$\dot{\underline{\omega}}^n_{en} \equiv \begin{bmatrix} \dot{\rho}_x \\ \dot{\rho}_y \\ \dot{\rho}_z \end{bmatrix} \tag{12}$$

$$\dot{\rho}_x = \frac{d}{dt}\,(-V_y/R) = -A_y/R \tag{13}$$

$$\dot{\rho}_y = \frac{d}{dt}\,(V_x/R) = A_x/R \tag{14}$$

$$\dot{\rho}_z = \frac{d}{dt}\left(-\frac{V_y}{R}\tan\theta\right) = -\frac{A_y}{R}\tan\theta - \frac{V_y}{R}\dot{\theta}\sec^2\theta \tag{15}$$

The angular rate of the navigation frame with respect to the inertial frame expressed in navigation coordinates is then,

$$\underline{\omega}^n_{in} = \underline{\omega}^n_{ie} + \underline{\omega}^n_{en} = \begin{bmatrix} \Omega\cos\theta \\ 0 \\ \Omega\sin\theta \end{bmatrix} + \begin{bmatrix} -V_y/R \\ V_x/R \\ -\frac{V_y}{R}\tan\theta \end{bmatrix} \equiv \begin{bmatrix} \omega_x \\ \omega_y \\ \omega_z \end{bmatrix} \tag{16}$$

(Reference 6:3-27 thru 3-43)

III. Satellite Geometry and Range Measurement Equation

In this chapter, theory which is peculiar to the use of Navigation satellites as updating aids to the INS is developed. First, the range measurement equation is derived. Next, a method for determining whether or not a satellite is observable or "in view" is presented. Finally, the satellite motion generator, a computer routine which calculates satellite orbital elements and unit vectors from the aircraft to the satellite as functions of time, is discussed.

Range Measurement Equation

The range divergence equations, characterizing the range measuring process, are generated by the user from a combination of INS and satellite information. The range measurement process involves the comparison of a measured value of range against a predicted value of range. The measured range to a satellite is determined by measuring the incremental phase shift between the user and satellite clocks which were synchronized at an earlier time. The computed range is obtained from satellite ephemeris data and user INS supplied position information. Both the measured and computed range values contain errors; however, if the measured and computed values are subtracted, the difference will contain only the errors. This difference is called the range divergence. If these errors can be modeled as the outputs of linear systems driven by white Gaussian noise, then a Kalman filter can be constructed to estimate these errors and greatly improve upon the accuracy of the raw range data.

In order to avoid the notational inconvenience of using subscripts to keep track of which satellite is being referred to, consider the case where a single satellite is observed. The results are identical for any

one of the 27 satellites and therefore easily extended. The range vector of interest is the vector $\underline{r}$ from the aircraft (or user) to the satellite. It is related to the two vectors $\underline{r}_a$ and $\underline{r}_s$ which are illustrated and defined in the following figure.

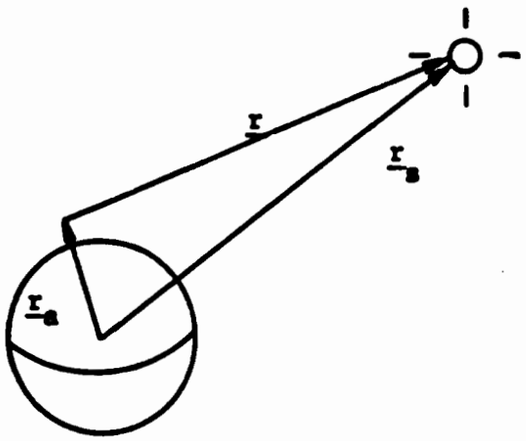

$\underline{r}$ = position vector from user to satellite

$\underline{r}_a$ = position vector from Earth's center to aircraft

$\underline{r}_s$ = position vector from Earth's center to satellite

Figure 3. Definition of Range Vector

It follows that

$$\underline{r} = \underline{r}_s - \underline{r}_a \tag{17}$$

$$r \equiv |\underline{r}| = |\underline{r}_s - \underline{r}_a| \tag{18}$$

$$r = \sqrt{\underline{r} \cdot \underline{r}} = \sqrt{(\underline{r}_s - \underline{r}_a) \cdot (\underline{r}_s - \underline{r}_a)} \tag{19}$$

The measured range to the satellite, r', is composed of two parts,

$$r' = r + \delta r' \tag{20}$$

where r is the true range, and $\delta r'$ is the error in the measured range.

The computed range to the satellite, r^*, is also composed of two parts,

$$r^* = r + \delta r^* \tag{21}$$

where r is the true range, and δr^* is the error in the value of the computed range. The quantity that is being observed is then the

difference of these two range values and is called the range divergence, Δr.

$$\Delta r = r' - r^* = \delta r' - \delta r^* \tag{22}$$

Errors in Computed Range. The computed satellite position is in error due to errors in the ephemeris data, while the INS errors account for the uncertainty in the aircraft's position.

$$\underline{r}_s^* = \underline{r}_s + \delta\underline{r}_s^* \tag{23}$$

$$\underline{r}_a^* = \underline{r}_a + \delta\underline{r}_a^* \tag{24}$$

The error equation is then obtained by noting from equation (19) that

$$(r^*)^2 = \underline{r}^* \cdot \underline{r}^* \tag{25}$$

Taking the differential of both sides of the equation,

$$2r^*\delta r^* = \underline{r}^* \cdot \delta\underline{r}^* + \delta\underline{r}^* \cdot \underline{r}^* \tag{26}$$

or,

$$\delta r^* = \frac{1}{r^*}(\underline{r}^* \cdot \delta\underline{r}^*) = \left(\frac{1}{r^*}\underline{r}^*\right) \cdot \delta\underline{r}^* \tag{27}$$

Noting that the quantity in parentheses on the right hand side of the above equation is simply a unit vector from the aircraft to the satellite

$$\underline{i}_{r^*} \equiv \frac{1}{r^*}\underline{r}^* \tag{28}$$

and also that

$$\delta\underline{r}^* = \delta\underline{r}_s^* - \delta\underline{r}_a^* \tag{29}$$

the computed error is then

$$\delta r^* = \underline{i}_{r^*} \cdot (\qquad\qquad) \tag{30}$$

Satellite orbital parameters are updated by the ground tracking network

on a periodic basis and relayed to the user along with the range data. This ephemeris data is highly accurate; any uncertainties in computed satellite range can be accounted for by increasing the satellite clock phase error. Thus, it is assumed that $\delta \underline{r}_s$ is approximately zero, and the computed range error is

$$\delta r^* \triangleq - \underline{i}r^* \cdot \delta \underline{r}_a^* \tag{31}$$

The computation of the above equation requires values for the unit vector from the aircraft to the satellite and current values for the x, y, and z INS position error states ($\delta \underline{r}_a^* = [\Delta x, \Delta y, \Delta z]^T$). Actually, the root-mean-squared (RMS) values of the covariance of the position errors are used, since this is a stochastic process simulation; this statistical aspect of the problem will be discussed in later chapters.

Errors in Measured Range. Modeling of the range measurement error requires a knowledge of the various error sources which are contained in the measurement and fitting these error sources with empirical data. The model used in this simulation is a somewhat simplified version of the one found in Reference 1. It is a linear combination of three components for each satellite measurement corrupted by white Gaussian noise (v). Each of the separate components is a linear system driven by white Gaussian noise. These linear models will be discussed in detail in Chapter V.

The range measurement error is modeled as

$$\delta r' = c\delta T_u - c\delta T_s + \delta b + v \tag{32}$$

where

c = the speed of light

δT_u = user clock phase error

δT_s = satellite clock phase error

δb = range bias

v = measurement noise

The bias term in the above equation accounts for the minor effect of both tropospheric delay and velocity of light bias uncertainties in each of the 4 satellite range measurements. The error due to ionosphere delay is a function of the elevation angle and on the order of 15 feet. As will be explained in Chapter V, this effect is assumed to be included in the satellite clock phase/range error (δT_s).

Substitution of equations (31) and (32) into equation (22) yields the final form of the range divergence equation.

$$\Delta r = \underline{i}r^* \cdot \delta \underline{r}_a^* + c\delta T_u - c\delta T_s + \delta b + v \qquad (33)$$

A minimum of four range divergence equations, or in other words at least four satellites, are required as observables to correct for the three components of position and the clock phase or time difference. Also note that for notational convenience the asterisk (*) will be dropped in subsequent equation development.

Satellite In-View Criterion

In order to obtain measurements from a given satellite, the satellite must be observable by the user; that is, it must be at some specified minimum angle above the aircraft's horizon for a useful signal. This minimum angle is arbitrary and dependent upon the capabilities of the user equipment. A nominal value of ten degrees was selected for implementation in this study. This in-view criterion along with the

selection of 27 for the number of satellites globally deployed insures that, regardless of the user's location, a reasonable number (say seven or eight) satellites will always be observable, from which a "best set" of the required four satellites may be chosen.

A method for determining whether or not a satellite is in-view using information calculated in the satellite orbit generating computer program is now presented.

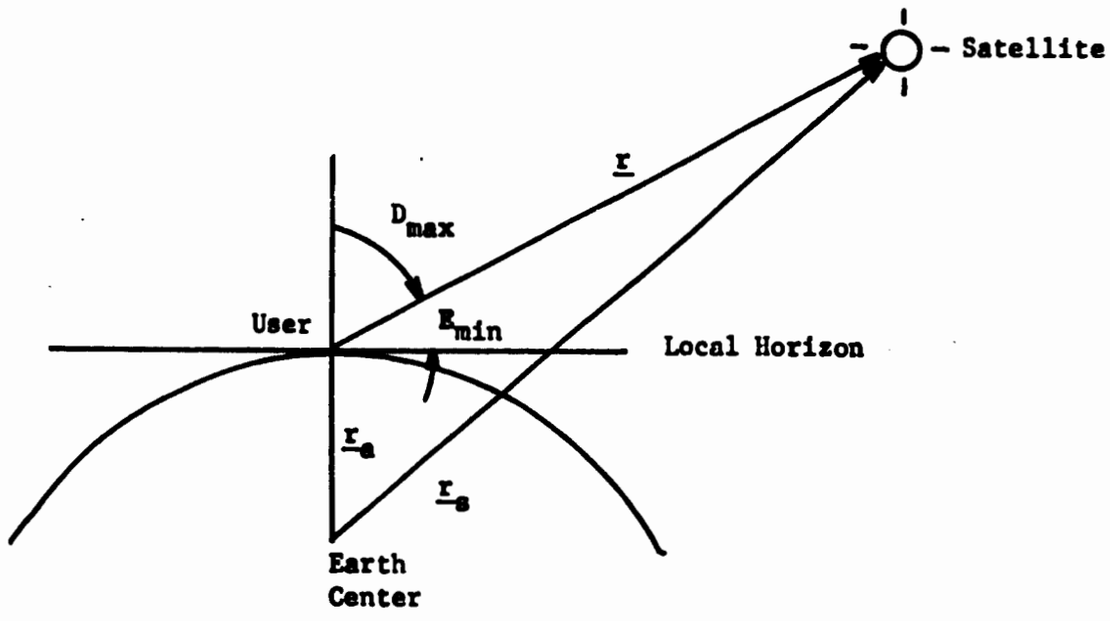

Figure 4. In-View Criterion Geometry

E_{min} = minimum angle of elevation for useful satellite signal

$$D_{max} = 90° - E_{min} \tag{34}$$

$\underline{r}$, $\underline{r}_s$, $\underline{r}_a$, and C_e^n are as defined in the previous section.

$\underline{r}_a$ is most readily expressed in the navigation frame,

$$\underline{r}_a^n = \begin{bmatrix} 0 \\ 0 \\ R + h \end{bmatrix} = \begin{bmatrix} 0 \\ 0 \\ R \end{bmatrix} \tag{35}$$

where R = radius of Earth, h = aircraft altitude, and the superscript

denotes the frame in which the vector is coordinatized. Since $\underline{r}_s^e$ is derived from the ground track latitude and longitude of the satellite in the orbit generator and readily available, the vector $\underline{r}$ from the aircraft to the satellite coordinatized in the navigation frame is written as

$$\underline{r}^n = \underline{r}_s^n - \underline{r}_a^n = C_e^n \underline{r}_s^e - \begin{bmatrix} 0 \\ 0 \\ R \end{bmatrix} \tag{36}$$

A unit vector along $\underline{r}^n$ is given by

$$\underline{i}_r = \underline{r}^n / r \tag{37}$$

where,

$$r = \sqrt{\underline{r}^n \cdot \underline{r}^n} \tag{38}$$

Noting that the z-component of the above unit vector is simply the sine of the elevation angle or the cosine of D,

$$\underline{i}_r \cdot \begin{bmatrix} 0 \\ 0 \\ 1 \end{bmatrix} = i_{r_z} = \cos D \tag{39}$$

It follows that if the unit vectors from the user to the satellite expressed in navigation coordinates are computed, the in-view criterion becomes

$$D < D_{max} \tag{40}$$

$$\cos D > \cos D_{max} \tag{41}$$

If $i_{r_z} > \cos D_{max}$ satellite is in view.

If $i_{r_z} \leq \cos D_{max}$ satellite is not in view.

For the arbitrarily selected minimum elevation angle of ten degrees this criterion requires the z-component of this unit vector to be greater than cos 80°.

$$i_{r_z} > \cos 80^\circ \quad (\cos 80^\circ \simeq 0.174) \tag{42}$$

A sample output from the satellite orbit generator program listing satellites which are in view at a particular time instant is included at the end of this chapter.

Satellite Motion Generator

It is apparent from previous sections that in order to simulate an INI flight, a satellite motion generator is required to provide necessary information regarding the satellites' orbital elements. This section presents the equations necessary to calculate required parameters of the satellites and also describes the selected arbitrary initial conditions on the satellite constellations. It should be noted that this particular configuration is a leading candidate for implementation in the proposed INI system.

Total deployment consists of three rings or "constellations" of nine satellites each. All satellite orbits are assumed to be circular; in fact, the orbital period (and thus the orbital velocity and altitude) of all satellites is assumed constant and equivalent. Since global coverage is desired, the satellites on any given ring are equally spaced; thus, the circular arc between any two adjacent satellites on a ring subtends a central angle of forty degrees. A satellite is identified by a two digit code, the first digit (1 through 9) indicates which satellite of the nine on the ring is referred to, and the second digit indicates the particular constellation (1, 2, or 3). Thus, satellite 62 is the sixth satellite on the second ring.

The Euler Angles. To specify the orientation of any one satellite with respect to the Earth-fixed frame requires three parameters; the

most convenient parameters are the Euler angles, from which the direction cosines or unit vector to the satellite may be determined. Figure 5 shows two unit orthogonal right-handed triads ($\underline{i}$, $\underline{j}$, $\underline{k}$) and ($\underline{I}$, $\underline{J}$, $\underline{K}$) with origins at point O. The triad ($\underline{i}$, $\underline{j}$, $\underline{k}$) has $\underline{k}$ pointing to the satellite, and the triad ($\underline{I}$, $\underline{J}$, $\underline{K}$) represents the Earth-fixed frame.

The first Fuler angle ξ is the angle between $\underline{i}$ and $\underline{I}$, and is the angle of inclination. The second angle η is the angle between the plane ($\underline{i}$, $\underline{I}$) and the plane ($\underline{I}$, $\underline{J}$); this is the angle resulting from the Earth's rotation. The third angle ζ is the angle between the plane ($\underline{i}$, $\underline{j}$) and the plane ($\underline{I}$, $\underline{i}$); this is the angle resulting from the satellites motion about the Earth.

Initially let the triad ($\underline{i}$, $\underline{j}$, $\underline{k}$) coincide with ($\underline{I}$, $\underline{J}$, $\underline{K}$). The triad ($\underline{i}$, $\underline{j}$, $\underline{k}$) can be brought to the general position shown in Figure 5 by applying the following rotations in order:

(i) A rotation η about $\underline{I}$; this brings the movable triad ($\underline{i}$, $\underline{j}$, $\underline{k}$) into coincidence with ($\underline{I}$, $\underline{J}'$, $\underline{K}'$).

(ii) A rotation ξ about $\underline{K}'$; this brings ($\underline{i}$, $\underline{j}$, $\underline{k}$) into coincidence with ($\underline{i}$, $\underline{J}''$, $\underline{K}'$).

(iii) A rotation ζ about $\underline{i}$; this brings ($\underline{i}$, $\underline{j}$, $\underline{k}$) into the required final position.

It is observed that all possible positions of the body can be obtained by assigning values to ξ, η, ζ in the ranges

$$0 \leq \xi \leq \pi \qquad 0 \leq \eta < 2\pi \qquad 0 \leq \zeta < 2\pi$$

Let A be the rotation matrix transforming a unit vector from the general coordinate frame ($\underline{i}$, $\underline{j}$, $\underline{k}$) to the Earth-fixed frame. Then,

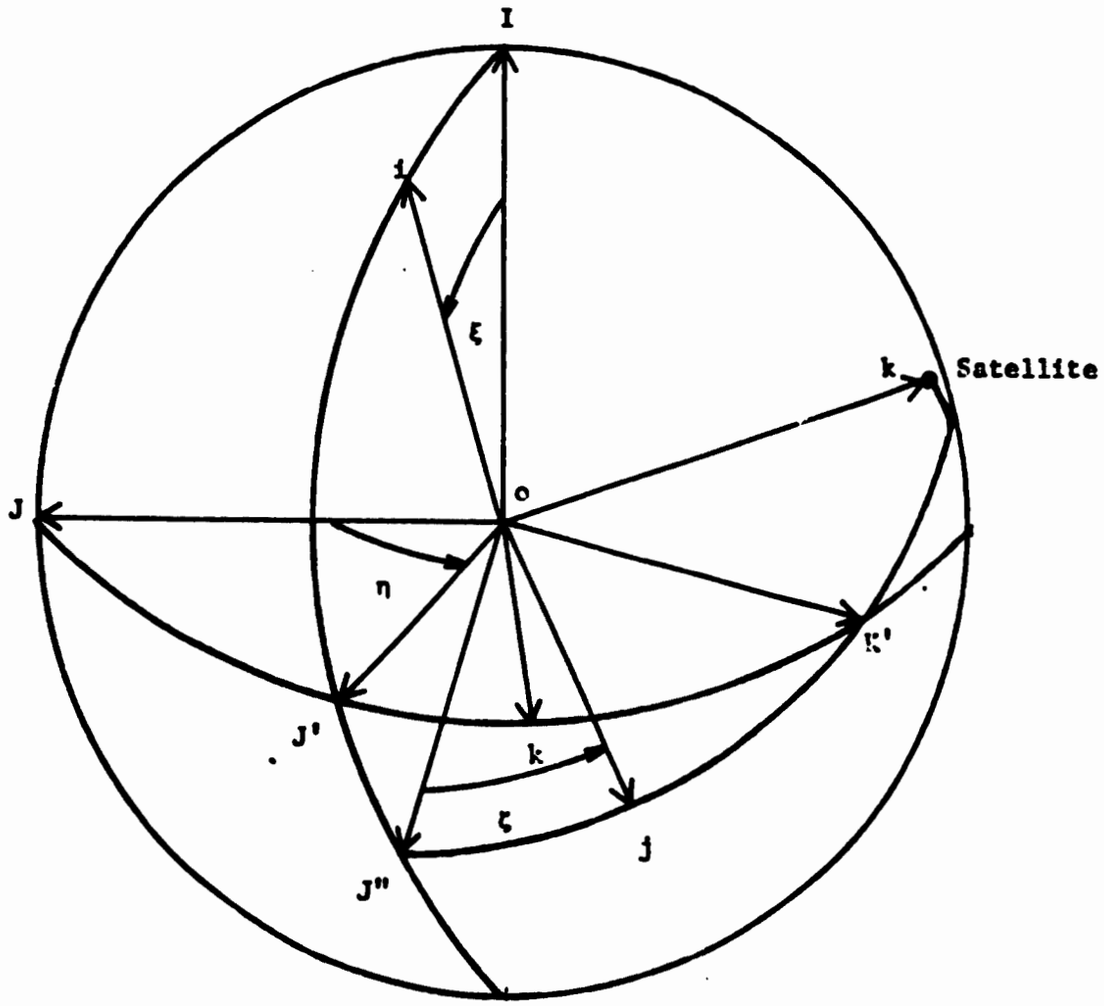

Fig. 5. The Euler Angles

$$\begin{bmatrix} I \\ J \\ K \end{bmatrix} = A \begin{bmatrix} i \\ j \\ k \end{bmatrix} = \begin{bmatrix} a_{11} & a_{12} & a_{13} \\ a_{21} & a_{22} & a_{23} \\ a_{31} & a_{32} & a_{33} \end{bmatrix} \begin{bmatrix} i \\ j \\ k \end{bmatrix} \tag{43}$$

Where I, J, K, i, j, k represent the scalar components along their respective axes. Since the unit vector to the satellite is coincident with $\underline{k}$ (i.e., i = j = 0, k = 1) this simplifies to,

$$\begin{bmatrix} I \\ J \\ K \end{bmatrix} = \begin{bmatrix} a_{13} \\ a_{23} \\ a_{33} \end{bmatrix} \tag{44}$$

These direction cosines may be obtained by resolving vectors in Figure 5. Alternately, the cosine law of spherical triangles may be applied at this point (See Ref 7:17-19). Using either method the following values are obtained.

$$a_{13} = \sin \zeta \sin \xi \tag{45}$$

$$a_{23} = -(\sin \eta \cos \zeta + \cos \eta \sin \zeta \cos \xi) \tag{46}$$

$$a_{33} = \cos \eta \cos \zeta - \sin \eta \sin \zeta \cos \xi \tag{47}$$

(Ref 8:259-261).

a_{13}, a_{23}, and a_{33} represent the components of the unit vector along $\underline{r}_s^e$, the vector from the center of the earth to the satellite expressed in Earth coordinates.

Initialization of Satellites. The initial conditions and constant parameters of the satellite orbits are given in the following two tables. Note that m refers to the m^{th} satellite on the designated ring; for example, the entry of m1 in the table of initial conditions represents the remaining eight satellites of the first constellation. The numbers

which are missing from the table (represented by ---) are dependent upon the initial values of ξ, η, and ζ which are specified. The latitude and longitude values refer to the ground track of the satellites.

TABLE I

Orbital Design Constants

Orbital Period	8 Hrs. (all satellites)
Angle of Inclination (ξ)	55° (all three satellite rings)
Altitude	7496 n. mi. (all satellites)

TABLE II

Navigation Satellite Initial Conditions

	Initial Latitude (deg)	Initial Longitude (deg)	ζ_o (deg)
11	0	0	0
m1	---	---	-40(m-1)
12	0	120	0
m2	---	---	-40(m-1)
13	0	-120	0
m3	---	---	-40(m-1)

These satellites may be initialized at any given time relative to the flight time since they are in reality not yet in orbit and their orbits remain arbitrary. For computational ease, the satellites will be given the above initial conditions at the start of the INI flight (t = 0). However, if the satellites were actually in orbit, then

initial positions would be dependent upon the user take-off time. A pictorial representation of the satellite orbits is shown in Figure 6.

Computational Sequence. The sequence of equations required to compute unit vectors for each of the 27 $\underline{r}^n$ is now presented.

$$\xi = 55° \tag{48}$$

$$\eta = 120°(n-1) - (1°/240 \text{ sec})t \tag{49}$$

$$\zeta = -40°(m-1) + Ct \tag{50}$$

Where m = satellite designator, n = ring designator, and 1°/240 sec represents the rotational speed of the Earth. Also,

$$C = \sqrt{G_e/r_s}^e = \text{orbital speed of the satellite} \tag{51}$$

The components of $\underline{r}_s^e$ are now computed using the Eulerian Angles.

$$\begin{bmatrix} a_{13} \\ a_{23} \\ a_{33} \end{bmatrix} = \begin{bmatrix} \sin\zeta \sin\xi \\ -(\sin\eta \cos\zeta + \cos\eta \sin\zeta \cos\xi) \\ \cos\eta \cos\zeta - \sin\eta \sin\zeta \cos\xi \end{bmatrix} \tag{52}$$

The ground track latitudes and longitudes are given by

$$\theta = \tan^{-1}\left(a_{13}/\sqrt{(a_{23})^2 + (a_{33})^2}\right) \tag{53}$$

$$\Lambda = \tan^{-1}\left(-a_{23}/a_{33}\right) \tag{54}$$

The required components of the unit vector along $\underline{r}^n$ may now be computed.

$$\underline{r}_s^n = C_e^n \, \underline{r}_s^e \tag{55}$$

$$\underline{r}^n = \underline{r}_s^n - \begin{bmatrix} 0 \\ 0 \\ R \end{bmatrix} = \begin{bmatrix} r_x \\ r_y \\ r_z \end{bmatrix} \tag{56}$$

$$r = \sqrt{(r_x)^2 + (r_y)^2 + (r_z)^2} \tag{57}$$

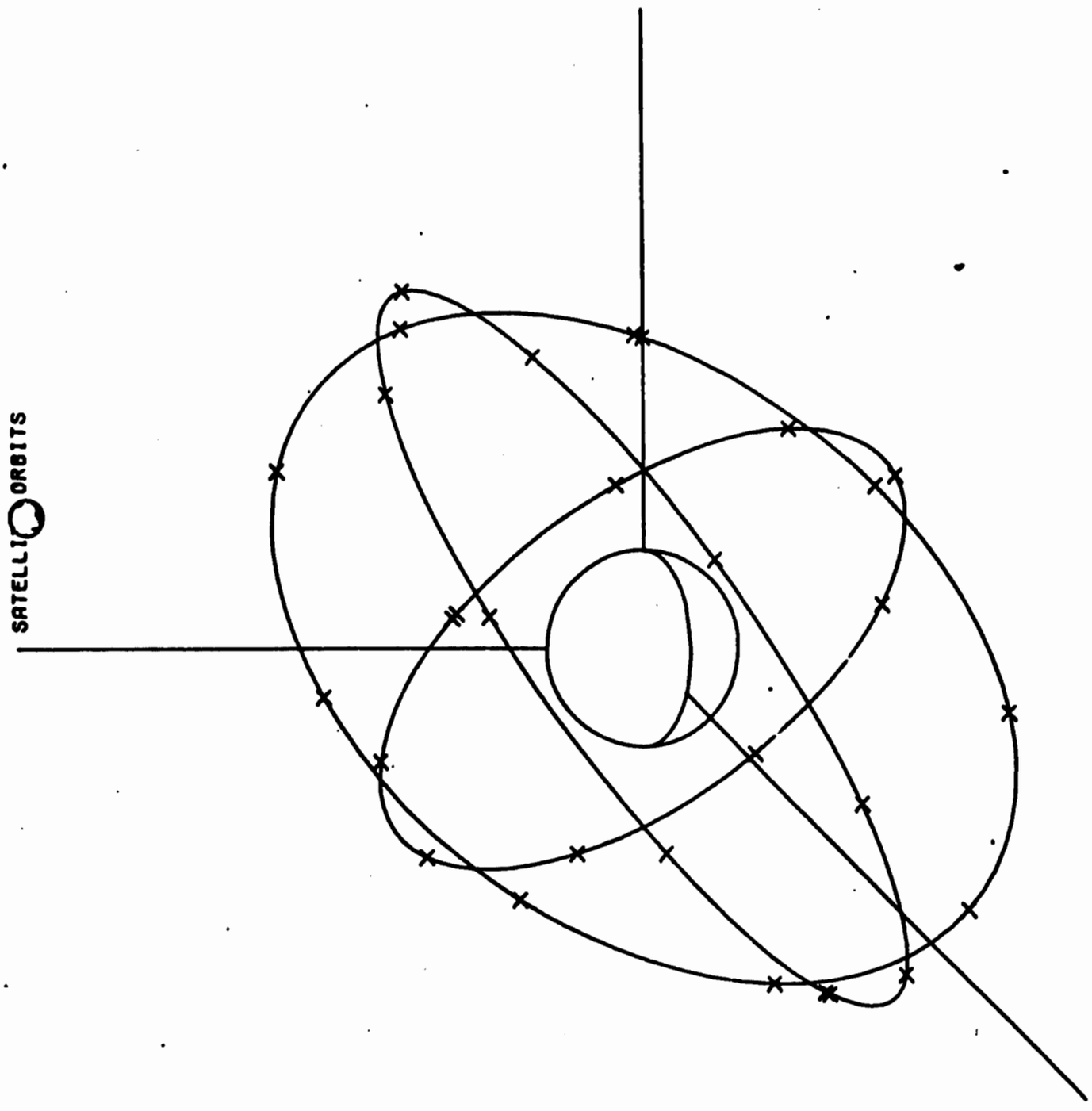

Fig. 6. Navigation Satellite Orbits

$$\underline{i}_{r_n} = \underline{r}^n/r = \begin{bmatrix} i_{r_x} \\ i_{r_y} \\ i_{r_z} \end{bmatrix} \tag{58}$$

A test on the in-view criterion is made

$$i_{r_z} > \cos 80^\circ \quad ? \tag{59}$$

The three components of the unit vector, the latitude, longitude, and in-view criteria for each of the 27 satellites is calculated and stored at each time increment of numerical integration along the flight path. A sample output of these values is presented in Table III. This table shows the output of the profile generator program for the 27 satellites. The first block is ring 1 consisting of nine satellites. Columns 1, 2, and 3 are the x, y, and z components of the unit vector from the aircraft to the satellite expressed in the navigation frame. Columns 4 and 5 are the satellite ground track latitude and longitude respectively (in degrees). Column 6 is the in-view criterion, the component of the unit vector in the z direction. If this value is greater than cos 80° ≈ 0.17, then column 7 will contain a T (for True) indicating the satellite is in-view. The 2nd and 3rd blocks represent rings 2 and 3. Note that the satellites in view of this particular time instant are satellites 52, 62, 72, 13, 83 and 93.

Table III

Satellite Position and In-View Criterion at Time = 360 sec

Satellite Number						
					Ring 1	
11	-.076	-.996	-.044	3.7	1.1	-.04 F
21	-.714	-.695	-.078	-28.4	-23.7	-.18 F
31	-.973	-.077	-.217	-52.5	-67.2	-.22 F
41	-.766	.517	-.382	-47.7	-131.2	-.38 F
51	-.243	.833	-.496	-19.9	-166.8	-.50 F
61	.363	.773	-.521	12.6	169.5	-.52 F
71	.817	.366	-.447	42.5	138.7	-.45 F
81	.923	-.243	-.299	54.6	79.6	-.30 F
91	.587	-.798	-.137	35.1	27.9	-.14 F
					Ring 2	
12	.447	.196	-.873	3.7	121.1	-.87 F
22	.045	-.129	-.991	-28.4	96.3	-.99 F
32	-.380	-.407	-.830	-52.5	52.8	-.83 F
42	-.724	-.561	-.400	-47.7	-11.2	-.40 F
52	-.836	-.486	.256	-19.9	-46.8	.26 T
62	-.466	-.058	.883	12.6	-70.5	.88 T
72	.303	.496	.814	42.5	-101.3	.81 T
82	.740	.656	.145	54.6	-161.0	.15 F
92	.723	.493	-.483	35.1	147.9	-.48 F
					Ring 3	
13	-.368	.849	.360	3.7	-118.9	.36 T
23	-.544	.780	-.311	-28.4	-143.7	-.31 F
33	-.448	.442	-.777	-52.5	172.8	-.78 F
43	-.206	.007	-.978	-47.7	108.8	-.98 F
53	.107	-.413	-.904	-19.9	73.2	-.90 F
63	.419	-.716	-.558	12.6	49.5	-.56 F
73	.635	-.772	.033	42.5	18.7	.03 F
83	.560	-.391	.719	54.6	-41.0	.71 T
93	.101	.391	.915	35.1	-92.1	.91 T

IV. Kalman Filter Equations

Design of an INI Kalman filter requires extensive computer simulation. This chapter is a discussion of the equations which are required not only for the mechanization of the filter but also those which are necessary to simulate the dynamics of the user, or aircraft, and the driving error sources.

The method of covariance analysis will be the principal tool used in solution of the problem. In this analysis, arbitrary initial conditions on the diagonal elements of the covariance matrix, P, are specified and the off-diagonal terms are assumed to be zero initially. The covariance is a measure of the uncertainty in the knowledge of the true values of the components of the state vector. In the simulation, the covariance matrix of both the system and the filter are propagated forward in time by numerical integration techniques. When the specified update time is reached, the best estimates of the states are determined, and control is applied to the system to adjust the values of the state variable to the best estimate obtained with the Kalman filter. The square root of the individual diagonal elements of the system covariance matrix are then plotted as a function of time to yield a basis for comparison of filters.

In this simulation, the error statistics are propagated; i.e., the standard deviation of the noise is always supplied when a noise value is required. This is in contrast to a "Monte Carlo" type simulation where an actual sequence of noise values is measured and recorded for use in the simulation. This is possible because the covariance is independent of actual measurement values, and can be computed without generating a sample sequence of measurement values.

System Model Equations

The basic equations used in this process are the differential equations that describe how the inertial navigator errors propagate with time. The equations are formulated into a set of first order, linear differential equations, driven by white Caussian noise. Linear measurements are made upon the actual system variables, and these are corrupted by white Gaussian noise. It is assumed that the equations representing a detailed model of the system are as follows:

$$\dot{\underline{x}}_s = F_s \underline{x}_s + G_s \underline{u}_s \tag{60}$$

where

$\underline{x}_s$ is an n_1 vector denoting the true state

F_s is an $n_1 \times n_1$ system dynamics matrix

G_s is an $n_1 \times m_1$ gain matrix

$\underline{u}_s$ is an m_1 vector of white noise inputs with zero mean and variance

$$E[\underline{u}(i)\underline{u}(j)^T] = \begin{cases} Q_s(i) & i = j \\ 0 & i \neq j \end{cases} \tag{61}$$

where i and j are instants in time.

The observations obtained from external references can be described by the linear measurement vector equation

$$\underline{z}_s = H_s \underline{x}_s + \underline{v}_s \tag{62}$$

where

$\underline{z}_s$ is an r vector of measurements

H_s is an $r \times n_1$ measurement matrix

$\underline{v}_s$ is an r vector of white noise inputs with zero mean and variance

$$E[\underline{v}(i)\underline{v}(j)^T] = \begin{cases} R_s(i) & i = j \\ 0 & i \neq j \end{cases} \qquad (63)$$

It is assumed that the system noise and measurement noise are uncorrelated for all time.

$$E[\underline{u}(i)\underline{v}(j)^T] = 0 \quad \text{all } i,j \qquad (64)$$

Filter Equations

The above set of equations are assumed to be a complete and accurate mathematical description of the INI system dynamics and measurement equations for the purpose of simulation. It is also the set of equations which would be utilized in the design of a fully optimal Kalman filter. However, due to the computational burden of the optimal filter, a suboptimal filter design is obtained by reducing the dimension of the state vector. The states that are eliminated are the ones that least affect the accuracy of the mathematical description of the INI. This suboptimal filter can then be implemented with an aircraft on-board computer.

The suboptimal filter structure is represented as follows where $\underline{x}_f$ is the design filter state and $\hat{\underline{x}}_f$ is the filter best estimate of the design filter state.

$$\dot{\underline{x}}_f = F_f\underline{x}_f + G_f\underline{u}_f \qquad (65)$$

where

$\underline{x}_f$ is an n_2 vector

F_f is an $n_2 \times n_2$ filter dynamics matrix

G_f is an $n_2 \times m_2$ gain matrix

$\underline{u}_f$ is an m vector of white noise inputs with zero mean and variance

$$E[\underline{u}_f(i)\underline{u}_f^T(j)] = \begin{cases} Q_f(i) & i = j \\ 0 & i \neq j \end{cases} \tag{66}$$

The filter measurement equation is

$$\underline{z}_f = H_f\underline{x}_f + \underline{v}_f \tag{67}$$

where

$\underline{z}_f$ is an r vector

H_f is an r x n_2 measurement matrix

$\underline{v}_f$ is an r vector of white noise inputs with zero mean and variance

$$E[\underline{v}_f(i)\underline{v}_f^T(j)] = \begin{cases} R_f(i) & i = j \\ 0 & i \neq j \end{cases} \tag{68}$$

The filter design based upon the above design state is given as follows:

Between measurements

$$\dot{\underline{\hat{x}}}_f = F_f\underline{\hat{x}}_f \tag{69}$$

$$\dot{P}_f = F_fP_f + P_fF_f^T + G_fQ_fG_f^T \tag{70}$$

At a measurement

$$K_f = P_f^-H_f^T[H_fP_f^-H_f^T + R_f]^{-1} \tag{71}$$

$$P_f^+ = P_f^- - K_fH_fP_f^- \tag{72}$$

$$\underline{\hat{x}}_f^+ = \underline{\hat{x}}_f^- + K_f[\underline{z}_s - H_f\underline{\hat{x}}_f] \tag{73}$$

where

$\underline{\hat{x}}_f$ is an n_2 vector denoting the best estimate

P_f is the filter covariance matrix

$-$ superscript indicates the time instant before update

$+$ superscript indicates the time instant after update

K_f Kalman gain matrix

The filter takes the actual measurement $\underline{z}_s$ and subtracts from it the best prediction of its value before the actual measurement is taken, $H_f\hat{\underline{x}}_f$. This difference is then passed through an optimal weighting matrix K_f, and used to correct $\hat{\underline{x}}_f$, the best prediction of the state at the time instant before the measurement is taken. This gives the best estimate after update. This estimate is propagated to the time of the next measurement sample with the above equations $\dot{\hat{\underline{x}}}$ and $\dot{P}$.

These recursive relationships are initiated from the assumed Gaussian density that describes the apriori knowledge of the state.

$$\hat{\underline{x}}(0) = \hat{\underline{x}}_o \tag{74}$$

$$P(0) = P_o \tag{75}$$

The Kalman filter will propagate the conditional probability density of the desired quantities, conditional on the actual measurements taken. The probability density function of a Gaussian noise amplitude takes on the shape of a normal bell-shaped curve. This assumption of Gaussian noise amplitude is justified by the fact that a system or measurement noise is typically caused by a number of small sources. It can be shown mathematically that when a number of random variables are added together the summed effect is very nearly a Gaussian probability density, regardless of the shape of the individual densities. Additionally, the use of Gaussian densities makes the mathematics tractable. The first and second order statistics (mean and variance or standard deviation) completely determine a Gaussian density. Thus, the Kalman filter, which propagates the first and second order statistics, includes all information contained in the conditional probability density (Ref 10:4-6 & 2:8-21).

The mean or expectation, (μ), of a density is defined as

$$E[X] = \mu = \int_{-\infty}^{\infty} xf(x)dx \tag{76}$$

This is interpreted as the weighted average of the values of X, using the probability density function f(x) as the weighting function. This value is assumed to be zero for all Gaussian white driving noises used in this simulation.

The variance (σ^2) of a density is defined as

$$Var[X] = \sigma^2 = \int_{-\infty}^{\infty} (x-\mu)^2 f(x)dx \tag{77}$$

σ^2 is the weighted average of the values of $(x-\mu)^2$; thus, σ^2 is a measure of the spread of the density. (Ref 11:136-146). It is a direct measure of the uncertainty: the larger σ is, the broader the probability peak is, spreading the probability weight over a larger range of χ values. For a Gaussian density, 68.3% of the probability weight is contained within the band σ units to each side of the mean (μ) which represents the area under the normal bell-shaped curve between $-\sigma$ and $+\sigma$ and 95.4% of the probability weight is contained between -2σ and $+2\sigma$.

Equations 76 and 77 give the first and second order statistics for the scalar case. These equations are easily extended to the vector case (as required in this study) and are

$$E[\underline{X}] = \underline{\mu} = \int_{-\infty}^{\infty} \cdots \int_{-\infty}^{\infty} \underline{x} f(\underline{x}) dx_1 \cdots dx_n \tag{76a}$$

$$Cov[\underline{X}] = P = \int_{-\infty}^{\infty} \cdots \int_{-\infty}^{\infty} (\underline{x} - \underline{\mu})(\underline{x} - \underline{\mu})^T f(\underline{x}) dx_1 \cdots dx_n \tag{77a}$$

V. System Model

To apply the Kalman Filter equations developed in the previous chapter, a reference system model that is a good approximation to the real world dynamics is needed. This chapter outlines the reference system equations selected for this design study. The chapter is presented in four sections. The first section defines the 44 error states incorporated in the system model along with their assumed initial conditions. Also, the system dynamic matrix F_s is presented in partitioned matrix form. The second section discusses the modeling of the INS plant error states. The third section presents INS and satellite error source models, linear systems driven by white Gaussian noise. The last section displays the measurement equation (62) explicitly in matrix form.

State Variable Definition & Initial Conditions

Table IV presents a detailed listing of the 44 states utilized in the reference system model. The initial conditions on the INS error states are highly arbitrary, and values similar to those used in other studies are selected. The initial conditions on the accelerometer and gyro error states are typical of an inertial navigation system in the one to two nautical mile per hour class. The initial conditions on the user clock are similar to those in Reference 1. The initial conditions on the satellite clock model are classified; therefore, reasonable order of magnitude numbers were selected in order to maintain the unclassified status of this report. It should be pointed out that whenever an integrator is required in the simulation diagram, the output of this integrator is a system state variable. Thus, the addition of an integrator to an error model increases the dimension of the error state

Table IV

System 44 State Vector Definition

Error State	Symbol	Definition	RMS Initial Condition
		INS Plant Error States	
1	Δx	x position error	3000 ft
2	Δy	y position error	3000 ft
3	Δz	z position (altitude) error	300 ft
4	$\Delta \dot{x}$	x velocity error	2 ft/sec
5	$\Delta \dot{y}$	y velocity error	2 ft/sec
6	$\Delta \dot{z}$	z velocity error	0.5 ft/sec
7	ϕ_x	x attitude error	0.14 millirad
8	ϕ_y	y attitude error	0.14 millirad
9	ψ_z	z attitude (heading) error	2.0 millirad
		INS Error Sources	
10	α_{rx}	x random accelerometer noise--expotentially correlated, τ = 600 sec	20 µg's
11	α_{ry}	y random accelerometer noise expotentially correlated, τ = 600 sec	20 µg's
12	α_{rz}	z random accelerometer noise--expotentially correlated, τ = 600 sec	20 µg's
13	α_{bx}	x accelerometer bias	66 µg's
14	α_{by}	y accelerometer bias	66 µg's
15	α_{bz}	z accelerometer bias	132 µg's
16	ϵ_{rx}	x random gyro drift expotentially correlated, τ = 3600 sec	0.012 deg/hr

Table IV

System 44 State Vector Definition

(Cont.)

Error State	Symbol	Definition	RMS Initial Condition
17	ϵ_{ry}	y random gyro drift expotentially correlated, τ = 3600 sec	0.012 deg/hr
18	ϵ_{rz}	z random gyro drift expotentially correlated, τ = 3600 sec	0.012 deg/hr
19	ϵ_{bx}	x gyro bias	0.025 deg/hr
20	ϵ_{by}	y gyro bias	0.025 deg/hr
21	ϵ_{bz}	z gyro bias	0.04 deg/hr
		User Clock Errors	
22	δT_u	user clock phase/range error	10,000 ft
23	x_{23}	user clock frequency offset	5 ft/sec
24	x_{24}	long term stability error	5×10^{-6} ft/sec^2
		Satellite Clock Errors	
25	δT_{s1}	sat. clock #1 phase/range error	100 ft
26	x_{26}	sat. clock #1 frequency offset	0.01 ft/sec
27	x_{27}	sat. clock #1 stability term	1×10^{-7} ft/sec^2
28	x_{28}	sat. clock #1 expotentially correlated noise, τ = 10000 sec	1×10^{-3} ft/sec
29	δT_{s2}	sat. clock #2 phase/range error	100 ft
30	x_{30}	sat. clock #2 frequency offset	0.01 ft/sec

Table IV

System 44 State Vector Definition

(Cont.)

Error State	Symbol	Definition	RMS Initial Condition
31	x_{31}	sat. clock #2 stability term	1×10^{-7} ft/sec^2
32	x_{32}	sat. clock #2 expotentially correlated noise, τ = 10000 sec	1×10^{-3} ft/sec
33	δT_{s3}	sat. clock #3 phase/range error	100 ft
34	x_{34}	sat. clock #3 frequency offset	0.01 ft/sec
35	x_{35}	sat. clock #3 stability term	1×10^{-7} ft/sec^2
36	x_{36}	sat. clock #3 expotentially correlated noise, τ = 10000 sec	1×10^{-3} ft/sec
37	δT_{s4}	sat. clock #4 phase/range error	100 ft
38	x_{38}	sat. clock #4 frequency offset	0.01 ft/sec
39	x_{39}	sat. clock #4 stability term	1×10^{-7} ft/sec^2
40	x_{40}	sat. clock #4 expotentially correlated noise, τ = 10000	1×10^{-3} ft/sec
		Satellite Range Bias Errors	
41	δb_1	sat. #1 range bias	10 ft
42	δb_2	sat. #2 range bias	10 ft
43	δb_3	sat. #3 range bias	10 ft
44	δb_4	sat. #4 range bias	10 ft

variable vector by one. Also, x, y, and z are navigation frame axes.

The initial covariance matrix P(0) has now been completely specified. Its diagonal elements are the squared values of the RMS initial conditions given in Table IV. The remaining off-diagonal elements are assumed to be zero initially. Propagation of the linear variance equation (70) requires additional knowledge of the two matrices F and Q' where

$$Q' = GQG^T \tag{78}$$

The F_s matrix is partitioned as follows

$$F_s = \begin{array}{c} \\ 1\text{-}9 \\ 10\text{-}15 \\ 16\text{-}21 \\ 22\text{-}24 \\ 25\text{-}40 \\ 41\text{-}44 \end{array} \begin{array}{c} \begin{array}{cccccc} 1\text{-}9 & 10\text{-}15 & 16\text{-}21 & 22\text{-}24 & 25\text{-}40 & 41\text{-}44 \end{array} \\ \begin{bmatrix} F_{11} & F_{12} & F_{13} & 0 & 0 & 0 \\ 0 & F_{22} & 0 & 0 & 0 & 0 \\ 0 & 0 & F_{33} & 0 & 0 & 0 \\ 0 & 0 & 0 & F_{44} & 0 & 0 \\ 0 & 0 & 0 & 0 & F_{55} & 0 \\ 0 & 0 & 0 & 0 & 0 & 0 \end{bmatrix} \end{array} \tag{79}$$

The submatrices of equation (79) will be displayed in explicit form as they are encountered in the following sections. The only non-zero elements of Q' are all diagonal and will be given in the following sections as q_i where the i subscript denotes the row and column of the value. For example, q_{10} indicates that this is the value belonging at the intersection of the 10th row and 10th column in the Q' matrix and corresponds to a white noise input on state variable number 10. There are eleven non-zero elements in the reference system Q' matrix corresponding to states 10, 11, 12, 16, 1 , 22, 25, 29, 33, and 37.

Plant Error States

The plant error state equations are the differential equations describing the natural unforced dynamic response of the errors in the inertial navigation system. This includes nine states: x, y, and z position, velocity, and attitude in the navigation frame. Additional state variables are usually added to these for the purpose of damping the inherently unstable vertical channel. Also, an altimeter measurement may be added to the measurement equations. However, since the navigation satellites provide position information along all three of the x, y, and z axes, inclusion of these additional states and measurements to control the altitude divergence is not absolutely necessary. In actual practice, an altimeter will be provided on the aircraft and may be used as a back-up for NAVSAT equipment failure or for temporary measurements during the period a satellite goes out of view and a new one is being acquired.

There are various models of these nine INS plant states available for implementation. The Pinson error model was selected as it was the model used in the SAMUS and profile generating computer programs which will be explained in a later chapter. A derivation of the Pinson error model is given in Chapter 4 of Reference 9. This model, which makes up the F_{11} matrix is shown in Figure 7.

Error Source Models

The error propagation equations given in Chapter IV were developed under the assumption that the system disturbances ($\underline{u}(t)$) are not correlated in time. The estimation of disturbances which have significant time correlation is done by means of "state vector augmentation."

	1	2	3	4	5	6	7	8	9
1	0	0	0	1	0	0	0	0	0
2	0	0	0	0	1	0	0	0	0
3	0	0	0	0	0	1	0	0	0
4	$\frac{A_z}{R} - \omega_s^2 + \omega^2 - \Omega^2 - (\omega_x + \Omega_x)\rho_x$	$\dot{\rho}_z - (\omega_y + \Omega_y)\rho_x$	$-\dot{\rho}_y - (\omega_z + \Omega_z)\rho_x$	0	$2\omega_z$	$-2\omega_y$	0	$-A_z$	A_y
5	$-\dot{\rho}_z - (\omega_x + \Omega_x)\rho_y$	$\frac{A_z}{R} - \omega^2 + \omega^2 - \Omega^2 - (\omega_y + \Omega_y)\rho_y$	$\dot{\rho}_x - (\omega_z + \Omega_z)\rho_y$	$-2\omega_z$	0	$2\omega_x$	A_z	0	$-A_x$
6	$\rho_y - \frac{A_x}{R} - (\omega_x + \Omega_x)\rho_z$	$-\dot{\rho}_x - \frac{A_y}{R} - (\omega_y + \Omega_y)\rho_z$	$\omega^2 - \Omega^2 + 2\omega_s^2 - (\omega_z + \Omega_z)\rho_z$	$2\omega_y$	$-2\omega_x$	0	$-A_y$	A_x	0
7	$-\frac{\omega_z}{R}$	0	0	0	$\frac{1}{R}$	0	0	ω_z	$-\omega_y$
8	0	$-\frac{\omega_z}{R}$	0	$\frac{1}{R}$	0	0	$-\omega_z$	0	ω_x
9	$\frac{\omega_x}{R}$	$\frac{\omega_y}{R}$	0	0	0	0	ω_y	$-\omega_x$	0

Figure 7. F_{11} Matrix (Pinson Error Model)

That is, the dimension of the system state vector in increased by including the correlated disturbances as well as descriptions of their dynamic behavior in the appropriate rows of an enlarged F matrix. Because these quantities are random, their behavior cannot be described deterministically. Instead, they are modeled as state variables of a fictitious linear dynamic system which is excited or driven by white noise. This model serves two purposes; it provides proper autocorrelation characteristics through specification of the linear system and strength of the driving noise, and the random nature of the signal follows from the random excitation.

The correlated system disturbances utilized in this study are each modeled by a combination of one or more of the several types of basic error models described in Figure 8.

Specification of the block diagram models of these error sources implies the structure of the F and Q' matrices.

The random constant or bias is a non-dynamic quantity meant to model a constant of unknown amplitude. It is simulated as the output of an integrator which has no input but has a random initial condition. Its constant nature is indicated by the fact that the corresponding rows of the F and Q' matrices contain only zeros.

Random walk, which derives its name from an illustration involving a man who takes fixed-length steps in arbitrary directions, is simulated by passing white noise through an integrator. In this case, the row of the augmented F matrix contains only zeros. However, the corresponding row and column of Q' is nonzero, the element at their intersection is q.

Random errors which exhibit a definite time-growing behavior may be described by the random ramp or the random parabola (which is formed

Type of Error Source	State Differential Equations	Block Diagram
Random Constant (Bias)	$\dot{x} = 0$	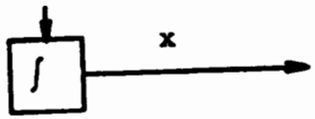
Random Walk	$\dot{x} = u$	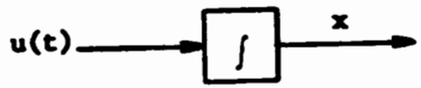
Expotentially Correlated Random Variable	$\dot{x} = -\beta x + u$	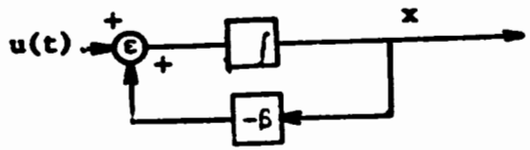
Random Ramp	$\dot{x}_1 = x_2$ $\dot{x}_2 = 0$	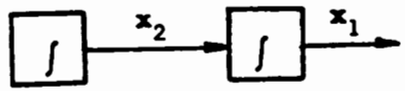
Random Parabola	$\dot{x}_1 = x_2$ $\dot{x}_2 = x_3$ $\dot{x}_3 = 0$	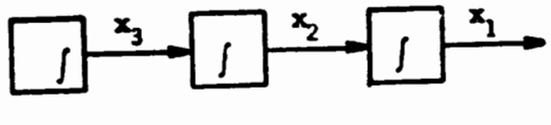

Fig. 8. Error Source Models for Random Variables

by adding a long-term stability state to the random ramp). These models will introduce non-zero elements into the F matrix, and when driven by white noise, into the Q' matrix.

The expotentially correlated random variable whose autocorrelation function is a decreasing expotential, provides a reasonable approximation for a band-limited signal whose spectral density is approximately flat for a finite bandwidth. This type of random variable introduces a single non-zero diagonal element $-\beta$ into the F matrix.

$$\beta = \frac{1}{\tau} \tag{80}$$

where τ = correlation time constant of the expotentially decaying function.

If the value of the corresponding element in the initial covariance matrix P(0) is specified, then the noise value required to drive the fictitious linear system for computer simulation is determined as follows. Since q is constant, in steady state $\dot{p} = 0$ so that from the linear variance equation

$$0 = FP + PF^T + Q' \tag{81}$$

or, in the scalar case

$$0 = -\beta p - p\beta + q \tag{82}$$

$$q = 2\beta p \tag{83}$$

Therefore, the expotentially correlated random variable requires a diagonal element in Q' whose value is two times the initial covariance value divided by the correlation time (Ref 5:3-36 thru 3-49).

INS Error Source Models. Through extensive testing and detailed knowledge of sensor dynamics many imperfections and errors of inertial navigation systems are removed by careful design. But when all the tests

for predictable errors and the ingenious design tricks have been exhausted, there still remain errors whose source defies compensation. The statistical behavior of these sensor errors can be obtained through testing and fitting curves to laboratory experimental data. The error models chosen for the gyros and the accelerometers are typical of an INS in the one to two nautical miles per hour class. They are both modeled as linear combinations of a random bias and an expotentially correlated random variable excited by white noise. Note that this requires two states for the x direction gyro drift and two states for the x direction accelerometer error, and similarly for the y and z directions. Therefore, modeling of the INS driving errors requires 12 additional states in the system error state vector. Block diagrams and corresponding elements of the F and Q' matrices are as follows.

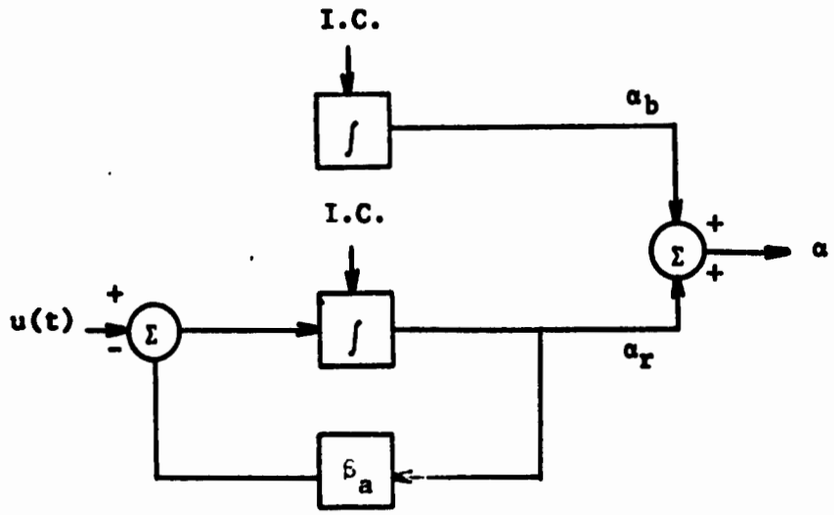

Fig. 9. Accelerometer Error Source Model

The F and Q' matrix terms are

$$F_{22} = \begin{array}{c} \\ 10 \\ 11 \\ 12 \\ 13\text{-}15 \end{array} \begin{array}{c} \begin{array}{ccc} 10 & 11 & 12 \end{array} \quad \begin{array}{c} 13\text{-}15 \end{array} \\ \left[\begin{array}{ccc|c} -\beta_a & 0 & 0 & \\ 0 & -\beta_a & 0 & 0 \\ 0 & 0 & -\beta_a & \\ \hline & 0 & & 0 \end{array}\right] \end{array} \tag{84}$$

$$F_{12} = \begin{array}{c} \\ 1\text{-}3 \\ 4 \\ 5 \\ 6 \\ 7\text{-}9 \end{array} \begin{array}{c} \begin{array}{ccc} 10 & 11 & 12 \end{array} \quad \begin{array}{c} 13\text{-}15 \end{array} \\ \left[\begin{array}{ccc|ccc} & 0 & & & 0 & \\ \hline 1 & 0 & 0 & 1 & 0 & 0 \\ 0 & 1 & 0 & 0 & 1 & 0 \\ 0 & 0 & 1 & 0 & 0 & 1 \\ \hline & 0 & & & 0 & \end{array}\right] \end{array} \tag{85}$$

$$q_{10} = 2\beta_a P_{10} \tag{86}$$

$$q_{10} = 2(1/600 \text{ sec})](20 \times 10^{-6} g)(32.2 \text{ ft/sec}^2\text{-g})]^2 \tag{87}$$

$$q_{10} = 1.382 \times 10^{-9} \text{ ft}^2/\text{sec}^5 \tag{88}$$

Similarly,

$$q_{11} = q_{12} = q_{10} \tag{89}$$

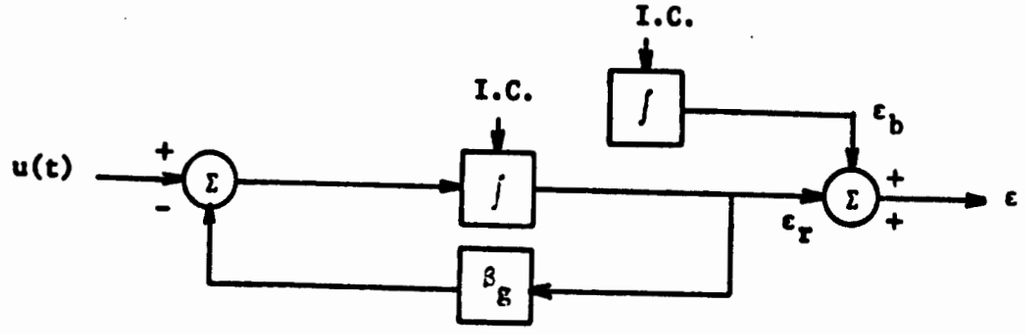

Fig. 10. Gyro Error Source Model

The F and Q' matrix terms are as follows

$$F_{33} = \begin{array}{c} \\ 16 \\ 17 \\ 18 \\ 19\text{-}21 \end{array} \begin{array}{c} \begin{array}{cccc} 16 & 17 & 18 & 19\text{-}21 \end{array} \\ \left[\begin{array}{cccc} -\beta_g & 0 & 0 & \\ 0 & -\beta_g & 0 & 0 \\ 0 & 0 & -\beta_g & \\ & 0 & & 0 \end{array}\right] \end{array} \tag{90}$$

$$F_{13} = \begin{array}{c} \\ 1\text{-}3 \\ 4\text{-}6 \\ 7 \\ 8 \\ 9 \end{array} \begin{array}{c} \begin{array}{cccccc} 16 & 17 & 18 & 19 & 20 & 21 \end{array} \\ \left[\begin{array}{cccccc} & 0 & & & 0 & \\ & 0 & & & 0 & \\ 1 & 0 & 0 & 1 & 0 & 0 \\ 0 & 1 & 0 & 0 & 1 & 0 \\ 0 & 0 & 1 & 0 & 0 & 1 \end{array}\right] \end{array} \tag{91}$$

$$q_{16} = 2\beta_g P_{16} \tag{92}$$

$$q_{16} = 2(1/3600 \text{ sec})](.012 \text{ deg/hr})(4.848 \times 10^{-6} \frac{\text{rad/sec}}{\text{deg/hr}})]^2 \tag{93}$$

$$q_{16} = 1.880 \times 10^{-18} \text{ rad}^2/\text{sec}^3 \tag{94}$$

Similarly,

$$q_{17} = q_{18} = q_{16} \tag{95}$$

Note that the accelerometer error sources are additive to the Δx, Δy, and Δz plant state differential equations requiring the non-zero terms of the F_{12} matrix. Similarly, the gyro error sources are additive to the differential equations of the plant attitude error states ϕ_x, ϕ_y, and ψ_z requiring the non-zero terms of the F_{13} matrix.

NAVSAT Error Sources. Modeling of the navigation satellite error

sources requires extensive testing, compiling of empirical data, and curve fitting. The error source models selected for this design study are a modified version of those found in Reference 1 and include: one user clock, four satellite clocks, and four range biases (one per satellite).

In operation, the range measuring process would be initialized by synchronizing the user's clock (i.e., oscillator) with the clock signal received from the satellite at some arbitrary starting time. Range increments would then be measured by counting incremental phase shift between satellite and user clocks as the vehicle moves. If either clock drifts, however, erroneous incremental phase shifts will be measured. During the tracking process the satellite clocks are in effect synchronized to the master tracking station clock by estimating the satellite clock drift model coefficients. These coefficients are to be updated every hour and relayed via the satellite user link to the user for use in correcting raw incremental range measurements. Thus the satellite clock error is a function of the accuracy of the drift model coefficient estimates (Ref 1:2-14 thru 2-18).

Reference 1 suggests the following model for both the user clock and the four satellite clocks. Note that although the structure of the user and satellite clock models are the same, the user clock initial errors are orders of magnitude greater than those of the satellite clock because of the greater accuracy of the periodically updated satellite clocks.

The mathematical equation representing the clock error is:

$$\delta T = C_o + C_1 t + C_2 t^2 + \varepsilon(t) \qquad (96)$$

where

$$\ddot{\varepsilon}(t) + \beta\dot{\varepsilon} = u(t) \tag{97}$$

$$E[u(t)] = 0 \tag{98}$$

$$E[u^2(t)] = 2\beta E\{[\dot{\varepsilon}(t)]^2\} \tag{99}$$

The block diagram of the fictitious linear system simulating this mathematical equation is given in Figure 11.

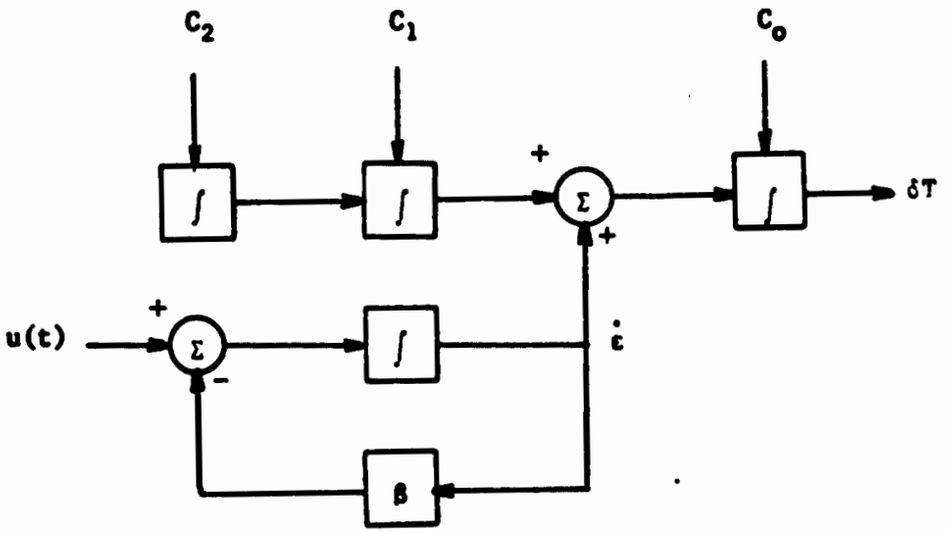

Fig. 11. Clock Error Model

The values suggested for the satellite clock error coefficients (C_o, C_1, C_2, $\dot{\varepsilon}$) are classified; arbitrary numbers selected for the design are given as initial conditions in Table IV.

The contributions to the system F and Q' matrices by the satellite clocks are then

$$F_{55} = \begin{array}{c|cccc|cccc|cccc|cccc|} & \multicolumn{4}{c|}{25-28} & \multicolumn{4}{c|}{29-32} & \multicolumn{4}{c|}{33-36} & \multicolumn{4}{c|}{37-40} \\ \hline 25-28 & 0 & 1 & 0 & 1 & & & & & & & & & & & & \\ & 0 & 0 & 1 & 0 & & & & & & & & & & & & \\ & 0 & 0 & 0 & 0 & & 0 & & & & 0 & & & & 0 & & \\ & 0 & 0 & 0 & -\beta_s & & & & & & & & & & & & \\ \hline 29-32 & & & & & 0 & 1 & 0 & 1 & & & & & & & & \\ & & 0 & & & 0 & 0 & 1 & 0 & & 0 & & & & 0 & & \\ & & & & & 0 & 0 & 0 & 0 & & & & & & & & \\ & & & & & 0 & 0 & 0 & -\beta_s & & & & & & & & \\ \hline 33-36 & & & & & & & & & 0 & 1 & 0 & 1 & & & & \\ & & 0 & & & & 0 & & & 0 & 0 & 1 & 0 & & 0 & & \\ & & & & & & & & & 0 & 0 & 0 & 0 & & & & \\ & & & & & & & & & 0 & 0 & 0 & -\beta_s & & & & \\ \hline 37-40 & & & & & & & & & & & & & 0 & 1 & 0 & 1 \\ & & 0 & & & & 0 & & & & 0 & & & 0 & 0 & 1 & 0 \\ & & & & & & & & & & & & & 0 & 0 & 0 & 0 \\ & & & & & & & & & & & & & 0 & 0 & 0 & -\beta_s \end{array} \quad (100)$$

$$q_{25} = 2\beta_s P_{25} \quad (101)$$

$$q_{25} = 2(1/10000 \text{ sec})(1 \times 10^{-3} \text{ ft/sec})^2 \quad (102)$$

$$q_{25} = 2 \times 10^{-10} \text{ ft}^2/\text{sec}^3 \quad (103)$$

Similarly,

$$q_{29} = q_{33} = q_{37} = q_{25} \quad (104)$$

The suggested user clock error coefficients are given in Table V.

Table V

Suggested User Clock Error Coefficients

Error Coefficients	RMS Value	Correlation Time
C_o	10000 ft	-
C_1	5 ft/sec	-
C_2	5×10^{-6} ft/sec^2	-
$\dot{\epsilon}$	2.5 ft/sec	.02 sec

These numbers are typical of a good quality, temperature controlled quartz crystal oscillator suitable for airborn application. These values are much higher than the satellites' but will be greatly reduced by the inherent calibration process of the INI Kalman filter. Random drift of the user clock is caused predominantly by the acceleration sensitivity of the crystal which responds to aircraft vibrations. The short correlation time of this process is due to the relatively wideband nature of the aircraft vibration spectrum (Ref 1:2-17 thru 2-18).

However, the correlation time of the $\dot{\epsilon}$ state variable in the user clock is so short in comparison to the numerical integration step size used in this simulation that a modification is necessary. The short correlation time and hence the wideband nature of this random variable may easily be approximated as a white noise input. Thus, the user clock error model used in this study is given in Figure 12.

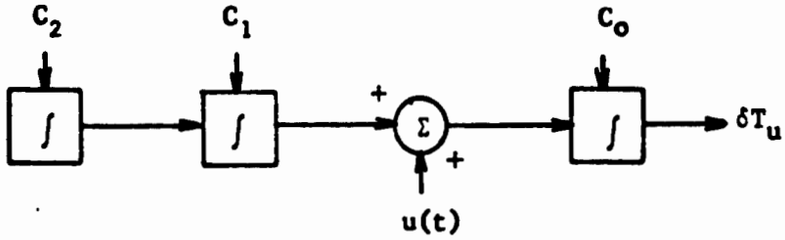

Fig. 12. Simplified User Clock Error Model for System

The suggested values for C_o, C_1, and C_2 are used; the initial RMS value of the covariance on the white noise input u(t) is assumed to be 6.25 ft/sec.

Thus,

$$F_{44} = \begin{array}{c} \\ 22 \\ 23 \\ 24 \end{array} \begin{array}{c} \begin{array}{ccc} 22 & 23 & 24 \end{array} \\ \begin{bmatrix} 0 & 1 & 0 \\ \cdot & \cdot & 1 \\ 0 & 0 & 0 \end{bmatrix} \end{array} \qquad (105)$$

and

$$q_{22} = 6.25 \text{ ft}^2/\text{sec} \tag{106}$$

When the satellite signal passes through the ionosphere, the signal is bent or refracted. Thus, the signal path is not a perfectly straight line but has a slight amount of curvature to it.

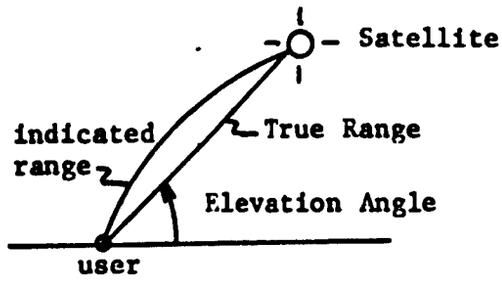

Fig. 13. Ionospheric Delay

This increase in signal path length due to unpredictable ionospheric delay is on the order of 15 to 25 feet depending upon the angle of elevation of the satellite with respect to the user. A detailed error source model for this ionospheric delay as applied to a set of synchronous satellites is given in Reference 1. However, it is felt that this particular model is not applicable to the non-synchronous satellite case. As mentioned in Chapter III the errors due to ionospheric delay will be assumed included in the phase/range satellite clock errors for the purpose of this report. An area for future study would be the synthesis of an accurate error source model for this ionospheric delay in the utilization of non-synchronous satellites.

The final error sources used in the system model are the range biases. These are modeled simply as arbitrary initial conditions on integrators and account for the effect of tropospheric delay and uncertainty in the speed of light. The cumulative magnitude of these two

error sources is on the order of 10 feet. This requires four additional state variables (one for each satellite) in the system state vector but adds no additional nonzero terms to the F or Q' matrices.

System Measurement Equation

The measurement equation consists of a set of four range divergence equations as derived in Chapter III (Equation 33). Three of these are needed to reduce the position error and the fourth is required to synchronize the user clock. This study is concerned with using only range measurements in the filter design. Incorporating an altimeter would require an additional measurement. If range-rate measurements were taken, four more equations would be required.

The system measurement equation is

$$\underline{z}_s = H_s \underline{x}_s + \underline{v}_s \tag{107}$$

where the 44 variables of $\underline{x}_s$ are listed in Table IV and

$$\underline{z}_s = \begin{bmatrix} \Delta r_1 \\ \Delta r_2 \\ \Delta r_3 \\ \Delta r_4 \end{bmatrix} \tag{108}$$

H_s is the 4 by 44 matrix shown in Figure 14. The white Gaussian noise vector $\underline{v}_s$ is described by the covariance matrix R_s where

$$R_s = \begin{bmatrix} \sigma_r^2 & 0 & 0 & 0 \\ 0 & \sigma_r^2 & 0 & 0 \\ 0 & 0 & \sigma_r^2 & 0 \\ 0 & 0 & 0 & \sigma_r^2 \end{bmatrix} \tag{109}$$

	1	2	3	4–21	22	23–24	25	26–28	29	30–32	33	34–36	37	38–40	41	42	43	44
1	i_{rx1}	i_{ry1}	i_{rz1}	0	1	0	-1	0	0	0	0	0	0	0	1	0	0	0
2	i_{rx2}	i_{ry2}	i_{rz2}	0	1	0	0	0	-1	0	0	0	0	0	0	1	0	0
3	[illegible]	i_{ry3}	i_{rz3}	0	1	0	0	0	0	0	-1	0	0	0	0	0	1	0
4	i_{rx4}	i_{ry4}	i_{rz4}	0	1	0	0	0	0	0	0	0	-1	0	0	0	0	1

Fig. 14. System Measurement Matrix H

The value σ_r is a measure of the white noise corrupting the high frequency satellite signal and a typical value of σ_r = 10 feet is used in this design.

VI. Filter Designs

This chapter discusses a few of the various Kalman filter designs which were simulated using the 44 state reference system of Chapter V. Not all of the filter designs which were analyzed are presented; only those which were significant and illustrate important design differences are outlined. These include: (1) the 44 state optimal filter, (2) a fully-coupled 15 state filter, (3) a 15 state filter with all weak coupling terms removed from the INS error model, and (4) a ten state filter illustrating degraded performance caused by eliminating too many states from the filter.

Selection of the "best" Kalman filter design involves a trade-off study between desired accuracy and the computational time required by an onboard computer. Obviously, the most accurate filter is the optimal 44 state filter; however, the burden this would place on the computer is unacceptable. On the other hand, the ten state filter would substantially reduce the computational time but yields unacceptable accuracy. Therefore, the procedure of this study was to successively eliminate a few states at a time from the filter state vector and simulate each of these reduced-order or suboptimal filter designs on the computer. So long as the accuracy of the filter performance was degraded only slightly in each step, this process was continued until a minimum acceptable filter state vector dimension was reached.

The Optimal Filter

The optimal filter is simply an exact replica of the system model (i.e., the same 44 state system and measurement model as given in Chapter V). This Kalman filter computes the optimal gains or weighting

coefficients from the filter design and applies them to the system. In the optimal filter, the values of the state variables for which these weighting coefficients are computed are identical to the state variable values to which the weighting coefficients are applied (the system model is theoretically assumed to be exact). This optimal 44 state filter will yield the most accurate performance possible for the given set of system state and measurement equations.

Plots of the RMS values of the nine plant state (position, velocity, and attitude) error covariances for the optimal filter are shown in Figures 15 through 23. These plots provide the basis against which all sub-optimal filter performance will be compared. Note that the time of flight is one hour (3600 seconds) for these and all plots in this report. Also, the vertical axes are automatically scaled in the computer plotting routine and may vary from one case to the next. For example, the optimal filter z-RMS velocity error is scaled from 0.14 ft/sec to 0.78 ft/sec, whereas the plot of this same variable for the 15 state filter presented later in this chapter is scaled from 0.32 ft/sec to 0.96 ft/sec.

Fully-Coupled 15 State Filter

The 44 state optimal filter was gradually reduced by eliminating the least significant variables of the state vector. No serious degradation of performance was noted as this state vector was reduced to the 15 state model. However, filter designs of lower dimension did diverge significantly, one example of this is given in the final section of this chapter. The intermediate designs between the 44 state optimal and the 15 state sub-optimal filter showed very little variation in performance. In fact, the increased accuracy provided by retention of

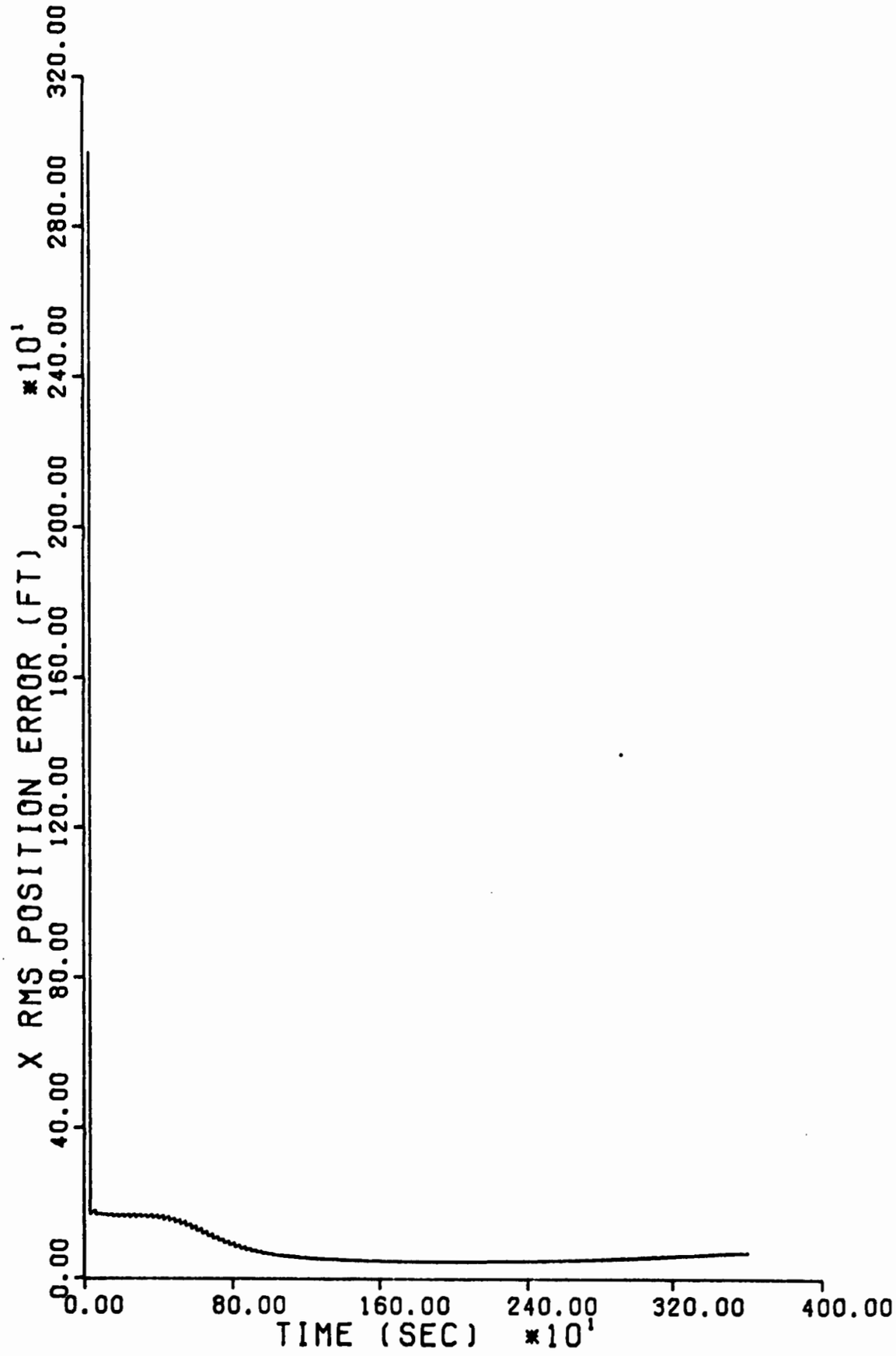

Fig. 15. Optimal Filter, x Position Error

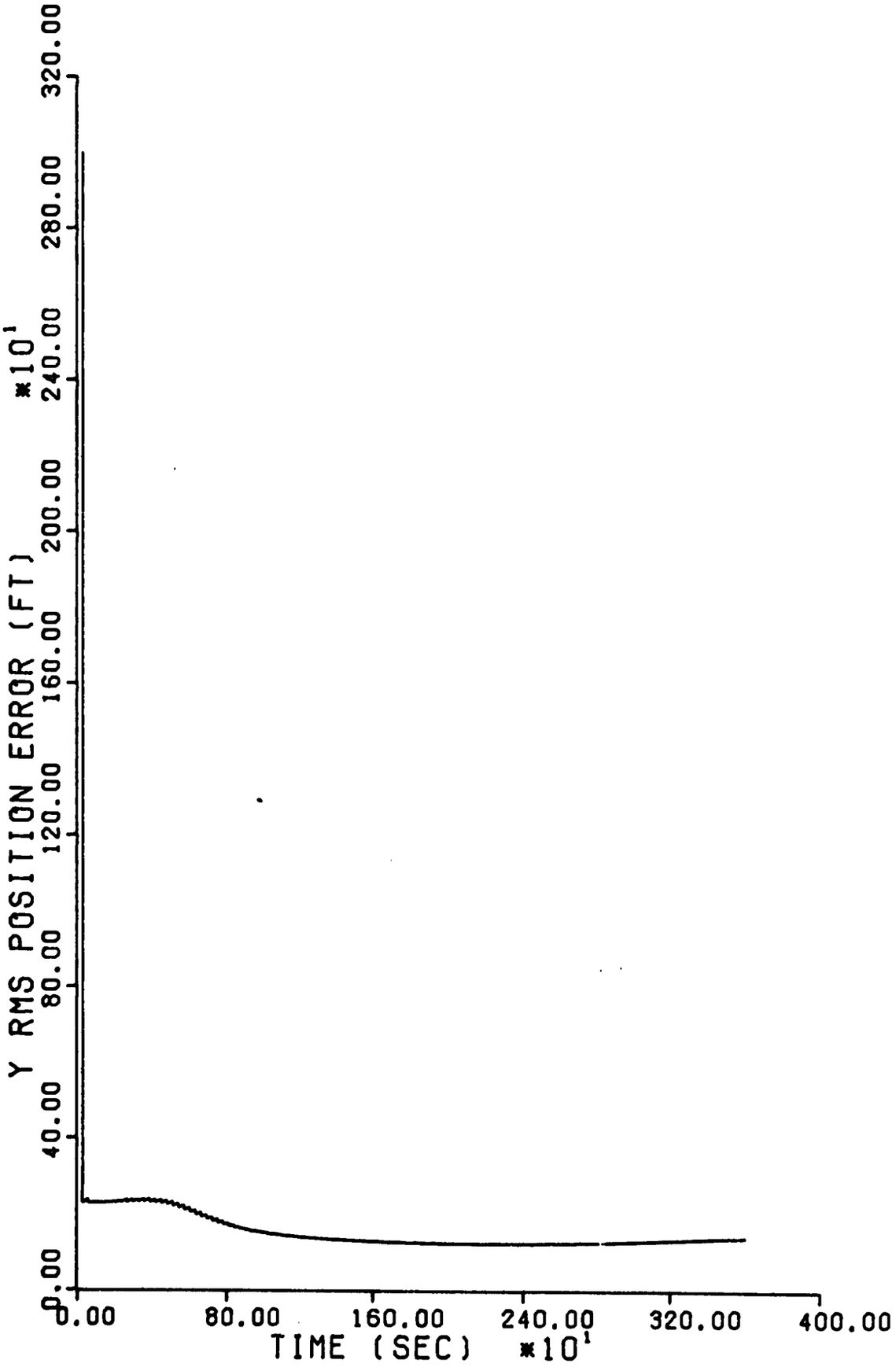

Fig. 16. Optimal Filter, y Position Error

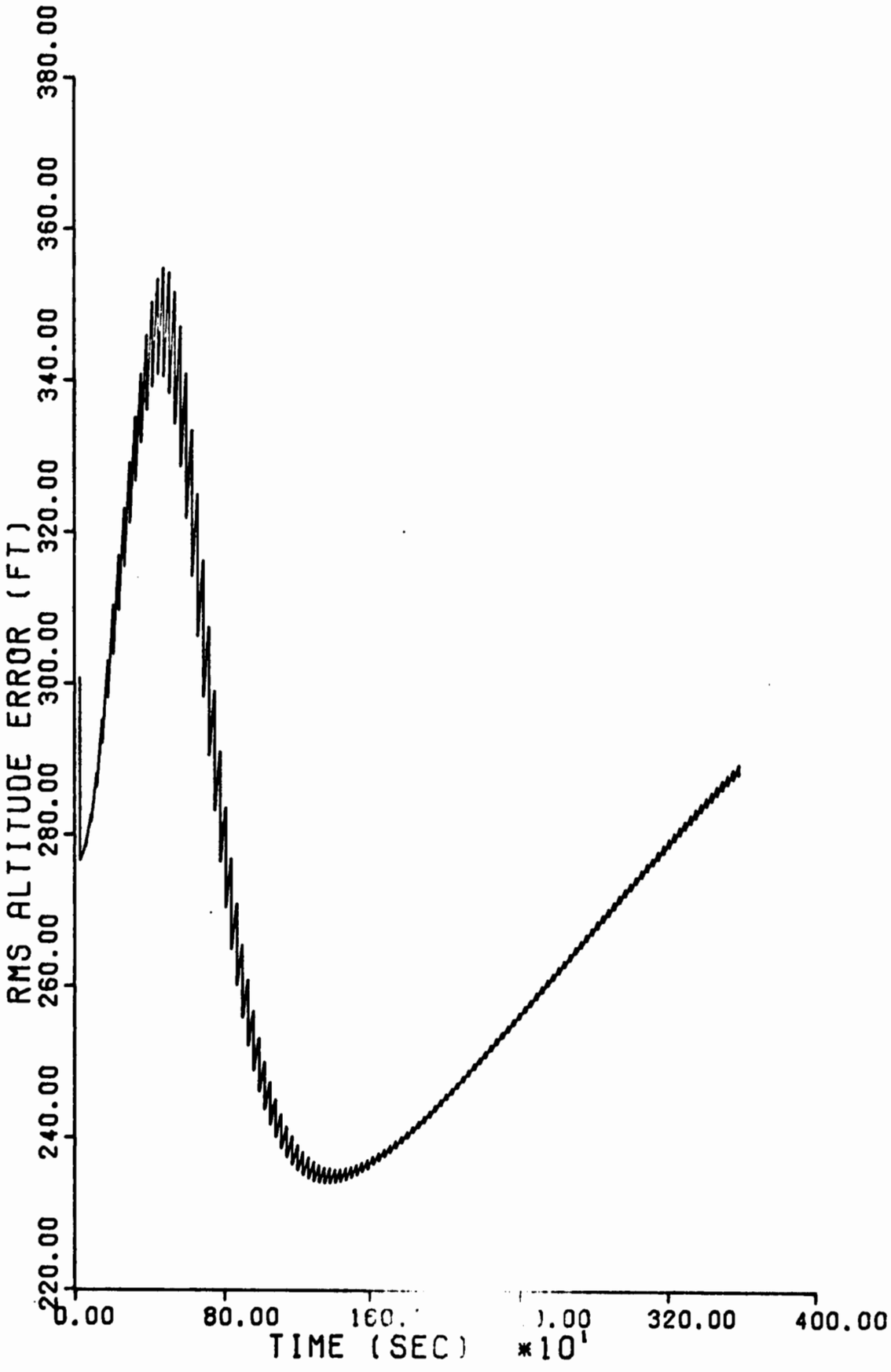

Fig. 17. Optimal Filter, Altitude Error

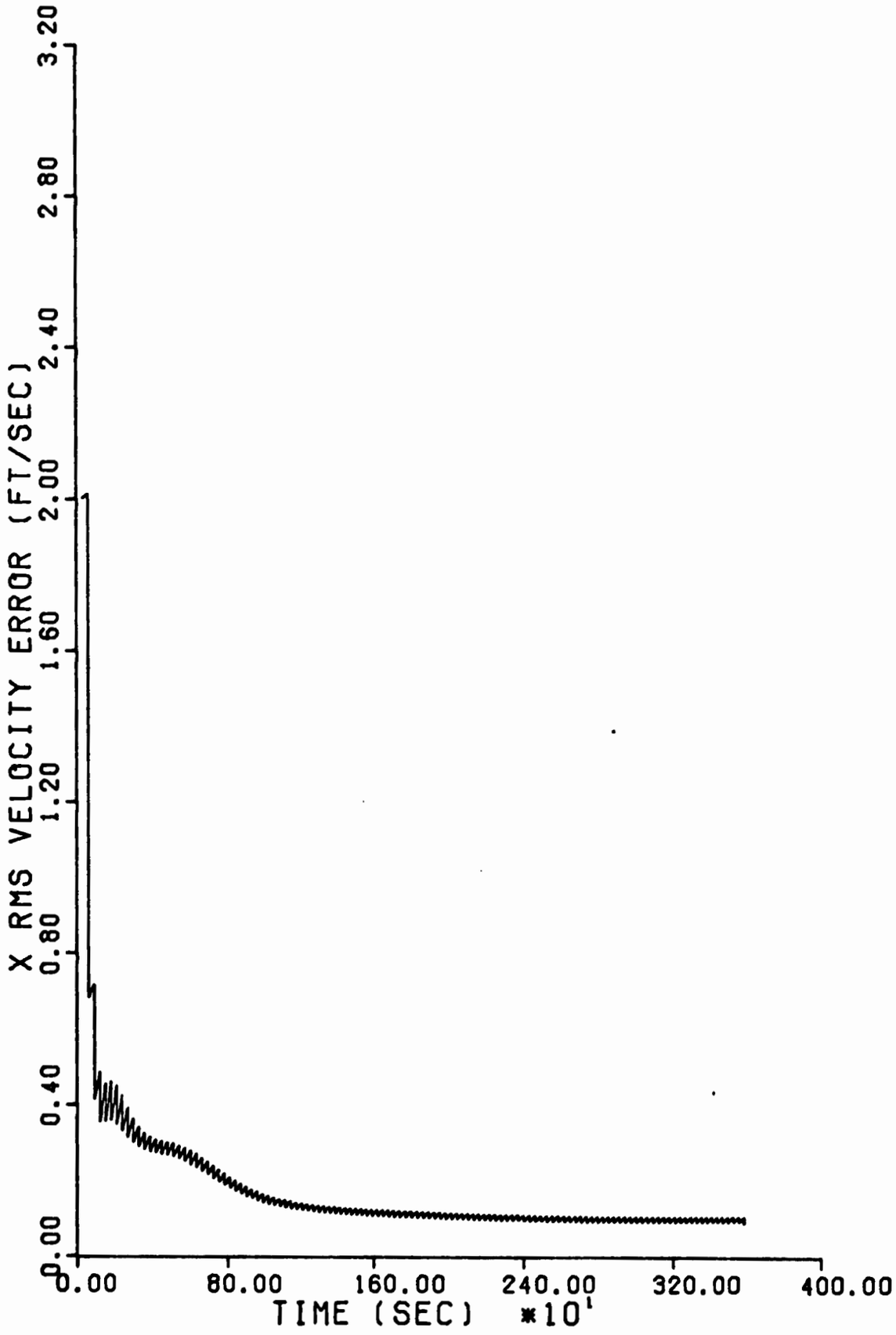

Fig. 18. Optimal Filter, x Velocity Error

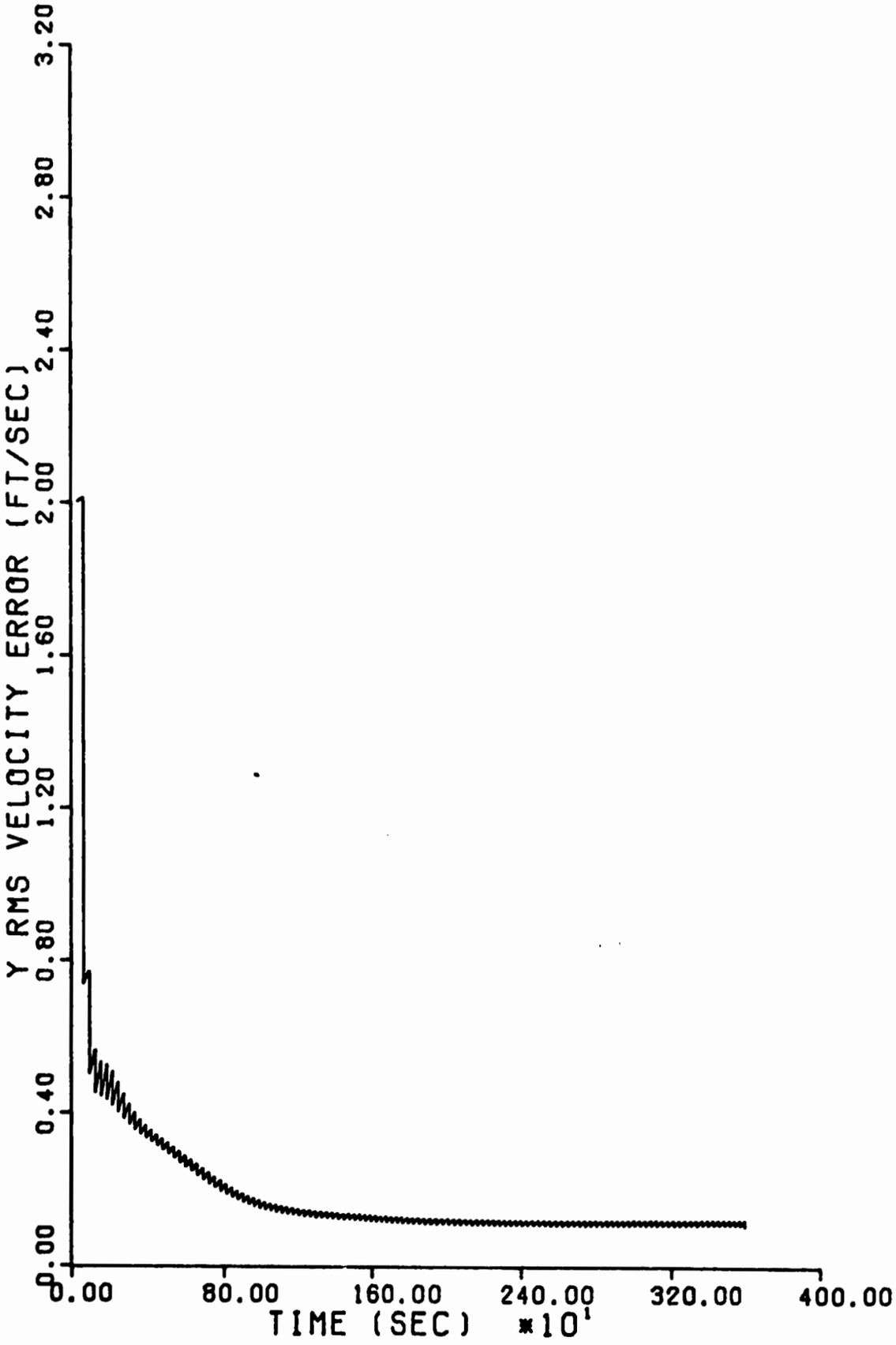

Fig. 19. Optimal Filter, y Velocity Error

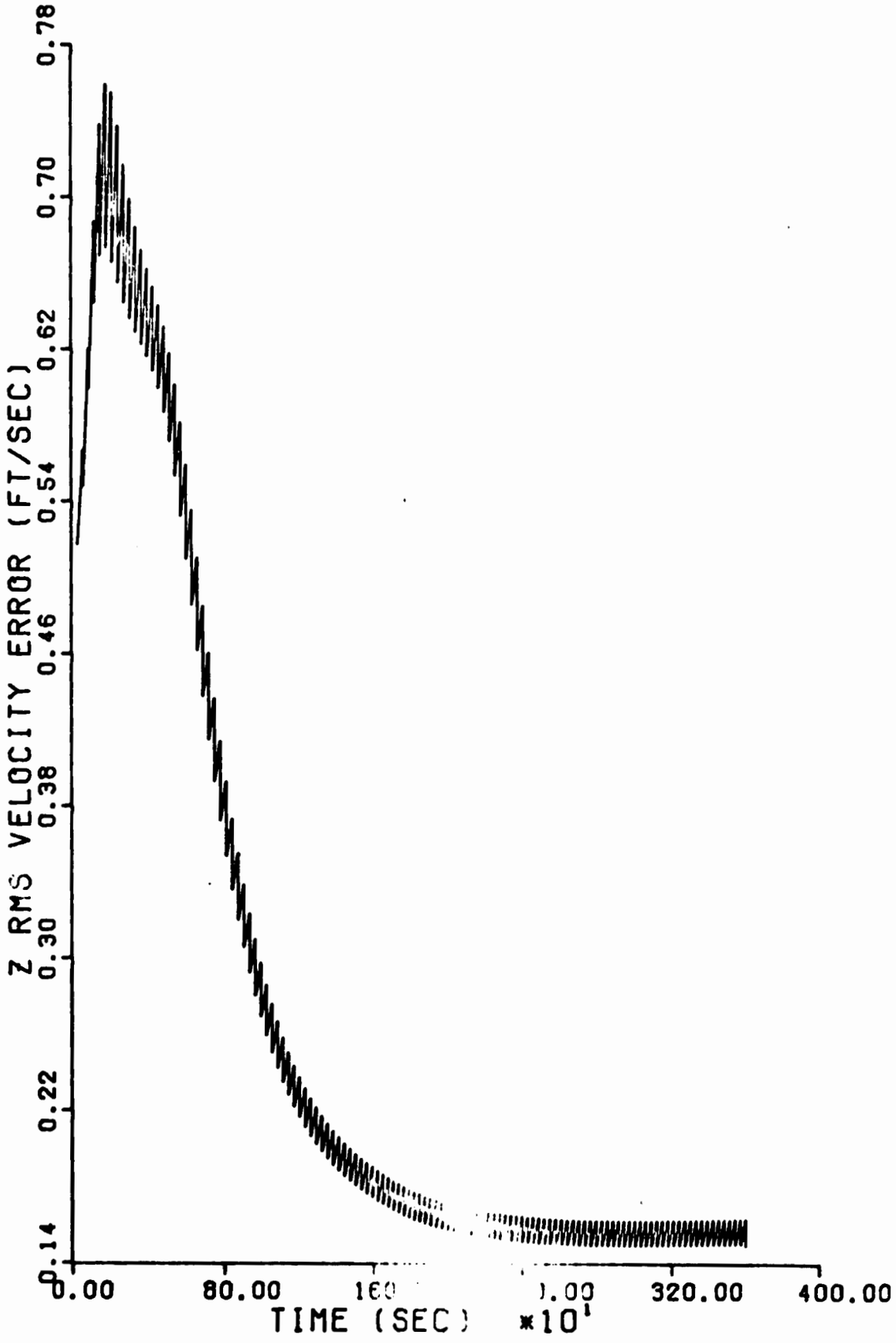

Fig. 20. Optimal Filter, z Velocity Error

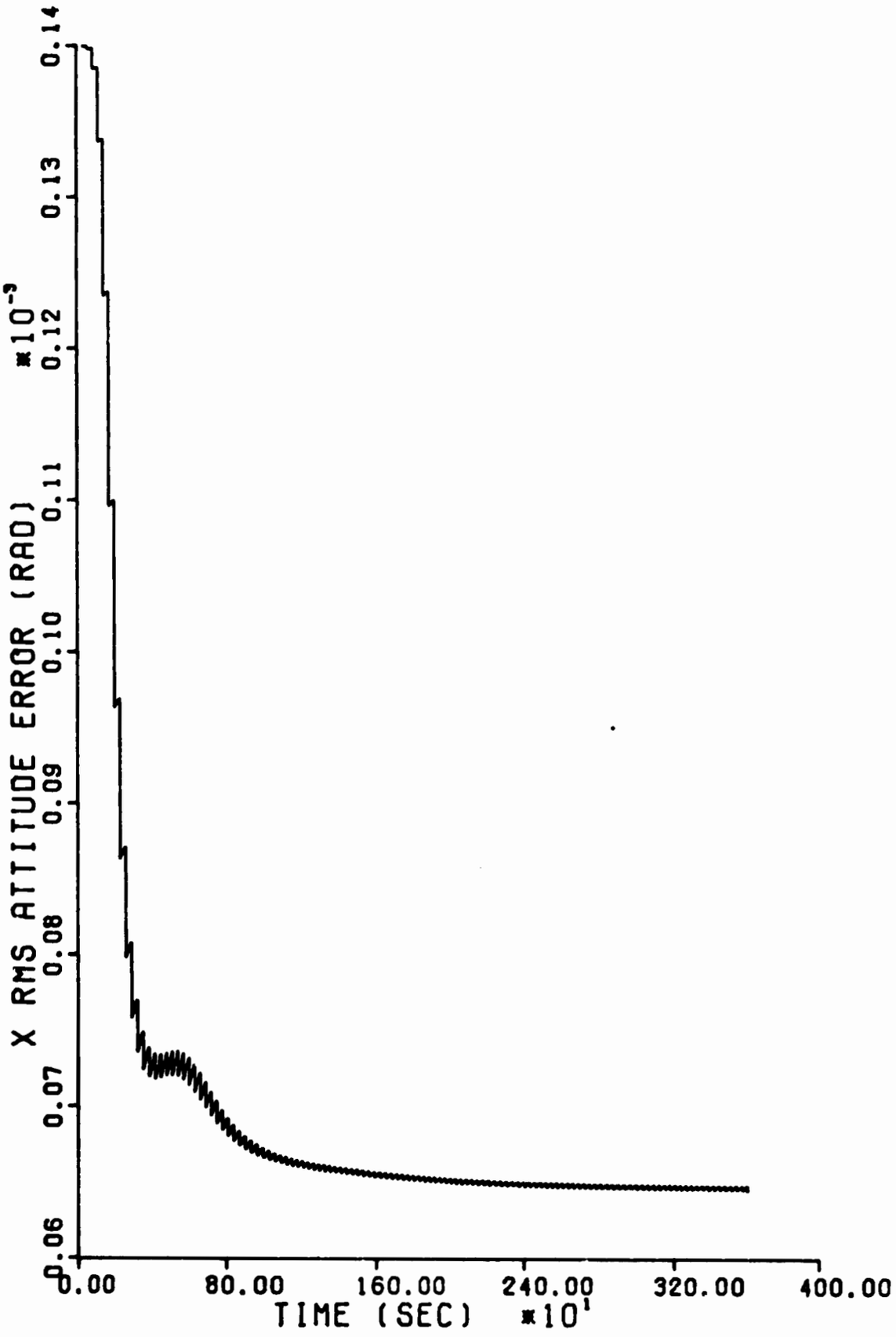

Fig. 21. Optimal Filter, x Attitude Error

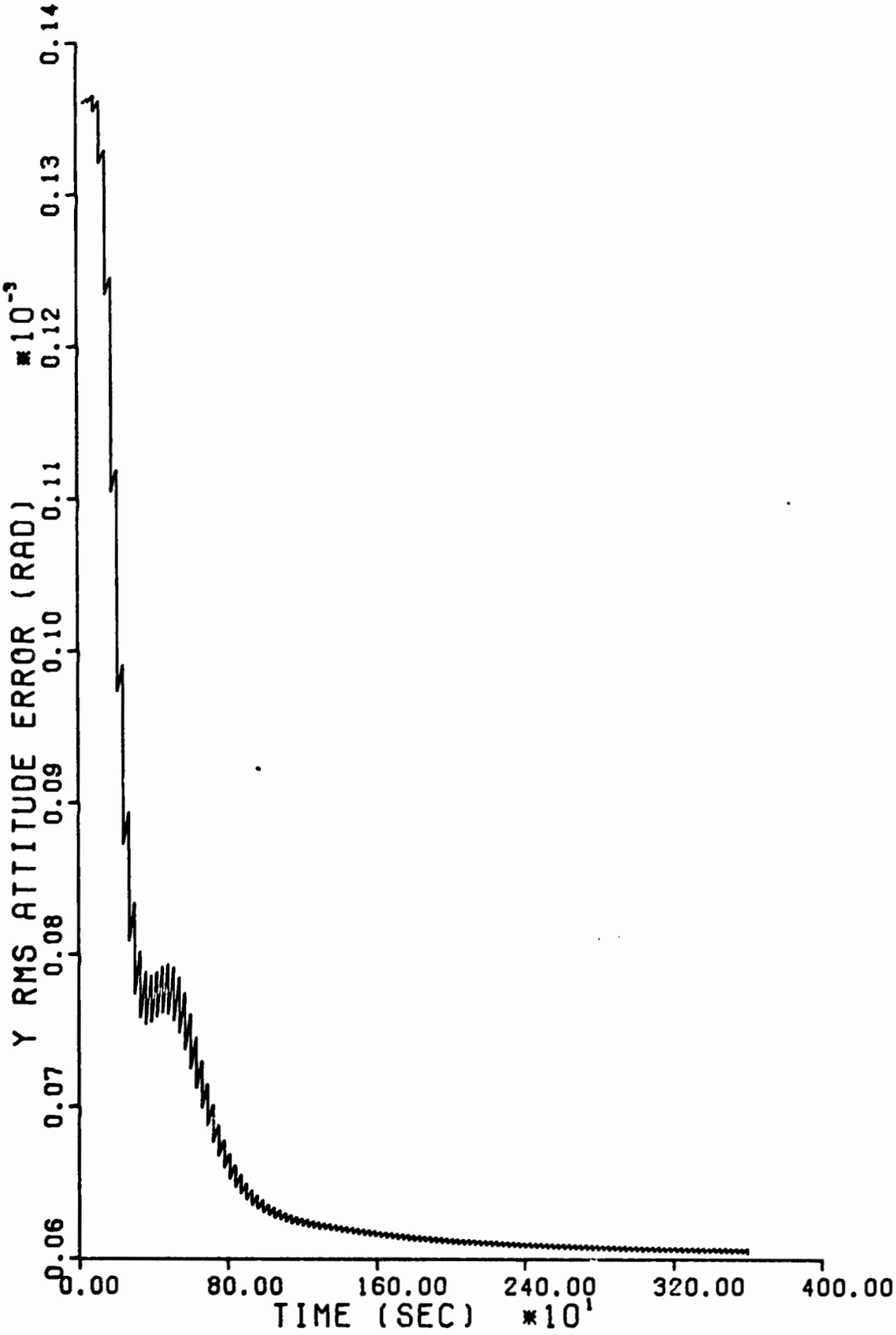

Fig. 22. Optimal Filter, y Attitude Error

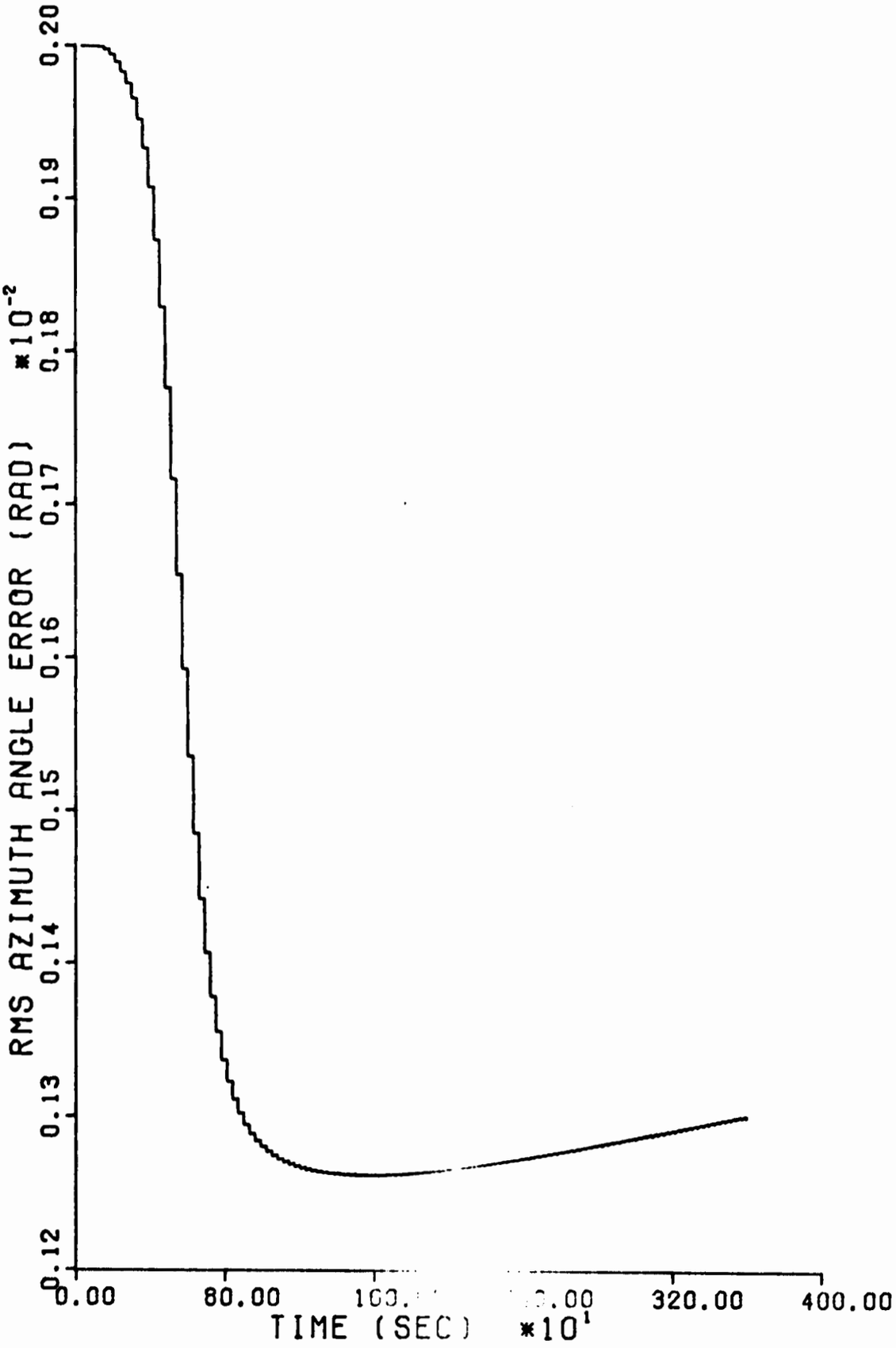

Fig. 23. Optimal Filter, Azimuth Error

any of the state variables in addition to the 15 selected is so slight that it is felt filter designs of higher dimension are unwarranted (except for the addition of one or two states when an altimeter is incorporated in the system). Filter designs whose state variable vectors were of lower dimension than this 15 state design exhibited significantly degraded accuracy in performance and are not recommended.

All sub-optimal filter designs presented in this report contain a model of the INS error states (position, velocity, attitude). These states are required to propagate the prediction of the predictor-corrector behavior of the filter. These INS plant error states comprise the first nine variables of the filter state vector which is shown in Table VI.

The INS error source models (gyro drift and accelerometer errors) required 12 state variables in the system model. These can be reduced to six state variables by approximating the linear combination of a random bias and an expotentially correlated random variable as a random walk (Ref 12:11-14 thru 11-16). However, <u>all</u> of the above 12 state variables can be eliminated from the filter design by approximating these error sources as white Gaussian noise on the plant states. The accelerometer error sources are modeled as equivalent driving white noises on the velocity error differential equations and the gyro error sources are modeled as equivalent white noise inputs on the attitude error differential equations.

These equivalent white noises are calculated as q_I^* values which provide approximately the same amount of RMS error build-up over the given interval of time (3600 sec) as the system error sources which have been discarded in the filter design. This may be done with little

Table VI

Filter 15 State Vector Definition

Error State	Symbol	Definition	RMS Initial Condition
		INS Plant Error States	
1	Δx	x position error	3000 ft
2	Δy	y position error	3000 ft
3	Δz	z position (altitude)	300 ft
4	$\Delta \dot{x}$	x velocity error	2.0 ft/sec
5	$\Delta \dot{y}$	y velocity error	2.0 ft/sec
6	$\Delta \dot{z}$	z velocity error	0.5 ft/sec
7	ϕx	x attitude error	0.14 millirad
8	ϕy	y attitude error	0.14 millirad
9	ψz	z attitude (heading) error	2.0 millirad
		Satellite and User Clock Errors	
10	δT_u	user clock phase/range error	10,000 ft
11	x_{11}	user clock frequency offset	5 ft/sec
12	δT_{s1}	sat. clock #1 phase/range error	100 ft
13	δT_{s2}	sat. clock #2 phase/range error	100 ft
14	δT_{s3}	sat. clock #3 phase/range error	100 ft
15	δT_{s4}	sat. clock #4 phase/range error	100 ft

loss in performance so long as the measurement sample frequency is high compared with dominant system time constants (Ref 1:4-3 thru 4-4). This requires six diagonal elements in the filter Q' matrix corresponding to these equivalent white noise inputs. The general equation used to calculate these q_i^* values is

$$q_i^* = \frac{2\sigma_{bi}^2}{\beta_i} = 2\sigma_{bi}^2\tau_i \tag{110}$$

where σ_{bi}^2 is the initial covariance of the corresponding system bias error source and β_i and τ_i are the inverse correlation time and correlation time, respectively, of the corresponding system expotentially correlated error source. The three equivalent noises on the velocity error differential equations are

$$q_4^* = 2\sigma_{\alpha bx}^2\tau_{\alpha rx} \tag{111}$$

$$q_4^* = (2)[(66 \times 10^{-6}\ g)(32.2\ ft/sec^2\text{-}g)]^2(600\ sec) \tag{112}$$

$$q_4^* = 5.411 \times 10^{-3}\ ft^2/sec^3 \tag{113}$$

Similarly,

$$q_5^* = q_4^* \tag{114}$$

$$q_6^* = 2.164 \times 10^{-2}\ ft^2/sec^3 \tag{115}$$

The three equivalent noises on the attitude error differential equations are

$$q_7^* = 2\sigma_{\varepsilon bx}^2\tau_{\varepsilon rx} \tag{116}$$

$$q_7^* = (2)[(0.025\ deg/hr)(4.848 \times 10^{-6}\ \frac{rad/sec}{deg/hr})]^2(3600\ sec) \tag{117}$$

$$q_7^* = 1.0576 \times 10^{-10}\ rad^2/sec \tag{118}$$

Similarly,

$$q_8^* = q_7^* \tag{119}$$

$$q_9^* = 2.7076 \times 10^{-10} \text{ rad}^2/\text{sec} \tag{120}$$

Note that since there are no white noise inputs on the position differential equations

$$q_1^* = q_2^* = q_3^* = 0 \tag{121}$$

The four range bias error sources (on the order of 10 ft) are easily eliminated by simply increasing the value of the diagonal elements of the measurement noise matrix (R) to 20 feet.

Upon examination of the clock error source models and the relative magnitudes of their state variable initial conditions as presented in Chapter V, it is apparent that the most significant variables are the four phase/range errors of the satellite clocks (in the order of 100 ft), the user clock phase/range error (on the order of 10,000 ft), and the user clock frequency offset error (on the order of 5 ft/sec). These six variables are, in fact, the only ones used in this 15 state filter design except for the nine INS plant error states.

The user clock is simplified by dropping the long term stability state. The filter model for the user clock is shown in Figure 24. Initial conditions and noise values remain unchanged from the system model.

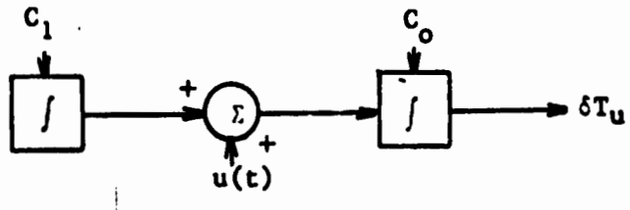

Fig. 24. Simplified User Clock Error Model

As in the system, the noise value input to the phase integrator is

$$q^*_{10} = 6.25 \text{ ft}^2/\text{sec} \tag{122}$$

The error source model for the four satellite clocks is greatly simplified by eliminating all satellite clock variables from the filter state vector except for the phase/range errors. The simplified satellite clock error model for the 15 state filter is given in the following figure.

Fig. 25. Simplified Satellite Clock Error Model

Although the satellite clock frequency offset state has been deleted from the filter state vector, the phase error build-up caused by this offset cannot be ignored. This effect is accounted for by finding the white noise input to the clock phase integrator which causes an equivalent build-up in phase error over a specified time. From Equation (96) it is seen that a frequency offset of C_1 will cause an RMS phase error build-up of

$$\delta T_s = C_1 \Delta t \tag{123}$$

Similarly, a white noise input of $q\Delta t$ to the phase integrator will cause an RMS build-up of

$$\delta T_s = (\quad)^{1/2} \tag{124}$$

Substitution of the right-hand side of Equation (123) into the left-hand side of Equation (124) and solving yields an equation for the

required equivalent q value of the Q' matrix (Ref 1:4-15 & 4-16).

$$q = C_1^2 \, \Delta t \tag{125}$$

This simple satellite clock model need be valid only over the satellite clock update interval, or flight time. Thus Δt was set at one hour (3600 sec).

$$q_{12}^* = (.01)^2(3600) = 0.36 \text{ ft}^2/\text{sec} \tag{126}$$

Similarly,

$$q_{13}^* = q_{14}^* = q_{15}^* = q_{12}^* \tag{127}$$

The F matrix representing this 15 state filter design is given in Equation (128). The "Pinson Error Model" is the same as given in Figure 7.

$$F_f = \begin{array}{c} \\ 1\text{-}9 \\ 10\text{-}11 \\ 12\text{-}15 \end{array} \begin{array}{c} \begin{array}{ccc} 1\text{-}9 & 10\text{-}11 & 12\text{-}15 \end{array} \\ \left[\begin{array}{ccc} \begin{array}{c}\text{Pinson}\\ \text{Error}\\ \text{Model}\end{array} & \begin{array}{cc} & \\ 0 & \end{array} & \begin{array}{c} \\ 0 \end{array} \\ \hline \begin{array}{ccc} & & \\ & 0 & \\ & & \end{array} & \begin{array}{cc} 0 & 1 \\ & \\ 0 & 0 \end{array} & \begin{array}{c} \\ 0 \\ \\ \end{array} \\ \hline \begin{array}{ccc} & & \\ 0 & & \end{array} & \begin{array}{cc} & \\ 0 & \end{array} & \begin{array}{c} \\ 0 \end{array} \end{array}\right] \end{array} \tag{128}$$

The Q', H, and R matrices are identical to those of the filter design presented next, and are not displayed here for the sake of brevity. Also, the RMS error plots for this filter design were indistinguishable from those of the decoupled version discussed next and are omitted.

This filter design and all others in this chapter were simulated using 30 second measurement rate. In the subsequent chapter, this 15 state filter is used as a basis of comparison for various measurement rates.

15 State Filter - Weak Coupling Removed

This filter provided the best tradeoff between accuracy and computational time for the particular problem of this study and is therefore the recommended Kalman filter design.

Incorporating the Pinson INS error model into the filter design requires the computation of 36 non-zero terms, in the F matrix many of which are complex (see Figure 7). However, for an aircraft cruising at subsonic speeds, as in the flight profile of this study, many of these terms are negligible and may be deleted from the F matrix. This includes terms on the order of magnitude of ω_{ie} such as V_x/R and V_y/R. However, the Schuler frequency terms (ω_s^2 and $2\omega_s^2$) are included so that the model applicability will not be restricted to short periods of time (on the order of 30 minutes). The simplified F matrix along with the Q', H, and R matrices for this 15 state filter design with weak coupling terms removed are given in Equations (129) through (132).

$$F_f = \begin{array}{c} \\ 1 \\ 2 \\ 3 \\ 4 \\ 5 \\ 6 \\ 7 \\ 8 \\ 9 \\ 10 \\ 11\text{-}15 \end{array} \begin{array}{c} \begin{array}{ccccccccccc} 1 & 2 & 3 & 4 & 5 & 6 & 7 & 8 & 9 & 10 & 11 \end{array} \quad 12\text{-}15 \\ \left[\begin{array}{ccccccccccc|c} 0 & 0 & 0 & 1 & 0 & 0 & 0 & 0 & 0 & 0 & 0 & \\ 0 & 0 & 0 & 0 & 1 & 0 & 0 & 0 & 0 & 0 & 0 & \\ 0 & 0 & 0 & 0 & 0 & 1 & 0 & 0 & 0 & 0 & 0 & \\ -\omega_s^2 & 0 & 0 & 0 & 0 & 0 & 0 & -A_z & A_y & 0 & 0 & \\ 0 & -\omega_s^2 & 0 & 0 & 0 & 0 & A_z & 0 & -A_x & 0 & 0 & \\ 0 & 0 & 2\omega_s^2 & 0 & 0 & 0 & -A_y & A_x & 0 & 0 & 0 & 0 \\ 0 & 0 & 0 & 0 & 0 & 0 & 0 & \omega_z & -\omega_y & 0 & 0 & \\ 0 & 0 & 0 & 0 & 0 & 0 & -\omega_z & 0 & \omega_x & 0 & 0 & \\ 0 & 0 & 0 & 0 & 0 & 0 & \omega_y & -\omega_x & 0 & 0 & 0 & \\ 0 & 0 & 0 & 0 & 0 & 0 & 0 & 0 & 0 & 0 & 1 & \\ \hline & & & & & & 0 & & & & & 0 \end{array}\right] \end{array} \quad (129)$$

$$Q_f' = \begin{array}{c} \\ 1\text{-}3 \\ 4\text{-}15 \end{array} \begin{array}{c} \begin{array}{cc} 1\text{-}3 & 4\text{-}15 \end{array} \\ \left[\begin{array}{c|ccc} 0 & & 0 & \\ \hline & \ddots & & \\ 0 & & \ddots & \\ & & & q_{15}^* \end{array}\right] \end{array} \quad (130)$$

The values for q_4 through q_{15} are as given in the preceding section of this chapter.

$$H_f = \begin{array}{c} \\ 1 \\ 2 \\ 3 \\ 4 \end{array} \begin{array}{c} \begin{array}{cccccccccc} 1 & 2 & 3 & 4\text{-}9 & & 10 & & 11 & 12\text{-}15 & \end{array} \\ \left[\begin{array}{ccc|c|c|c|cccc} i_{rx1} & i_{ry1} & i_{rz1} & 0 & 1 & 0 & -1 & 0 & 0 & 0 \\ i_{rx2} & i_{ry2} & i_{rz2} & 0 & 1 & 0 & 0 & -1 & 0 & 0 \\ i_{rx3} & i_{ry3} & i_{rz3} & 0 & 1 & 0 & 0 & 0 & -1 & 0 \\ i_{rx4} & i_{ry4} & i_{rz4} & 0 & 1 & 0 & 0 & 0 & 0 & -1 \end{array}\right] \end{array} \tag{131}$$

$$R_f = \begin{array}{c} \\ 1 \\ 2 \\ 3 \\ 4 \end{array} \begin{array}{c} \begin{array}{cccc} 1 & 2 & 3 & 4 \end{array} \\ \left[\begin{array}{cccc} \sigma_r^2 & 0 & 0 & 0 \\ 0 & \sigma_r^2 & 0 & 0 \\ 0 & 0 & \sigma_r^2 & 0 \\ 0 & 0 & 0 & \sigma_r^2 \end{array}\right] \end{array} \tag{132}$$

Where σ_r = 20 ft.

The system RMS position, velocity, and attitude error plots for this filter design are given in Figures 26 through 34 and should be compared with those for the optimal filter. Table VII following these plots compares the system plant and user clock phase/range error values for both the optimal and the 15 state decoupled filter at 2400 seconds with the initial values to provide a quick comparison of performance. These are "average" values as explained in the next chapter.

Note that the effectiveness of both the optimal and the 15 state sub-optimal filter is approximately the same in controlling the x, y, z position and user clock phase/range errors. Also, the 15 state filter yields attitude accuracy close to that of the optimal filter. However, the x and y velocity errors are reduced to approximately 10% of their

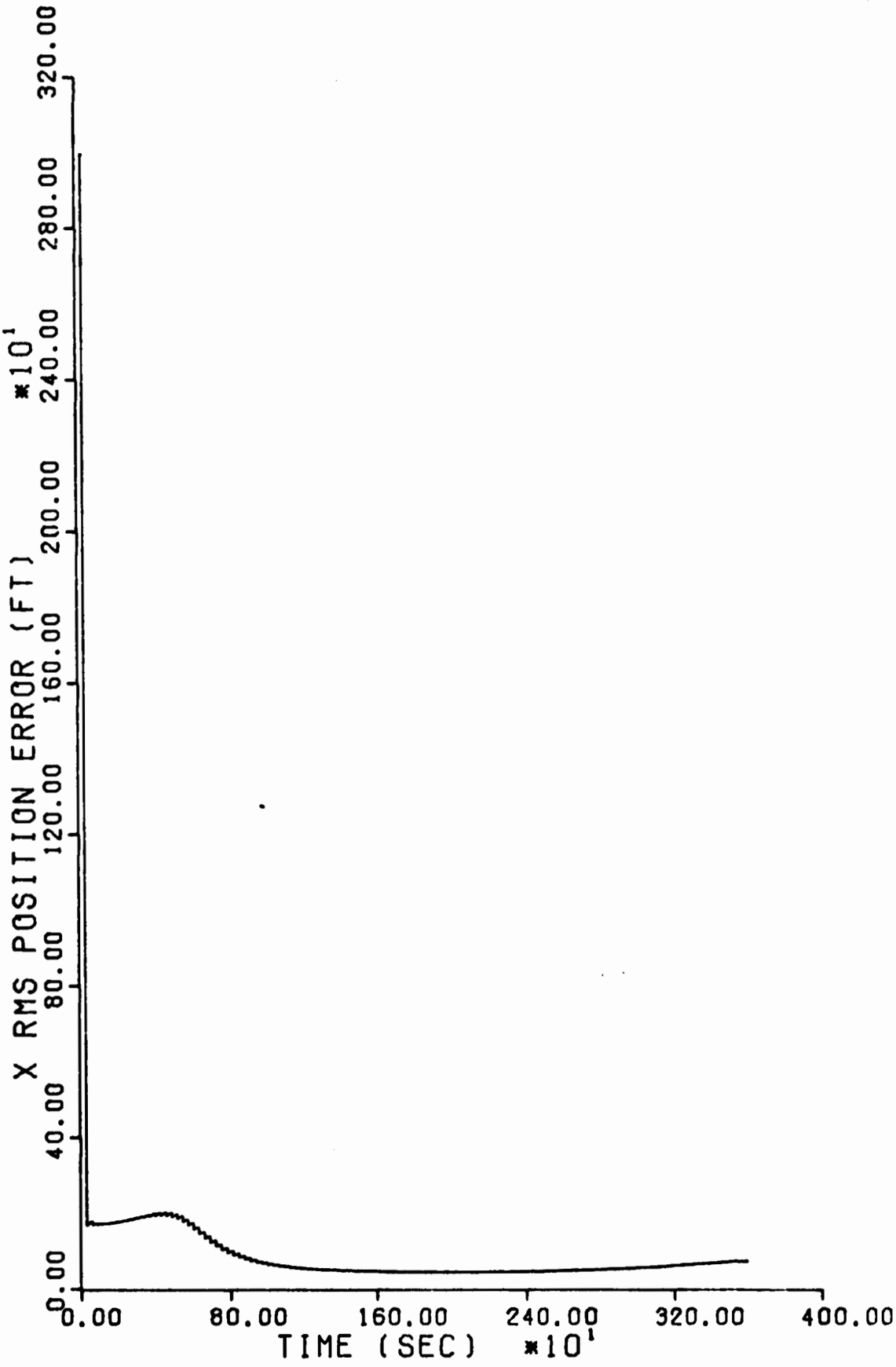

Fig. 26. 15 State Filter, x Position Error

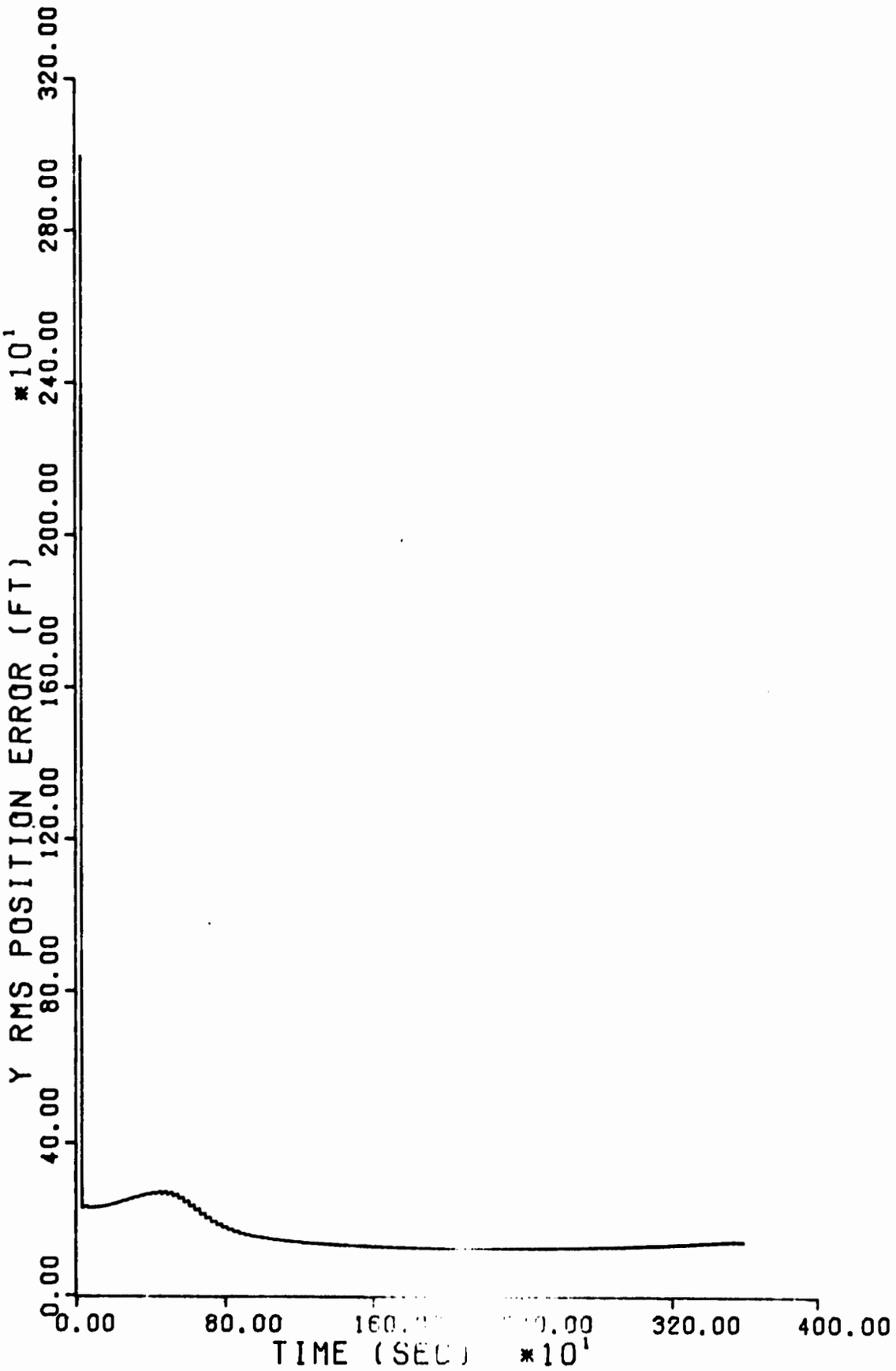

Fig. 27. 15 State Filter, y Position Error

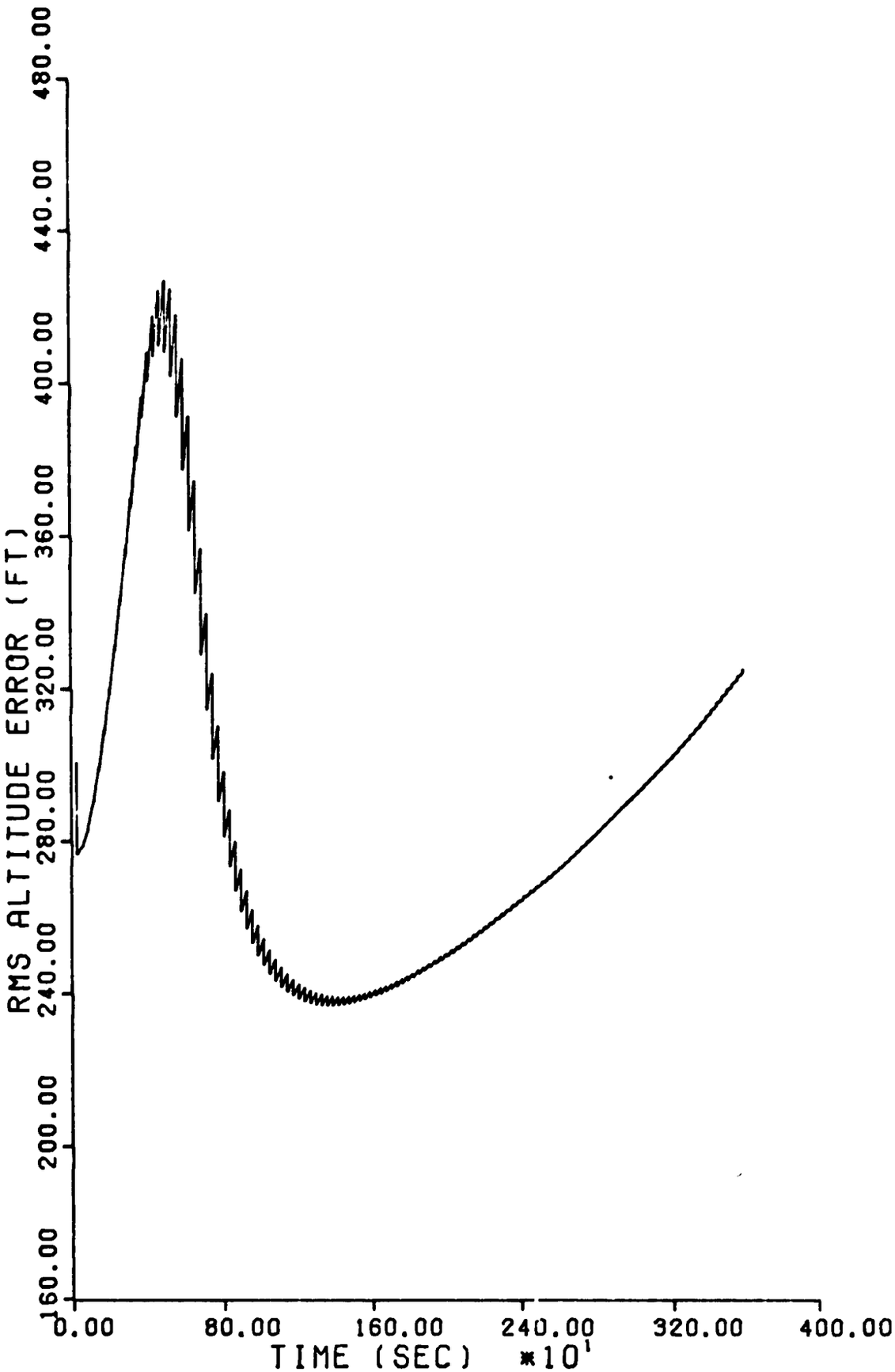

Fig. 28. 15 State Filter, Altitude Error

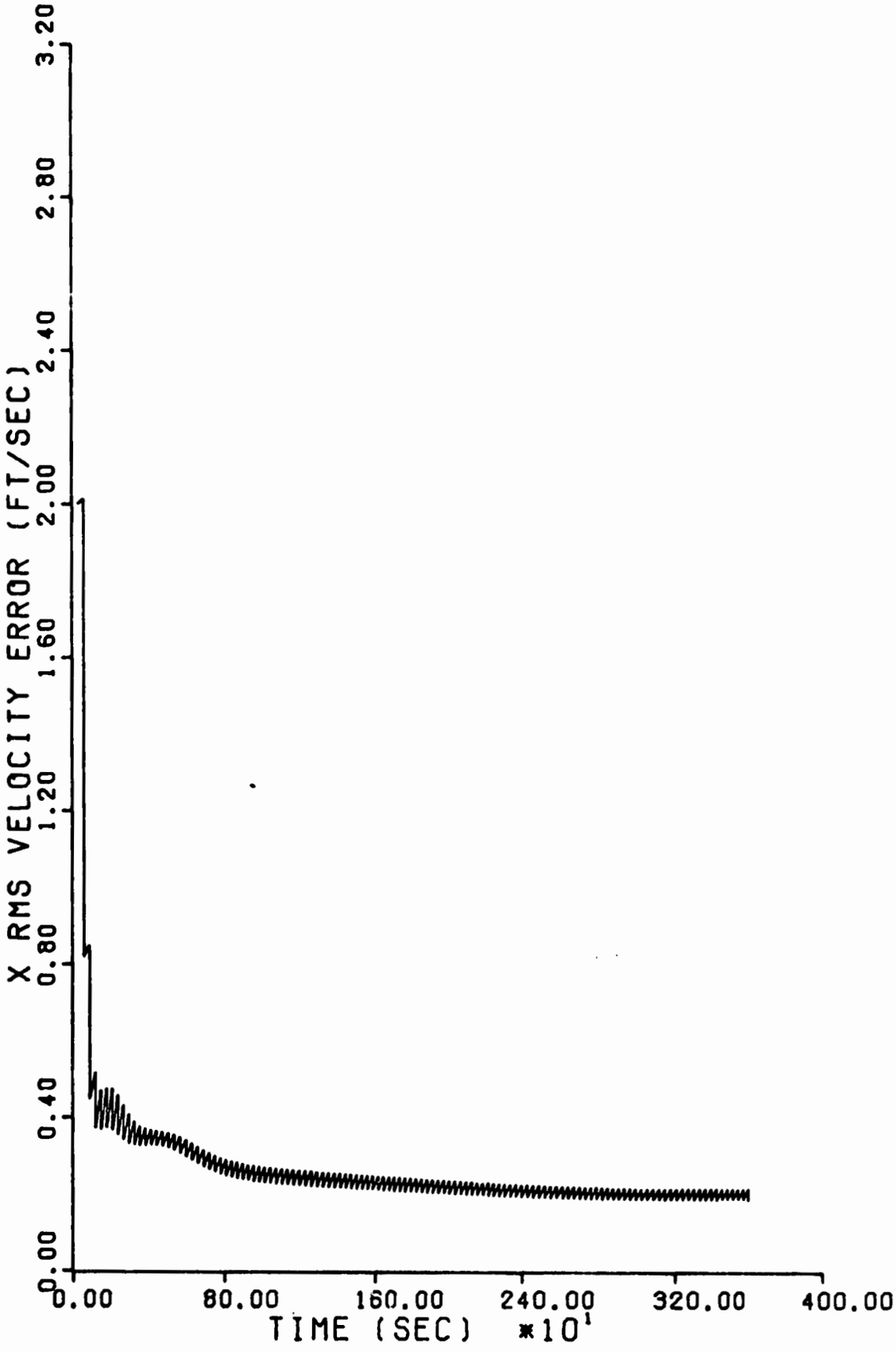

Fig. 29. 15 State Filter, x Velocity Error

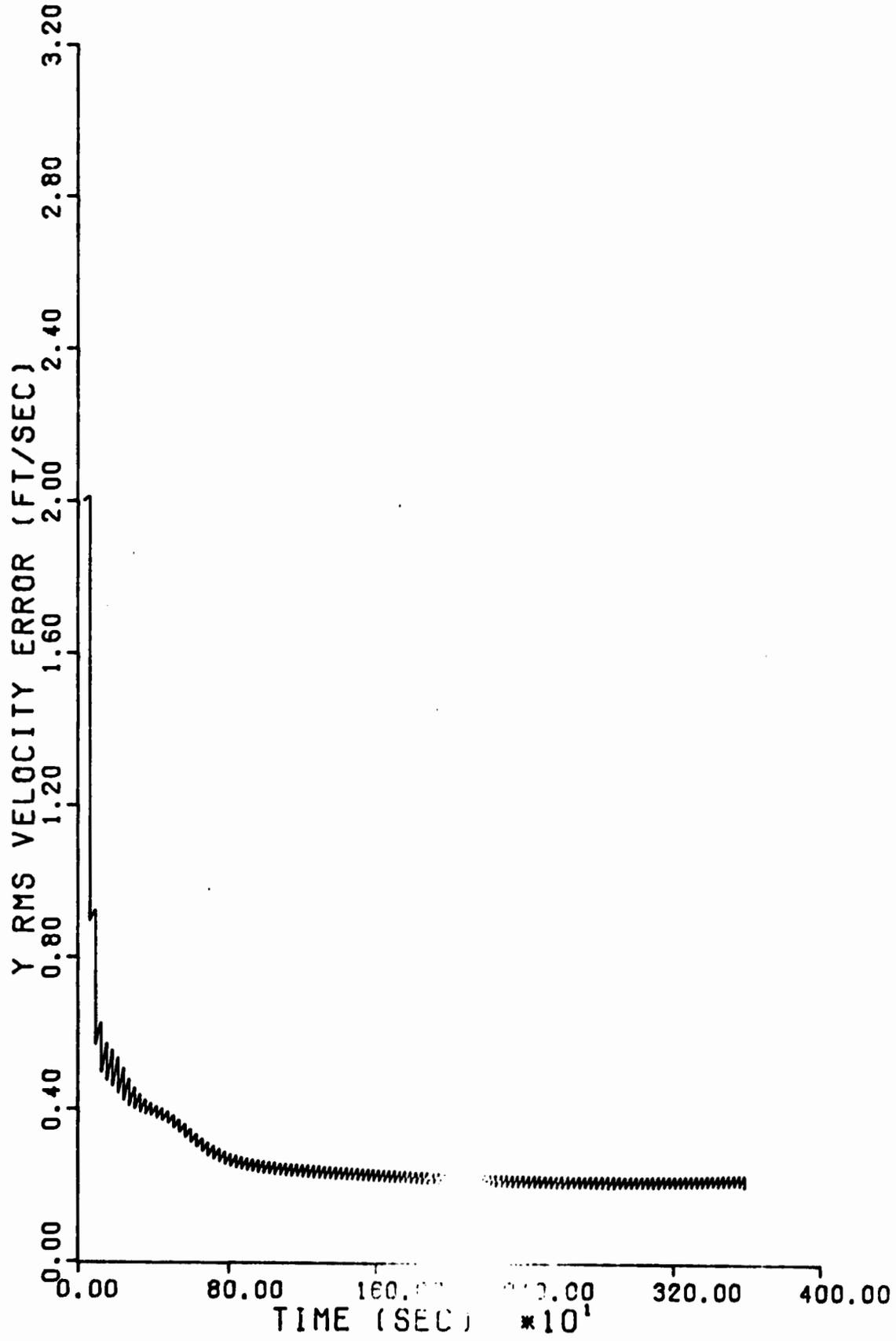

Fig. 30. 15 State Filter, y Velocity Error

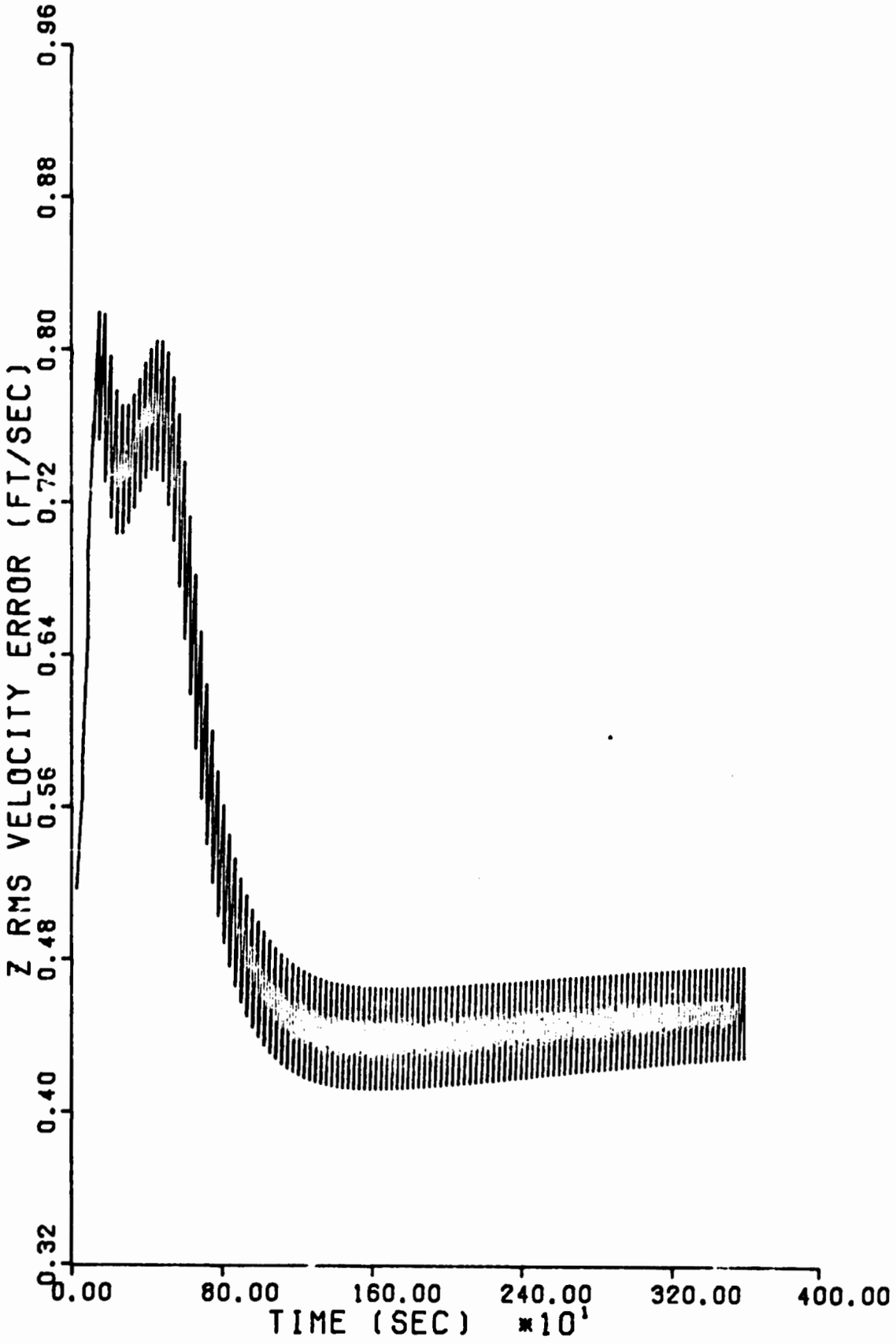

Fig. 31. 15 State Filter, z Velocity Error

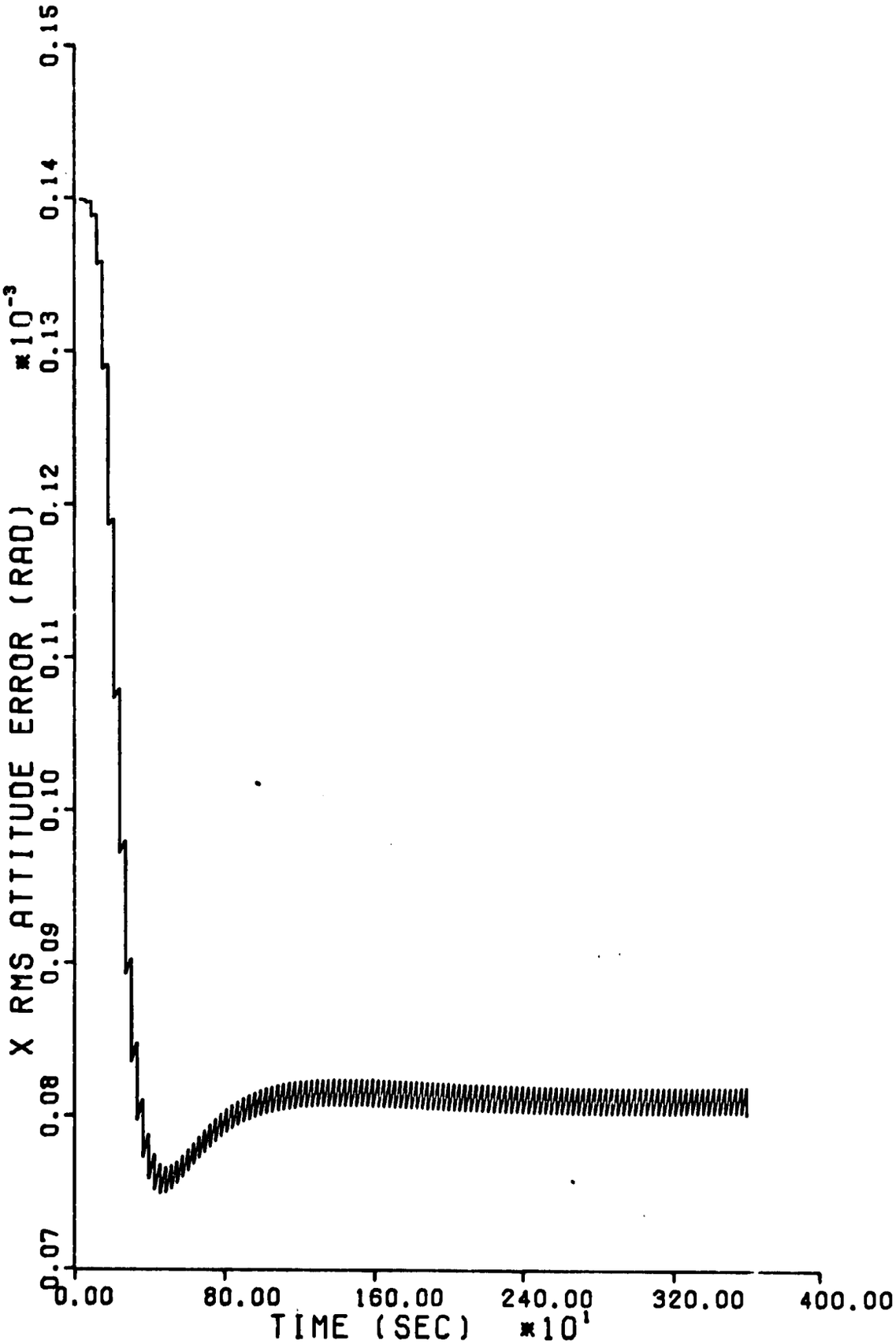

Fig. 32. 15 State Filter, x Attitude Error

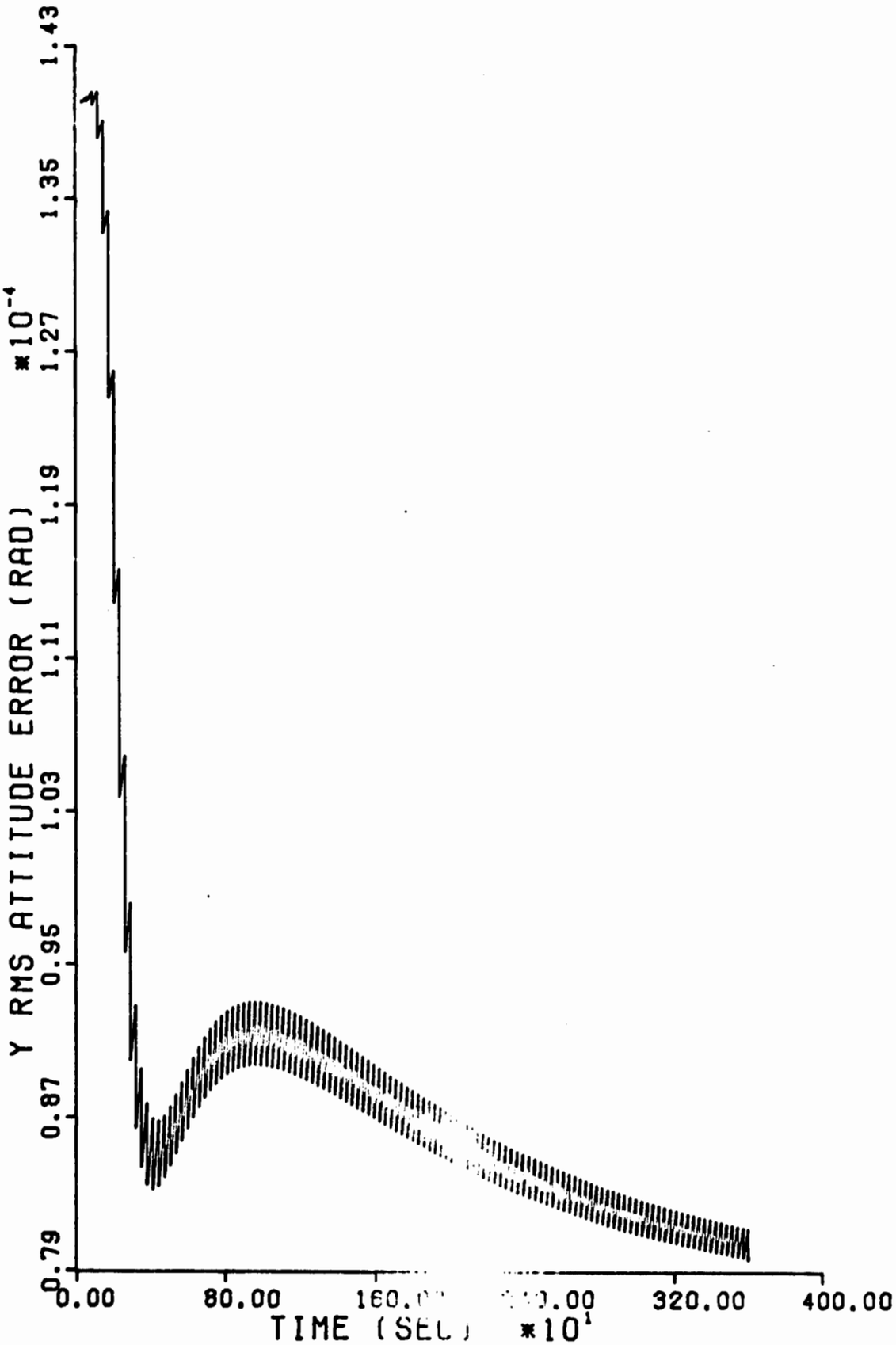

Fig. 33. 15 State Filter, y Attitude Error

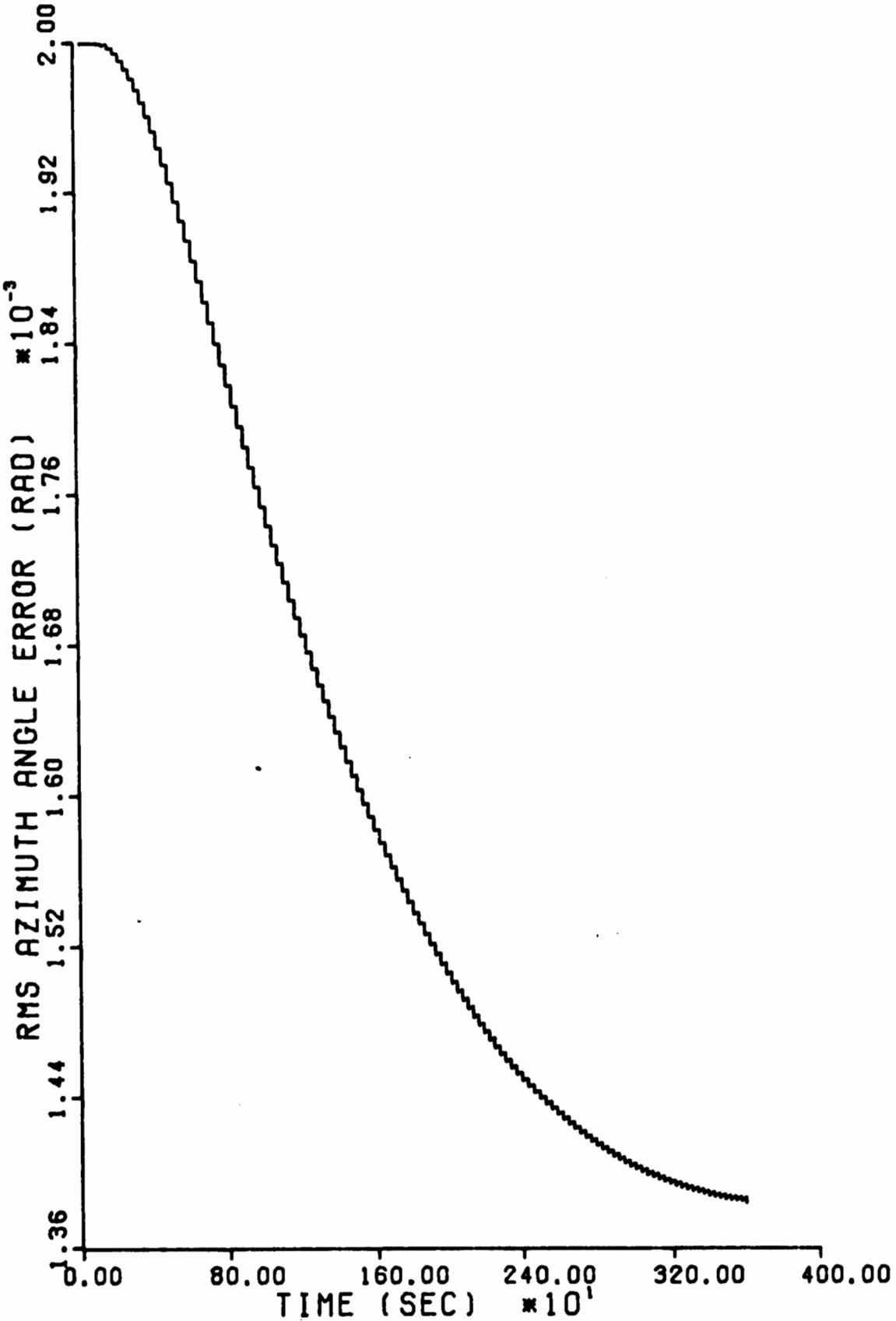

Fig. 34. 15 State Filter, Azimuth Error

Table VII

Average RMS Errors of INS Plant States

15 state filter and optimal 44 state filter performance compared against initial values. User clock phase/range is also included.

Variable	Initial Condition	Optimal Filter (t = 2400 sec)	15 State Filter (t = 2400 sec)
Δx	3000 ft	45.85 ft	47.47 ft
Δy	3000 ft	125.2 ft	126.1 ft
Δz	300 ft	256.3 ft	264.6 ft
$\Delta \dot{x}$	2 ft/sec	0.103 ft/sec	0.213 ft/sec
$\Delta \dot{y}$	2 ft/sec	0.117 ft/sec	0.217 ft/sec
$\Delta \dot{z}$	0.5 ft/sec	0.158 ft/sec	0.444 ft/sec
ϕx	0.14 millirad	0.065 millirad	0.082 millirad
ϕy	0.14 millirad	0.065 millirad	0.084 millirad
ϕz	2 millirad	1.27 millirad	1.45 millirad
δT_u	10,000 ft	199.0 ft	205.6 ft

initial values by the sub-optimal filter as compared to about 5% for the optimal case. The vertical velocity error is reduced only slightly below the initial value in the sub-optimal case, whereas it is reduced to approximately 1/3 its initial value by the optimal filter. Also note that the altitude error is merely kept from growing above its initial value in both cases and altitude accuracy is not significantly improved. These results suggest two areas for future investigation. First, range-rate measurements could be effective in improving upon velocity errors; and secondly, the addition of altimeter measurements would almost certainly reduce the magnitude of the altitude error. However, x and y position error, which is usually of primary importance, is very effectively controlled by this 15 state filter design.

10 State Filter

A filter design utilizing only ten states is presented here for the purpose of illustrating degraded performance characterized by reducing the dimension of the filter state vector too far. In this case, the Kalman gains computed by the filter do not include the effect of significant variables which have been deleted from the filter. Thus, when these gains are applied to the system, the divergent growth of the error equations is not effectively controlled.

In this case, the nine plant error state variables and the user clock phase/range error are the only ones retained in the filter. Thus, this design is obtained from the 15 state filter by discarding the four satellite clock phase/range error states and the user clock frequency offset error. The decoupled version of the INS error model (Equation (129)) is used in the F matrix and the user clock is modeled in a manner

similar to the simplified satellite clock model of the 15 state filter. The H matrix is obtained by deleting the four satellite clock terms (-1's) from the 15 state design. Also, the RMS value of the measurement noise (σ_r) is increased to 100 feet to account for the increased uncertainty in the range measurement value. The RMS error plots for this ten state filter design illustrate its unacceptable performance and are shown in Appendix A.

VII. Measurement Update Rate and Selection of Observables

The first section of this chapter investigates the effect of varying the measurement update rate. The fully coupled 15 state filter design of the previous chapter is used in this investigation. The measurement update rate requirements may vary greatly from system to system depending on the accuracy required as well as the capabilities of the equipment used to take the measurements for the update. For example, a smaller onboard computer would normally require a larger computational time. Additionally, a comparison is made between obtaining measurements from satellites which are randomly selected from those in view and obtaining measurements from a sequence of "optimum" sets of four satellites, three of which form a "most nearly orthogonal" set at the time of measurement.

The update rates used in this report are as follows: 5 seconds, 15 seconds, 30 seconds, 60 seconds, and 90 seconds. The results of these update rates are compared, at a specified time in the flight profile, in Table VIII at the end of this chapter.

Comparison of Update Rates

A few representative plots of the RMS errors for the nine INS plant error states are shown on the following pages. In the previous chapter, a 30 second update rate was used in determining the Kalman filter state vector dimension. Therefore, plots of the nine plant error states with this update rate are included in that chapter and will not be repeated here. Plots of the three error state variables; x position, y attitude and z velocity for update rates of 5 seconds, 15 seconds, 60 seconds, and 90 seconds appear in Figures 35 through 46. Plots of

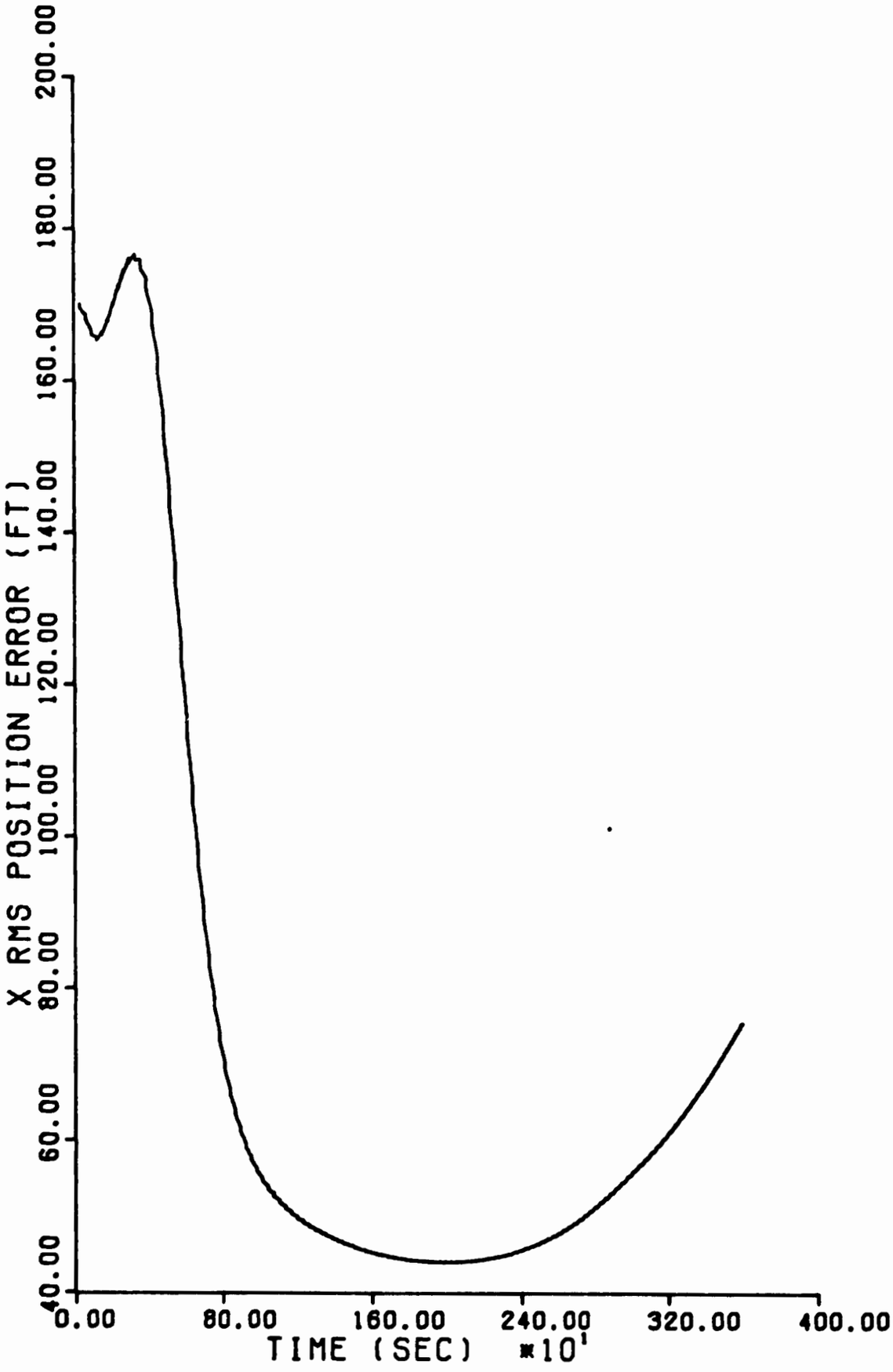

Fig. 35. x Position Error, 5 Second Update Rate

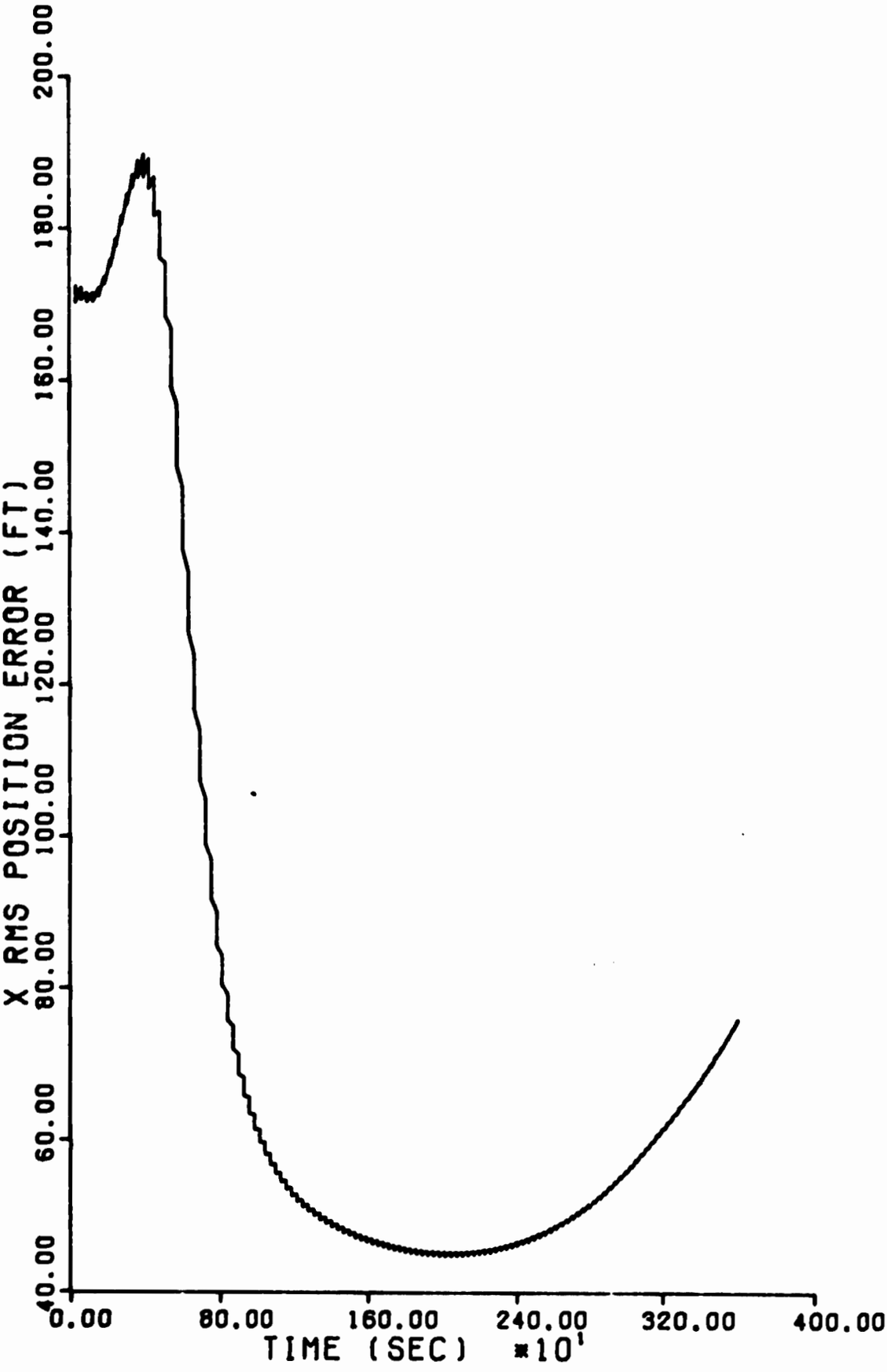

Fig. 36. x Position Error, 15 Second Update Rate

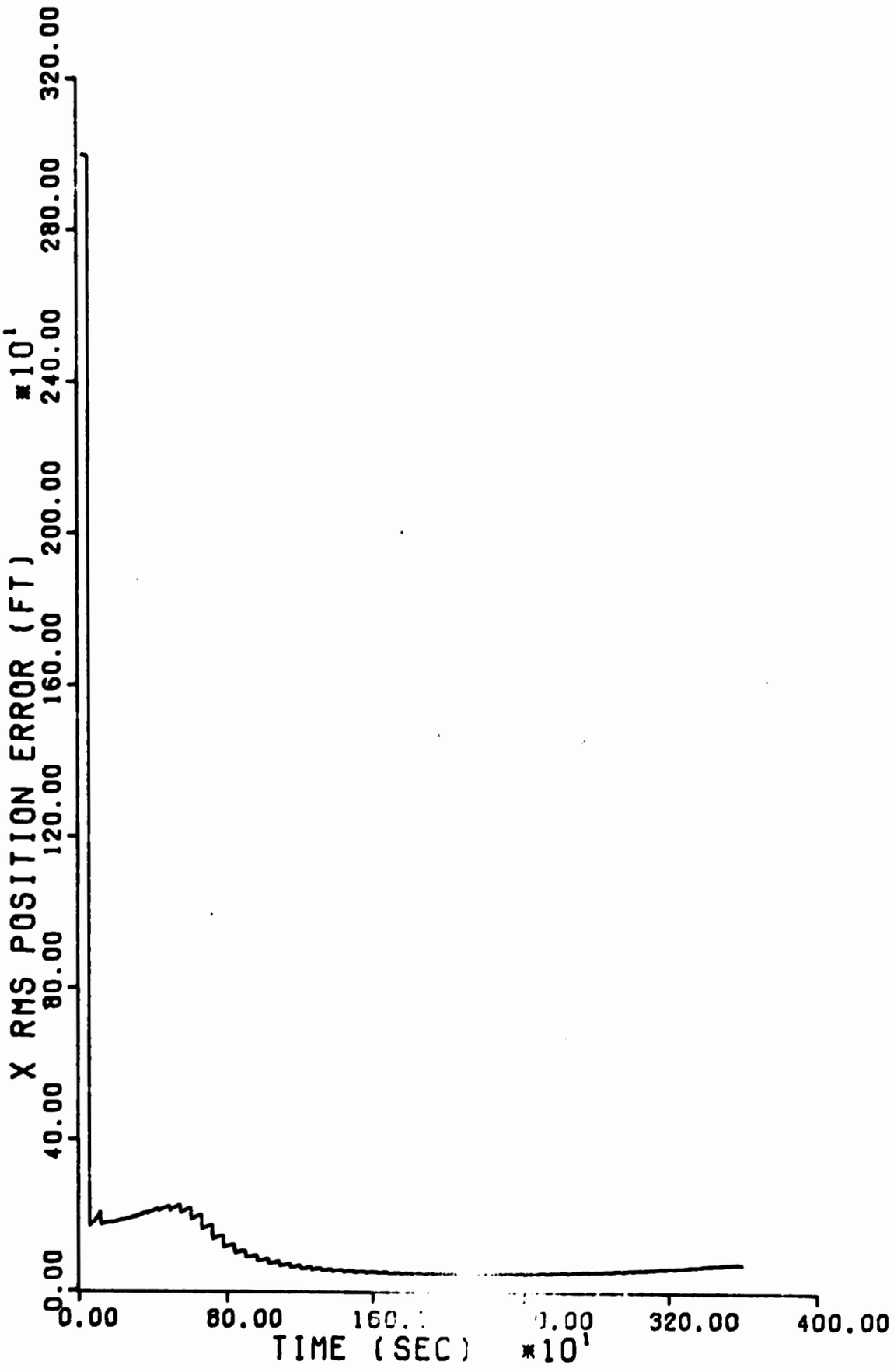

Fig. 37. x Position Error, 60 Second Update Rate

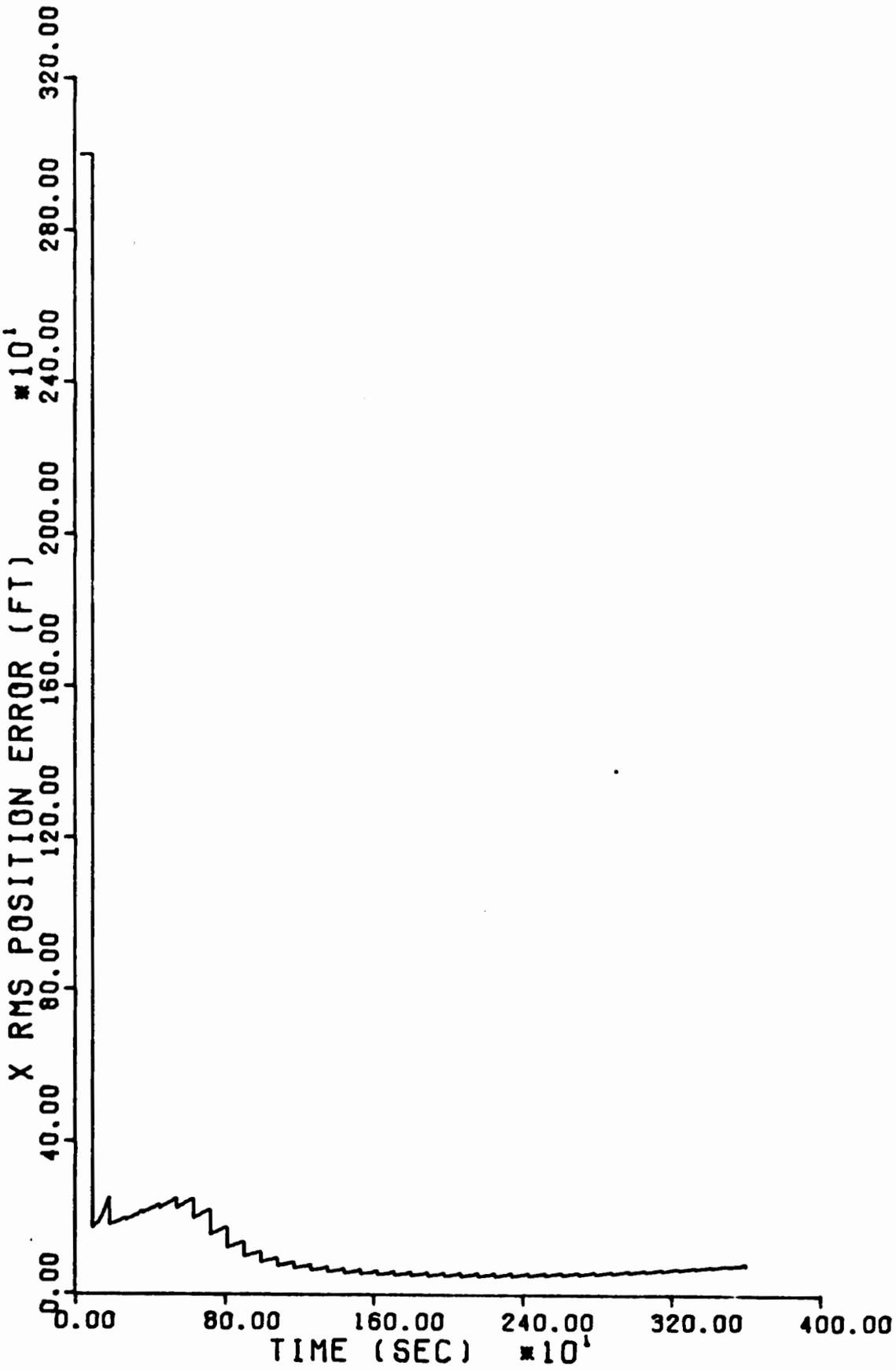

Fig. 38. x Position Error, 90 Second Update Rate

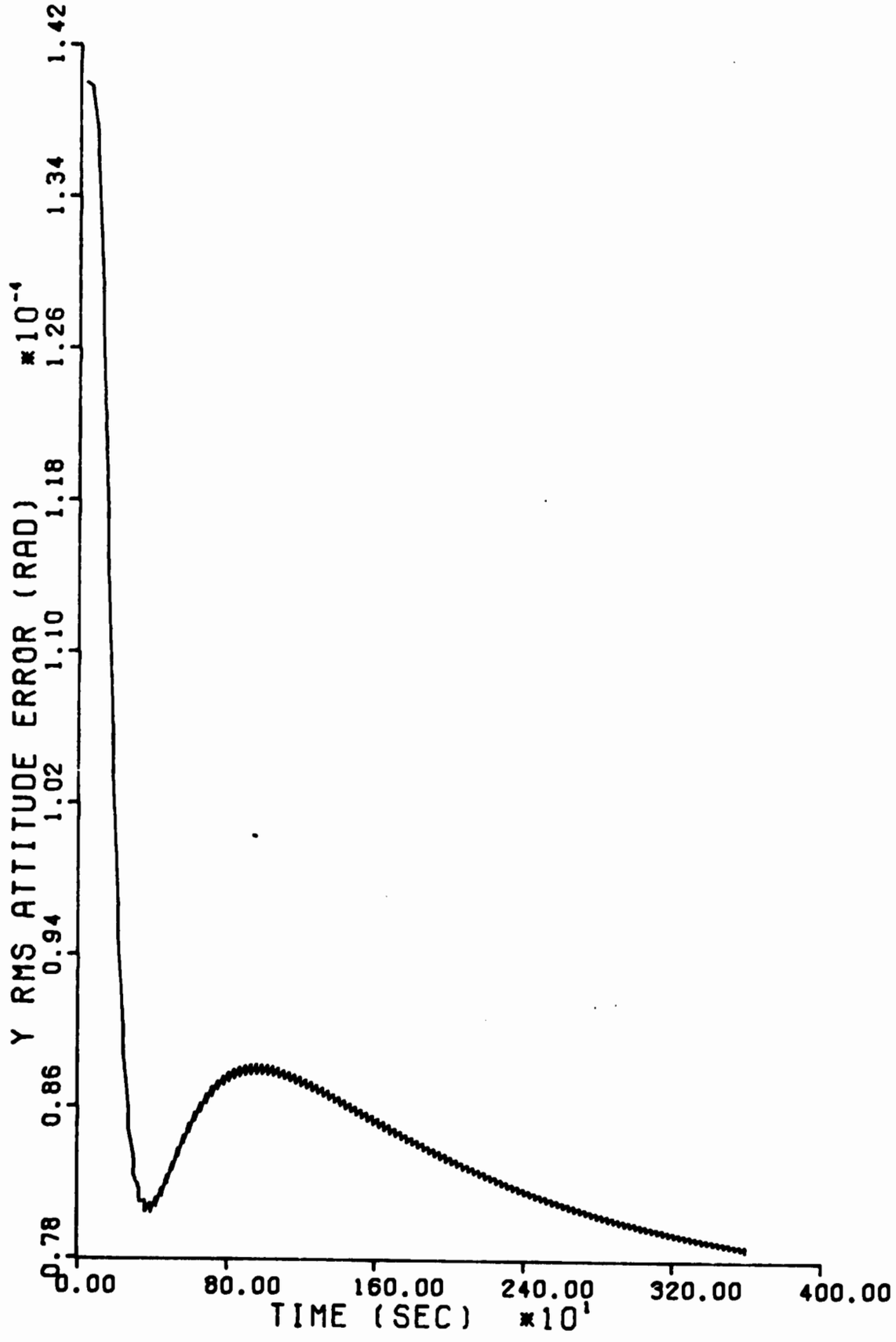

Fig. 39. y Attitude Error, 5 Second Update Rate

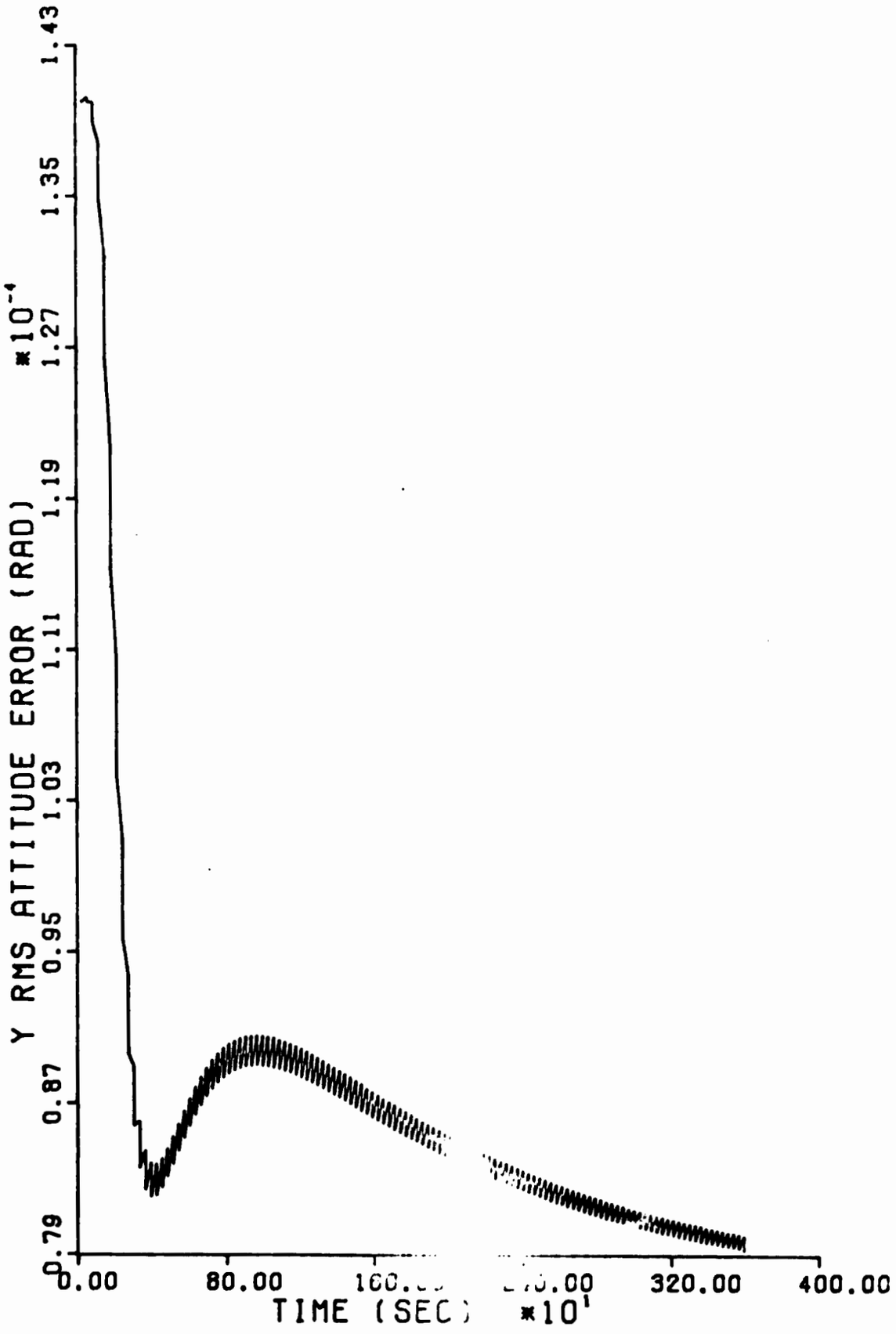

Fig. 40. y Attitude Error, 15 Second Update Rate

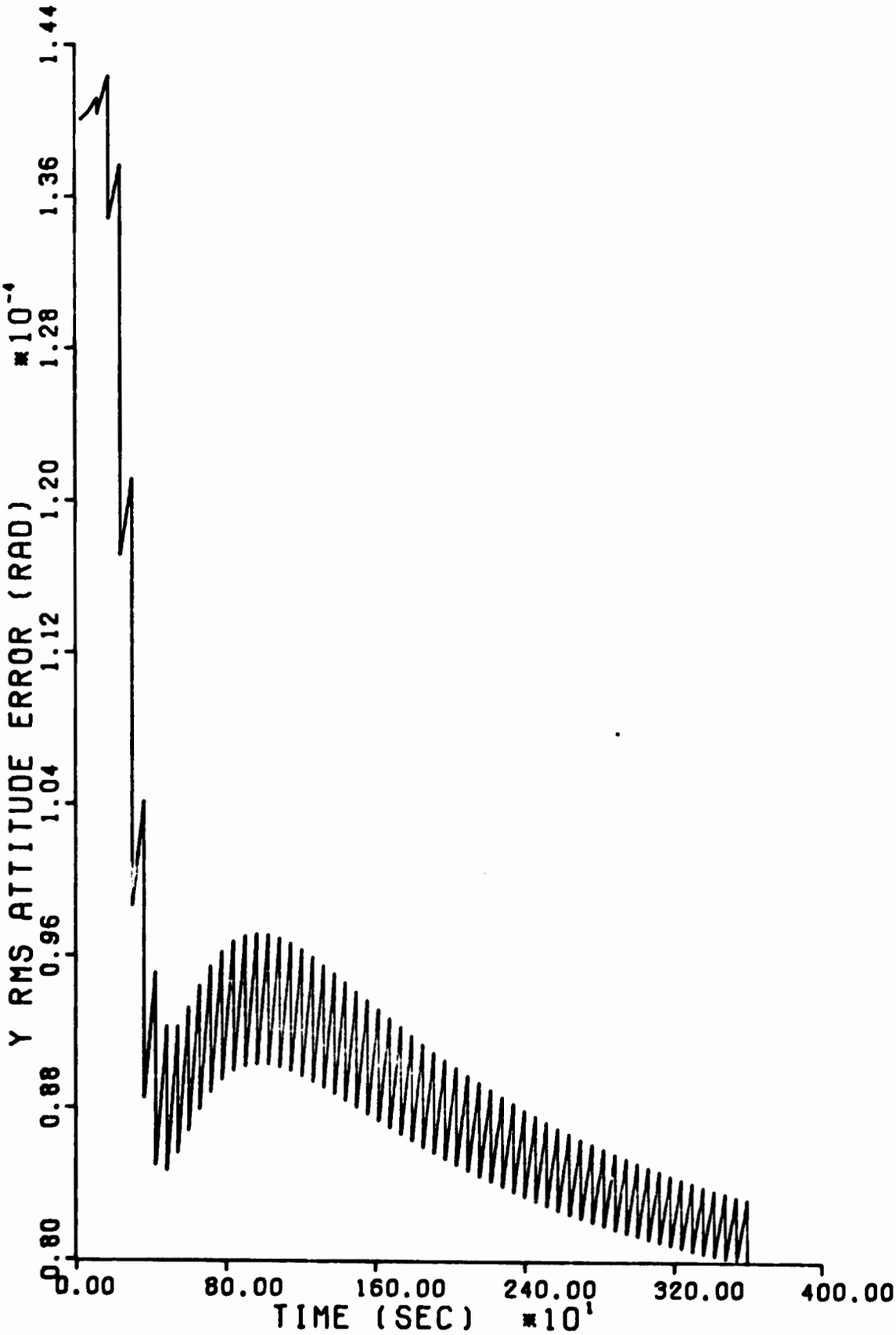

Fig. 41. y Attitude Error, 60 Second Update Rate

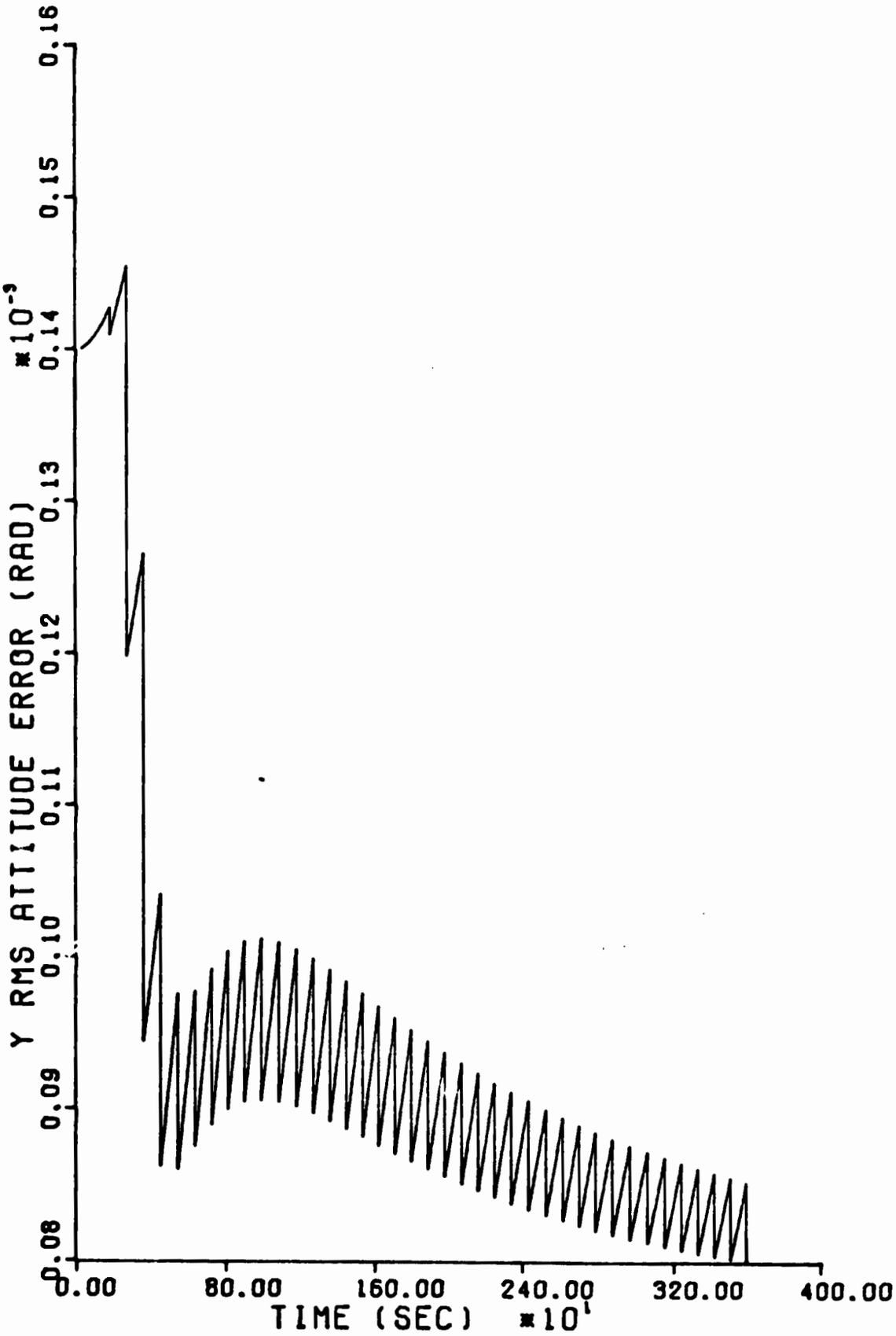

Fig. 42. y Attitude Error, 90 Second Update Rate

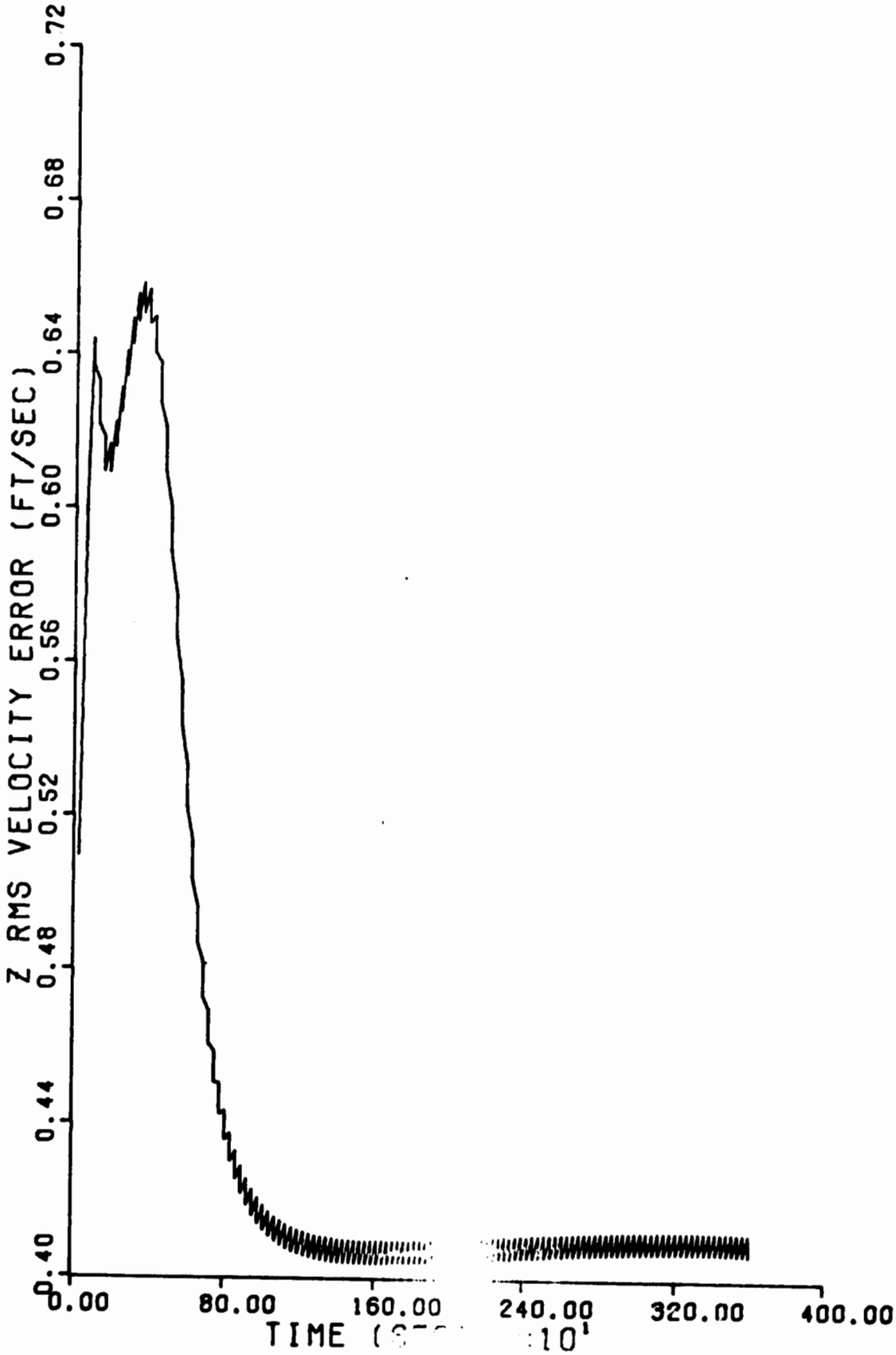

Fig. 43. z Velocity error, 5 Second Update Rate

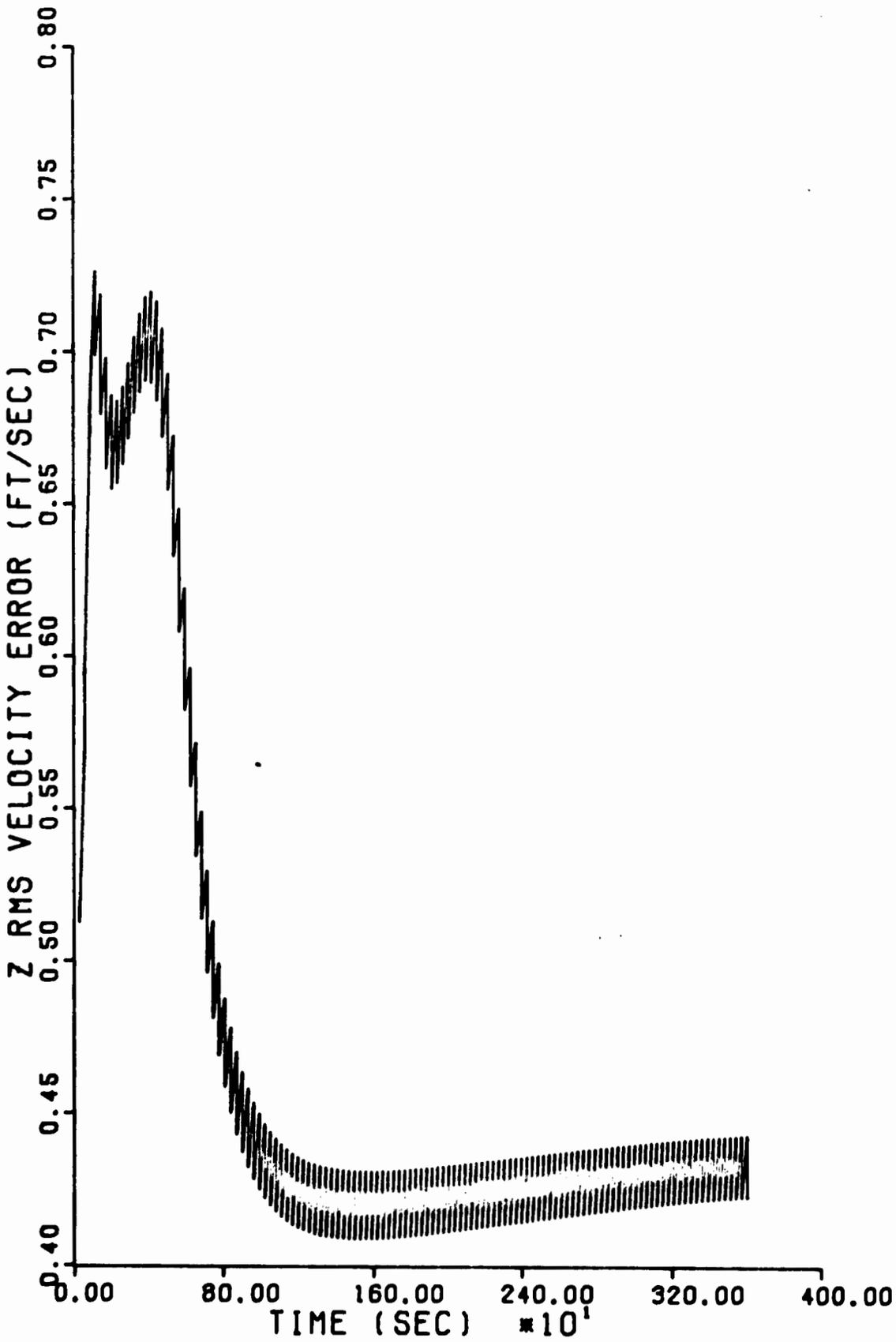

Fig. 44. z Velocity Error, 15 Second Update Rate

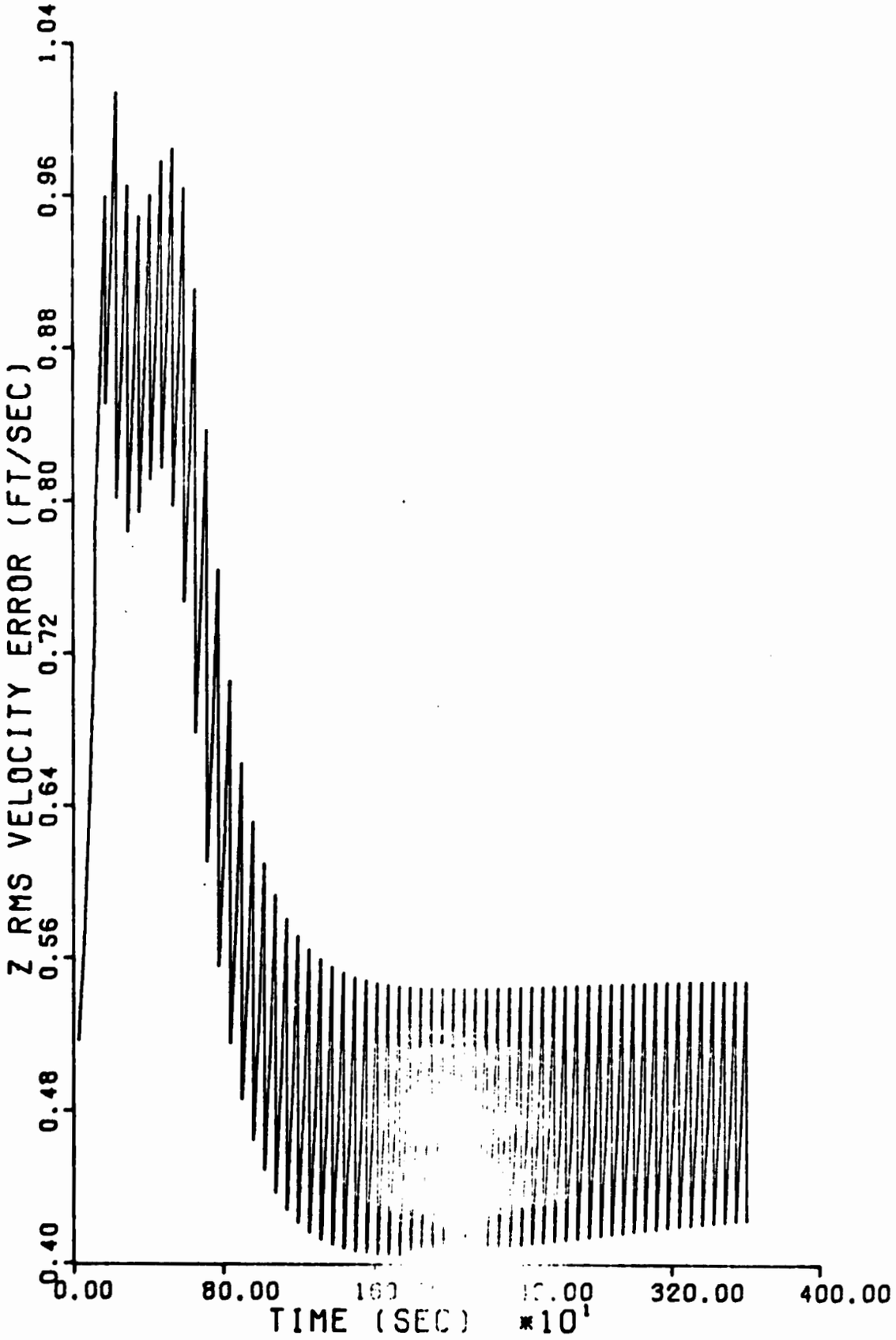

Fig. 45. z Velocity Error, 60 Second Update Rate

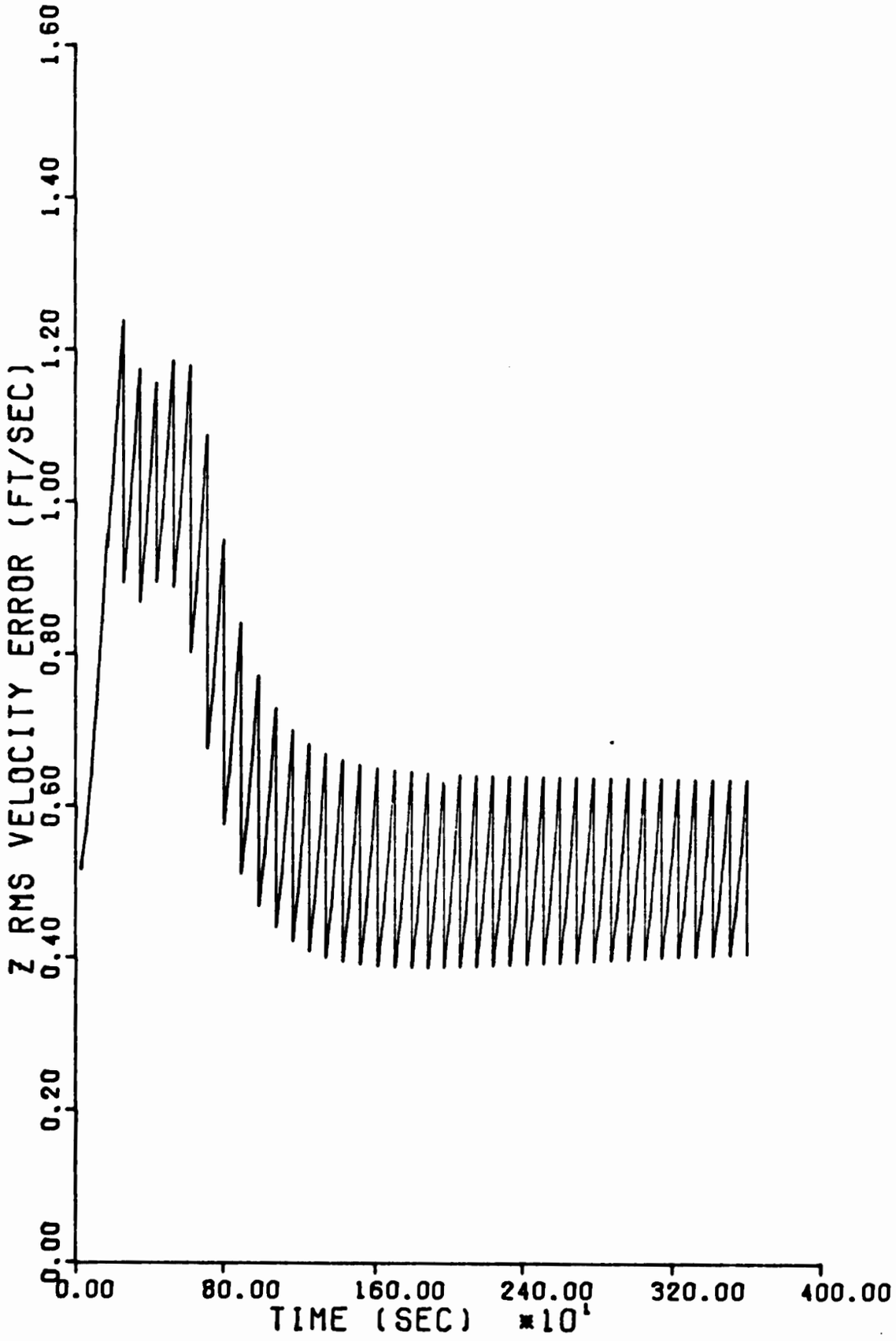

Fig. 46. z Velocity Error, 90 Second Update Rate

Table VIII

Average RMS Errors of Plant Error States at 1800 Seconds

Plant States	Update Rate 5 Sec	15 Sec	30 Sec	60 Sec	90 Sec	% Improvement from 90 to 5
x RMS Position (ft)	44.40	45.63	47.27	50.57	54.34	18.3
y RMS Position (ft)	129.26	129.59	130.11	131.10	132.4	2.3
RMS Altitude (ft)	240.48	242.09	244.40	249.41	255.27	5.8
x RMS Velocity (ft/sec)	.178	.204	.227	.259	.285	37.5
y RMS Velocity (ft/sec)	.179	.205	.226	.255	.268	33.2
z RMS Velocity (ft/sec)	.407	.421	.440	.475	.517	21.3
x RMS Attitude (Rad)	7.929×10^{-5}	8.047×10^{-5}	8.127×10^{-5}	8.282×10^{-5}	8.396×10^{-5}	5.6
y RMS Attitude (Rad)	8.43×10^{-5}	8.581×10^{-5}	8.676×10^{-5}	8.913×10^{-5}	9.093×10^{-5}	7.3
RMS Azimuth (Rad)	1.533×10^{-3}	1.537×10^{-3}	1.548×10^{-3}	1.547×10^{-3}	1.553×10^{-3}	1.3

the remaining six plant error states for these measurement rates are included in Appendix B.

It should be noted that the horizontal axis or time scale remains constant for all the plots, but the vertical axis, RMS error, was scaled for each plot to effectively show the results of the update rate. The plotting program was set to plot points at a minimum interval of 30 seconds. Because of this plot control the initial updates occuring in the 0 to 30 second time period are not shown for the 5 and 15 second measurement rates. In these two cases the errors have been greatly reduced by the time the first points are plotted and the lower region of the vertical axis has been greatly magnified. This illustrates the divergent behavior of the position error states at the end of this flight profile. This aspect will be discussed in the final section of this chapter.

These plots indicate that increasing the update rate does not greatly improve the RMS errors. In general, a slower update rate allows the errors to grow to higher values during the initial portion of the flight (first 15 minutes). The error states after this initial time period exhibit an almost "steady state" time behavior. The slower update rates provide RMS error values which are a little higher on the average than the faster measurement rates. This fact is illustrated in Table VIII. This table shows the average RMS errors of the plant error states at each update rate, for a particular time during the flight profile. Also shown in the table is the per cent improvement from the 90 second update rate to the 5 second update rate. "Average" values are obtained by fitting a smooth curve to the data points. This is accomplished by adding the RMS error values of a variable at the time

instant before a measurement to its value just after the measurement and dividing by two. Also, slower update rates permit the errors to grow to substantially higher values between measurements.

Selection of Observables

When using SAMUS (a computer program detailed in Chapter VIII), two test cases were executed using a twenty-two state optimal filter. In both cases four satellites, or observables, were selected for each reset segment by studying data output of the profile generator program of Chapter III, which calculates unit vectors in the navigation frame from the user to each satellite. Three of these range measurements are required for correcting x, y, and z position and the fourth measurement is needed for synchronization of the user clock. Three satellites having the largest components along the x, y, and z axes, respectively, when compared with all other satellites in-view at a particular time, are chosen. These form a most nearly orthogonal set of measurements. The fourth satellite is chosen as the one having the second largest component along the z axis. For example, the "optimal" set of satellites at the particular time instant shown in Table III is composed of satellites 52, 13, 93, and 62.

In case one, the flight time was divided equally into two reset segments. Since the satellite unit vectors are time varying, the satellites chosen for each reset segment provide the best information, on the average, over the given time interval. SAMUS was then executed, using these two reset segments, to calculate the values of the INS error states as a function of time over the one hour flight profile. The data from this run was next input to a general covariance plotting

program that provided the plots for the root mean square (RMS) error of the diagonal elements of the covariance matrix for the twenty-two error states. Figure 47 is a plot of the x and y position error, in nautical miles, for the time period of the profile. Figure 48 is a plot of the altitude error, in feet, for the same period. The results for the position error indicate a decrease from .5 nautical mile initially to .005 nautical mile after the first reset. The error remains constant for about 30 minutes then the error starts to increase. The altitude error indicates a decrease from 100 feet initially to 15 feet after the first reset. At this time the error starts to increase until it reaches approximately 50 feet at the end of the flight profile.

In case two of the same 22 state optimal filter was used; however, this run contained six reset segments. Since the satellite unit vectors were time varying, more accurate satellite information could be acquired by changing the observables, satellites, at shorter intervals. Figure 49 shows the plot of the x and y position error for this run. The results show that the position errors did not diverge at the end of the profile. Figure 50 illustrates the elimination of divergent behavior in the altitude error.

A comparison of the two cases indicates that by increasing the number of reset segments so that measurements are taken from "optimal" sets of satellites throughout the flight, the INS plant errors reach almost steady-state values and the tendency toward divergent behavior in the latter part of the flight disappears. However, the general covariance program used in generating the bulk of the plots appearing in this report does not have the capability for multiple reset segments. Thus, a set of 4 satellites giving reasonably good performance throughout the

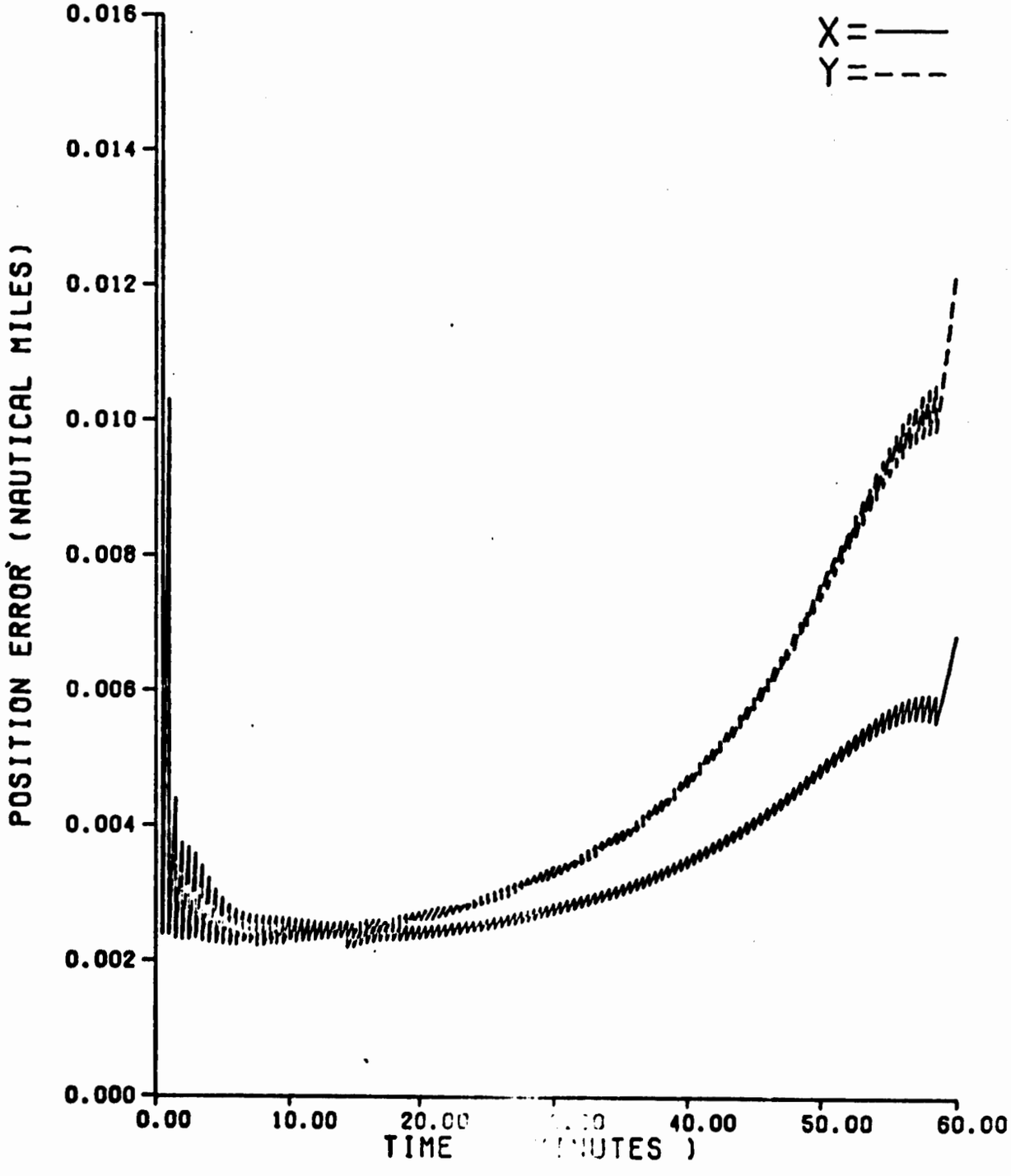

Fig. 47. Case One, Two Reset Segments, Position Error Diverges

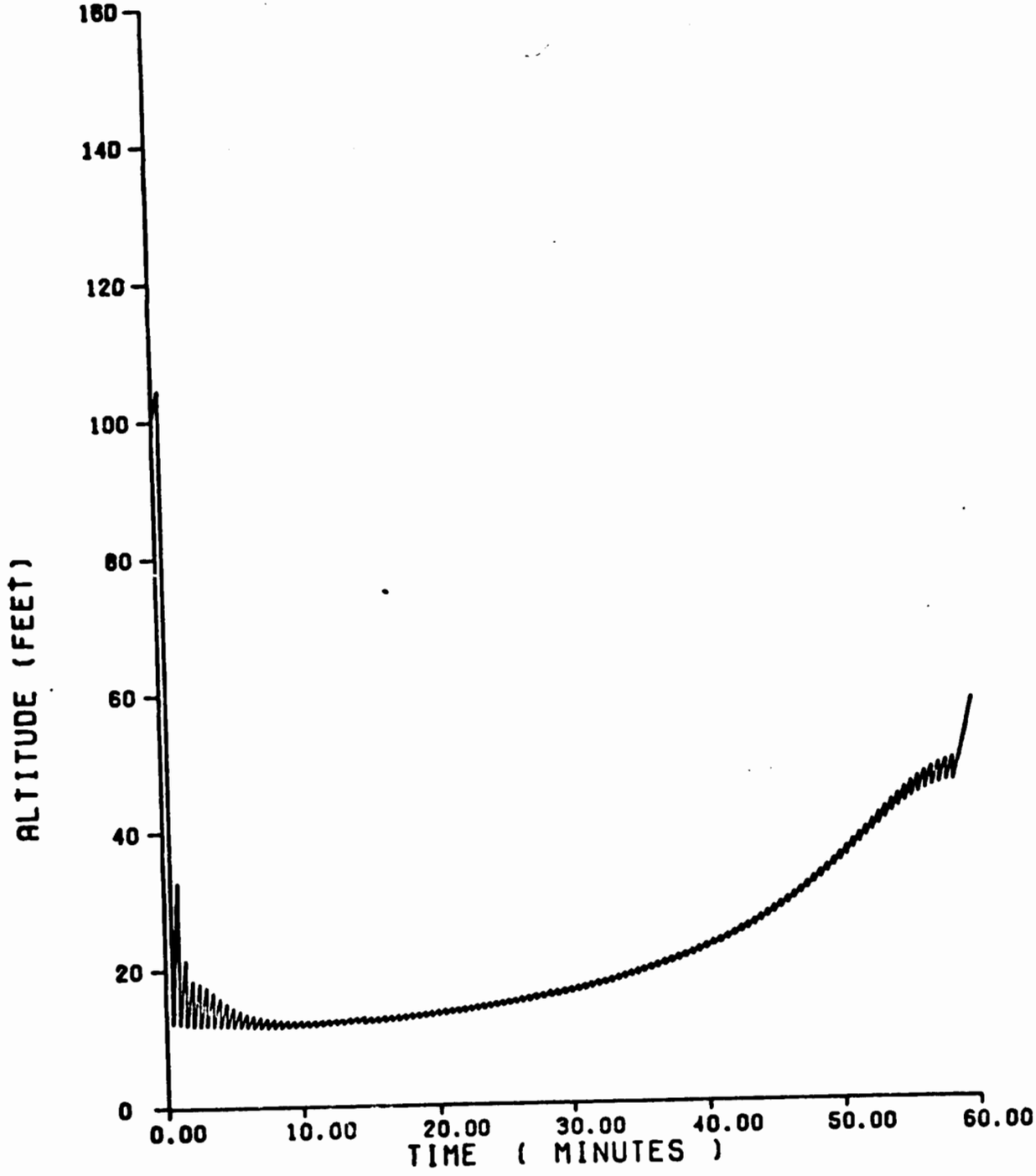

Fig. 48. Case One, Two Reset Segments, Altitude Error Diverges

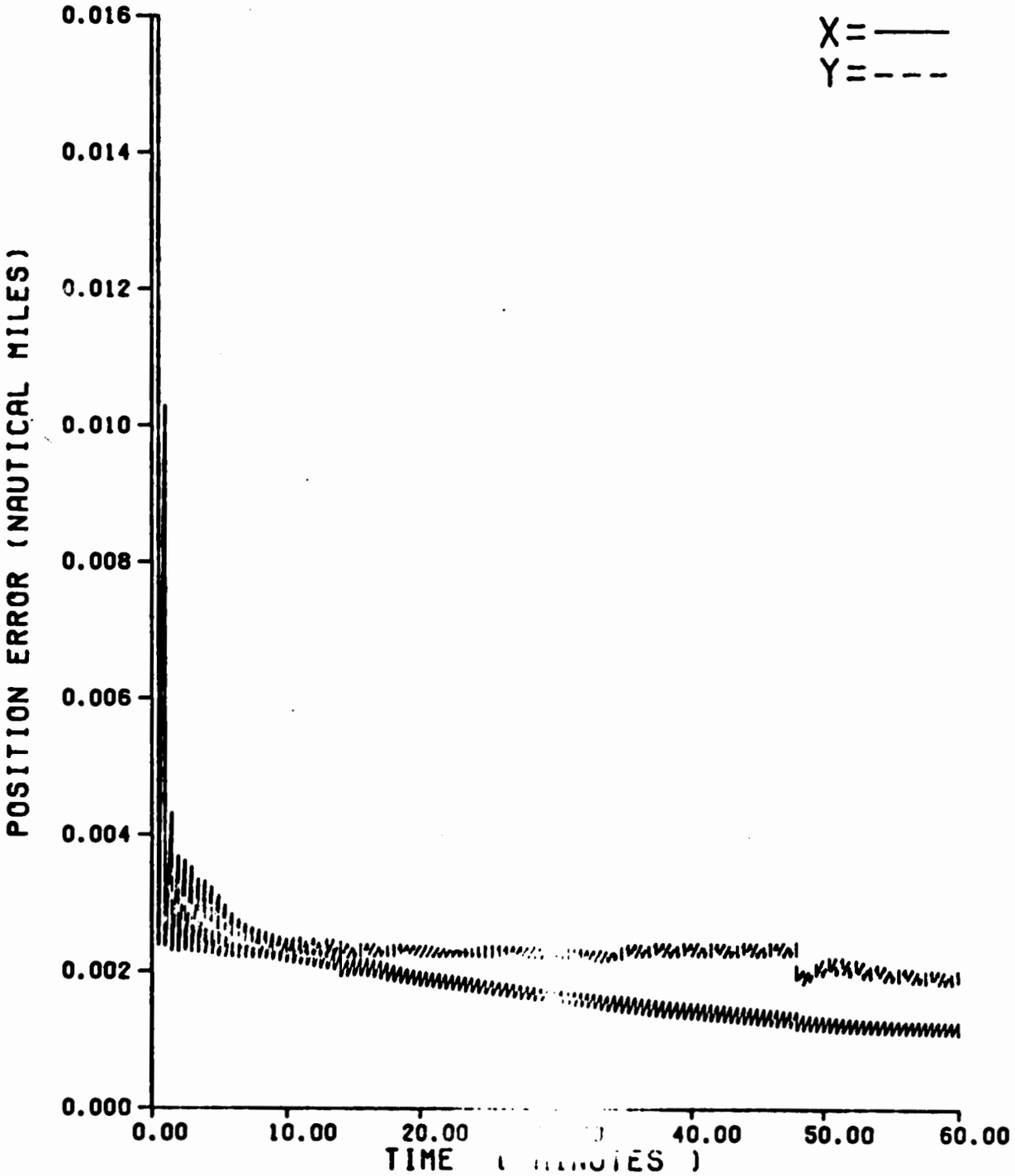

Fig. 49. Case Two, "Optimal" Set of Six Reset Segments, Position Error Does Not Diverge

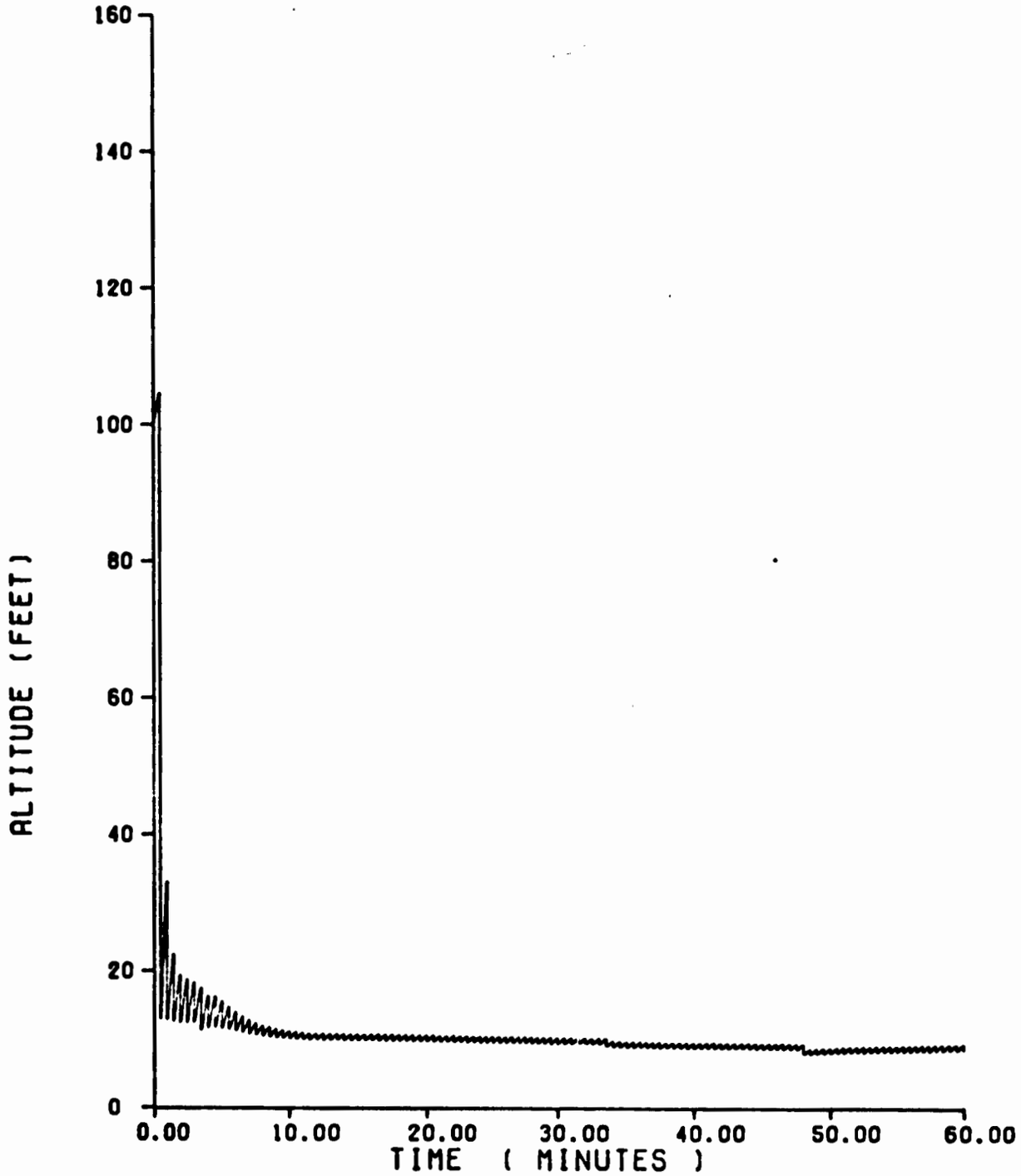

Fig. 50. Case Two, "Optimal" Set of Six Reset Segments, Altitude Error Does Not Diverge

one hour flight was used in the simulation work of Chapters VI and VII. Therefore, the divergent behavior illustrated in Figures 35 and 36 can probably be eliminated by obtaining measurements from a sequence of "optimal" sets of satellites. Incorporating this capability into the present covariance analysis program is an area suggested for future study.

VIII. Computer Simulation Programs

This chapter will outline the computer programs utilized in the simulation of an INI flight. The first section is a discussion of the State space Analysis of MUltisensor Systems (SAMUS) program. SAMUS was used in the early stages of this design study, and later abandoned in favor of a set of two computer programs which will be discussed in the second section. This second set of computer programs, consisting of a flight profile generator and a covariance analysis program, forms the analysis tool used in this study.

SAMUS

The first computer program utilized was the State space Analysis of MUltisensor Systems (SAMUS). This is a general purpose computer program for performing error analysis of cruise inertial navigation systems. SAMUS was developed and documented (kef 6) under a computer aided design effort funded by North American Rockwell Corporation.

The program was written to allow the user to perform analytical statistical error analysis of typical cruise system problems with little or no programming required. It has been preprogrammed to give the equations of motion, a master system description matrix, a master measurement matrix, and the error source statistics and coordinate frames which are normally used. In a typical cruise system utilizing a Kalman filter, estimation and control occur at short, regular intervals. This precludes specifying each control occurrence individually. Thus, the program was written so that the resets could be specified for segments. Each observable specified in a segment has an initial [illegible] time in the segment and is observed at a regular interval for the rest of the reset segment.

Cruise system problems require investigation of a variety of error source statistics. The SAMUS program allows the user to specify error statistics ranging from a constant to a second order noise. The program has the system distribution matrices of the typical cruise error sources preprogrammed. The user can specify required error sources by means of an error source code list (Ref 6:1-2).

However, the program was not designed to provide the necessary measurement error sources that are needed for the problem undertaken in this report. In the system under investigation the measurements are taken from satellites. A model of a clock was necessary for the user and each satellite. A major modification of the program would have been required to model the error sources for these clocks. Also, the computational burden of SAMUS was prohibitive; for example it required approximately one hundred and forty thousand octals of computer memory and six hundred seconds of computer time to perform the calculations for a simplified 22 state filter pass. It was for these reasons that a more adequate and efficient program was needed for this investigation.

Computer Program Final Selection

A combination of two separate computer routines was adopted to perform the required analysis of this report. The first program is a flight profile generator. This program, given the necessary initial conditions, computes the parameters of the flight profile. This information is then stored in a permanent file. The second program is a general covariance program. This program propagates the system and filter state variable covariances forward in time by numerical integration techniques, reading from the flight profile the values for aircraft latitude,

longitude, altitude, range, velocity, acceleration and satellite position information. These values are calculated in the flight profile generator at the time instant corresponding to the numerical integration step size of the general covariance program. The filter covariances are propagated forward until the update time is reached. The system is then propagated forward to the update time. Because the filter and the system are propagated in a parallel manner requiring duplicate information, two identical flight profiles were generated. Logic was incorporated in the general covariance program to read data from the first flight profile for the filter propagation and from the second flight profile for the system propagation. By precalculating the flight profile and storing the data, computer memory and time were saved.

Profile Generator. The flight profile generator (PROFGEN) was written to compute the position, velocity and acceleration of a point mass that is moving above the earth's surface. The user must supply the program initial values for position, attitude, and velocity plus commands to turn, fly straight, change heading in sinusoidal fashion, accelerate or decelerate. The program puts out position data including latitude, longitude, altitude and range from the earth's center and velocity and acceleration data in the North-West-Up navigation coordinate frame. Additionally, the flight profile generator was modified to calculate the latitude, longitude, in-view criterion, and unit vector components for each of the 27 satellites at every specified integration time step. This portion of the flight profile generator comprises the satellite motion generator discussed in Chapter III.

The investigation undertaken in this report used one of the two straight flight options available in the program. This option was a

sector of a great circle path around the earth. The great circle path varies the heading angle to maintain flight in a fixed plane passing through the earth's center. This option was used with a constant velocity for a straight and level flight of one hour duration. Table IX specifies the values for the flight profile used in this investigation.

Table IX

Flight Profile

Initial Head	45°
Initial Latitude	30°N
Initial Longitude	75°W
Altitude	10,000 ft.
Velocity	600 mph
Duration of Flight	60 minutes

Note that the above parameters must first be projected onto the navigation frame (for example, $\underline{V}^n = [V_x, V_y, V_z]^T$) before they are utilized in the problem solution.

The input data that the user supplies to execute this program specifies the initial conditions, the flight maneuvers of the aircraft, and the method of solution of the differential equations. The program uses a NAMELIST data input format that permits the entry of character strings consisting of parameter names with their values in the user's choice of format specification. Two NAMELIST input lists are used, PRDATA and PASDATA. The PRDATA (Problem Data) list is called at the start of each problem. This list contains nine problem parameters, all of which must be specified and none of which change during execution of the problem. The purpose of these parameters is to specify all initial conditions.

Values from the PASDATA (Path Segment Data) list are called at the start of each path segment. This contains twelve path parameters that specify the maneuver to be followed in a segment and the method of integration to use. A problem may be divided into a maximum of 20 path segments (Ref 13:1-5).

General Covariance Program. The second program used in this investigation was a general covariance program. This program propagates the system and filter state variables forward in time by numerical integration techniques. There are four subroutines in this program that the user must modify for the particular system under study. The first subroutine to be modified (FLMAT) supplies the filter matrix elements. Each non zero element of the F matrix is input as either a constant or a function of time. A set of indices for each non-zero element is then specified. The indices are used to locate the numbered elements in the F_f matrix, for example; the element A(4) may have indices 3,4 which would locate it in the third row and the fourth column of the F_f matrix. The H_f matrix was specified the same way.

The system matrix (SYSMAT) is the second subroutine to be modified. This routine is set up the same as FLMAT, specifying only the non-zero elements of the F_s and H_s matrices.

The next subroutine to be changed is Trajectory (TRAJ). This subroutine is called at each integration time instant and reads the flight profile information from one of the two permanent files, depending on the type of pass being made, filter or system. The profile generator provides the values for aircraft latitude, longitude, altitude, range, velocity, acceleration and satellite position information. The angular rates and angular accelerations of the coordinate frames which are used

to form the Pinson error model are then calculated using this information. This data was placed in a labeled common statement so that it could be used in the other subroutines requiring these values.

The last subroutine to be modified is User Input (USRIN). The values for Q and R are specified for both the filter and the system. This information was also placed in a labeled common statement so that the values could be used in FLMAT and SYSMAT subroutines.

This program proved to be much more efficient than SAMUS. The 22 state filter that was executed using SAMUS required approximately one hundred and fourty thousand octals of computer memory and six hundred seconds of computer time. The general covariance program required only forty-five thousand octals of memory and two hundred seconds of computer time to execute the same 22 state filter pass. The efficiency of this program comes primarly from the fact that it only performs operations on the non zero elements of the F, H, Q, and R matrices. This saves computer memory as well as execution time. For example, the forty-four state system model would require nineteen hundred octals of memory for the entire F_s matrix. However, there were only seventy-three non zero elements in this matrix. This resulted in a savings of over eighteen hundred octals of memory.

Covariance Plotting Program. Once the general covariance program has calculated the diagonal elements of the covariance for each state at a particular time instant, they are read into a permanent file. The plotting program reads these values from this file and prepares them for off-line plotting. This information is then placed on a magnetic tape and can be plotted at any time. This program plots the RMS error versus time for the system and the filter over the sixty minute flight profile.

The program is capable of plotting the RMS values on a regular linear scale or a log scale.

A brief description of the computer tools used in this investigation was presented in this chapter. It was shown that the computational burden of the original computer program (SAMUS) was prohibitive. The programs used in the final analysis proved to be much more efficient. A listing of these programs was not included in this report because of their extensive length.

IX. Conclusions and Recommendations

Conclusions

Based on the material presented in this thesis, as well as knowledge gained throughout this study, the following conclusions are drawn:

1. The 15 state filter vector consisting of nine INS error states, two user clock errors, and four satellite clock errors, provides the best performance tradeoff between high accuracy and low computational time.

2. The 15 state filter with weak coupling terms removed from the Pinson INS error model provides almost identical performance as the fully-coupled filter for this particular flight profile. This simplification results in a substantial reduction of the computational burden on the user's computer.

3. Measurement rates of once every 5, 15, 30, 60, or 90 seconds all provide satisfactory filter performance (depending upon the user's requirements). The slower update rates provide slightly larger RMS errors, on the average, and allow more error build-up between measurements.

4. Frequent changing of satellite observables so that measurements are taken from "optimal" sets of satellites (as explained in Chapter VII) prevents divergence of the error states in the latter part of the flight.

5. The vertical velocity and altitude errors are the most difficult to control. Use of an altimeter in conjunction with the filter should eliminate this divergent tendency.

6. Acceptable accuracy of the INS errors is obtained in this study using only range measurements. The simulation results suggest

that inclusion of range-rate measurements could possibly increase the filter accuracy (especially in the velocity errors).

7. Finally, it should again be emphasized that this type of covariance analysis is very sensitive to (a) the arbitrary initial conditions of the covariance matrix P(0) (in the initial transient portion), (b) erroneous system reference models, and (c) the dynamics of the flight profile.

Recommendations

The following recommendations are made for continued study in the subject area of this thesis and for improvement of the existing computer program:

1. Incorporation of an altimeter into the filter and system should provide more effective control of the vertical velocity and altitude errors. This would require the addition of two or three INS plant error states in both the reference system and the filter state variable vector. Additionally, this would add one equation to the system and filter set of measurement equations.

2. Inclusion of an accurate linear model of the ionospheric delays would improve the reference system's accuracy in describing the "real world" problem. A model applicable to the non-synchronous satellite case might be derived through modification of the ionospheric delay model presented in Reference 1 for the synchronous case.

3. The effect upon filter performance of including range-rate measurements should be investigated. A comparison with the usage of only range measurements could then be drawn. Use of satellite bearing measurements might also be studied.

4. An optimal sequencing scheme should be developed to automatically select the best satellites from which to take measurements of those in-view. (In our simulation, satellites were selected from prior knowledge of the flight profile). This would also require building into the computer simulation programs the capability of multiple reset segments (such as in SATUS).

5. Another area of interest would be comparison of sequential versus simultaneous measurements. For example, a sequential measurement scheme might take single measurements from satellite number one at t = 15 seconds, satellite number two at t = 30 seconds, satellite number three at t = 45 seconds, and satellite number four at t = 60 seconds. This sequence would then be repeated throughout the reset segment. The performance of such a filter could then be compared with one such as in this thesis where measurements and updates are performed with four satellites simultaneously. This comparison is of interest primarily because of the increased cost of equipment required to perform simultaneous measurements and computations as compared to the sequential case.

6. Various flight profiles (for example a "figure 8") should be simulated to investigate the dynamic effects of climbing, driving and turning upon the filter design of this thesis.

Bibliography

.vionics

2. Maybeck, P. S. The Kalman Filter, An Introduction for Potential Users. TM-72-3. Wright-Patterson Air Force Base, Ohio: Air Force Flight Dynamics Laboratory, 1972.

3. Meditch, J. S. Stochastic Optimal Linear Estimation and Control. New York: McGraw-Hill, 1969.

4. Maybeck, P. S. Kalman Filtering Applied to Inertial Systems. Course Notes from EE 7.35, Air Force Institute of Technology, Wright-Patterson Air Force Base, Ohio, 1972.

5. "A Short Course on Kalman Filter Theory and Application." The Analytic Science Corporation, Reading, Massachusetts, 1971.

6. Osborn, R. F. and I. J. Dotterer. SAMUS A Program for State Space Analysis of MUltisensor Systems. California: Autonetics Division North American Rockwell, 1971.

7. Battin, R. H. Astronautical Guidance. New York: McGraw-Hill, 1964.

8. Synge, J. L. and B. A. Griffith. Principles of Mechanics. New York: McGraw-Hill, 1959.

9. Leondes, C. T. Guidance and Control of Aerospace Vehicles, New York: McGraw-Hill, 1963.

10. Asher, R. B. and R. M. Reeves. Performance Evaluation of Sub-Optimal Filters. Unpublished. Wright-Patterson Air Force Base, Ohio: Air Force Avionics Laboratory, 1972.

11. Clarke, A. B. and R. L. Disney. Probability and Random Processes for Engineers and Scientists. New York: John Wiley and Sons, Inc., 1970.

12. DeVries, T. W., et al. Inertial Navigation System Mechanization for Fast Reaction At-Sea Alignment. Contract No. N00163-70-C-0054. California: Autonetics Division North American Rockwell, 1970.

13. Musick, S. A Users Guide to Profgen, A Flight Profile Generator. Unpublished. Wright-Patterson Air Force Base, Ohio: Air Force Avionics Laboratory, 1973.

Appendix A

Ten State Filter Plots

Plots of the RMS values of the nine INS plant error states are presented in Figures 51 through 59 of this appendix. The structure of this 10 state filter is detailed in Chapter VI. These plots illustrate the effect of eliminating too many states from the filter state variable vector

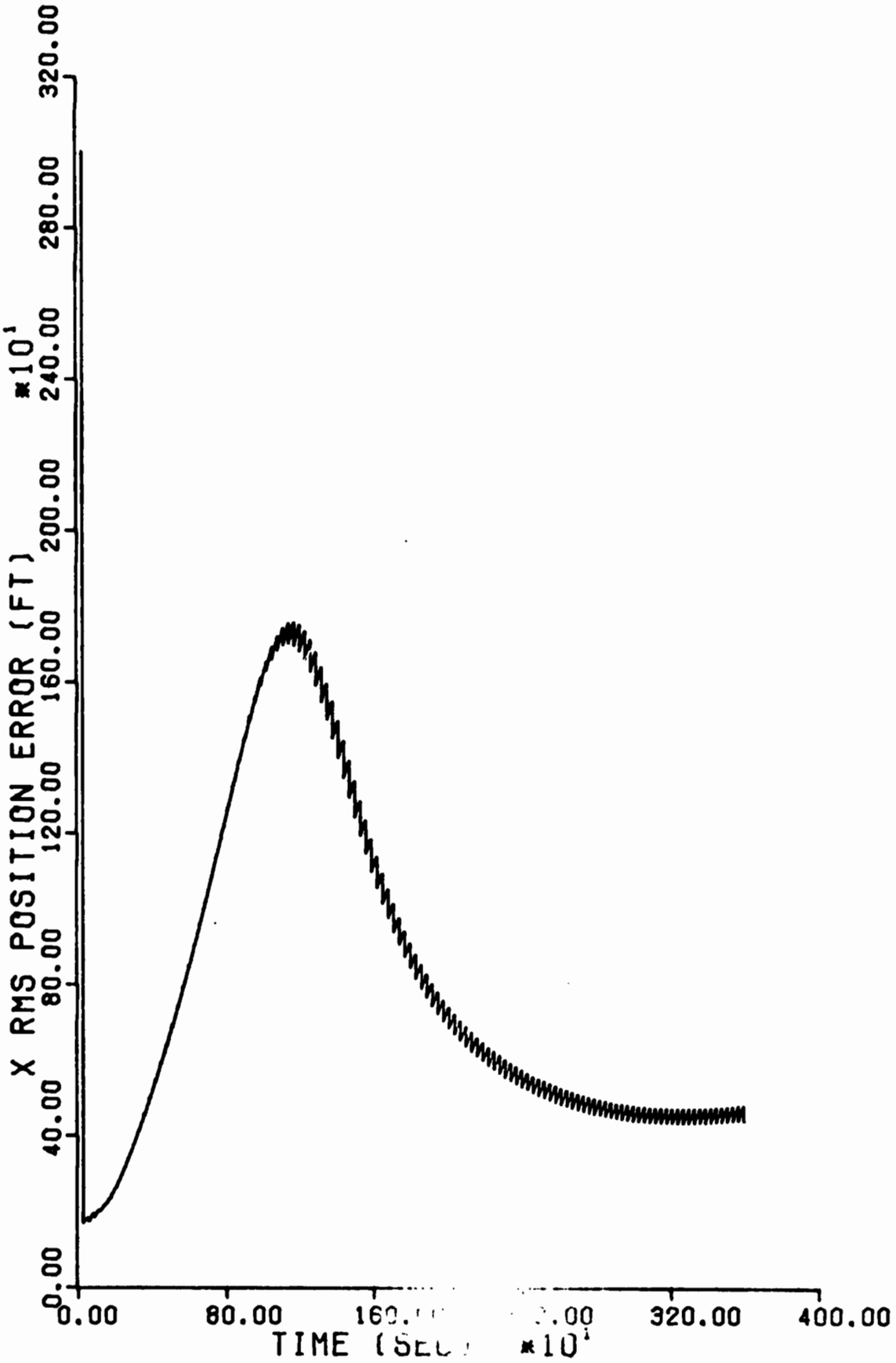

Fig. 51. 10 State Filter, x Position Error

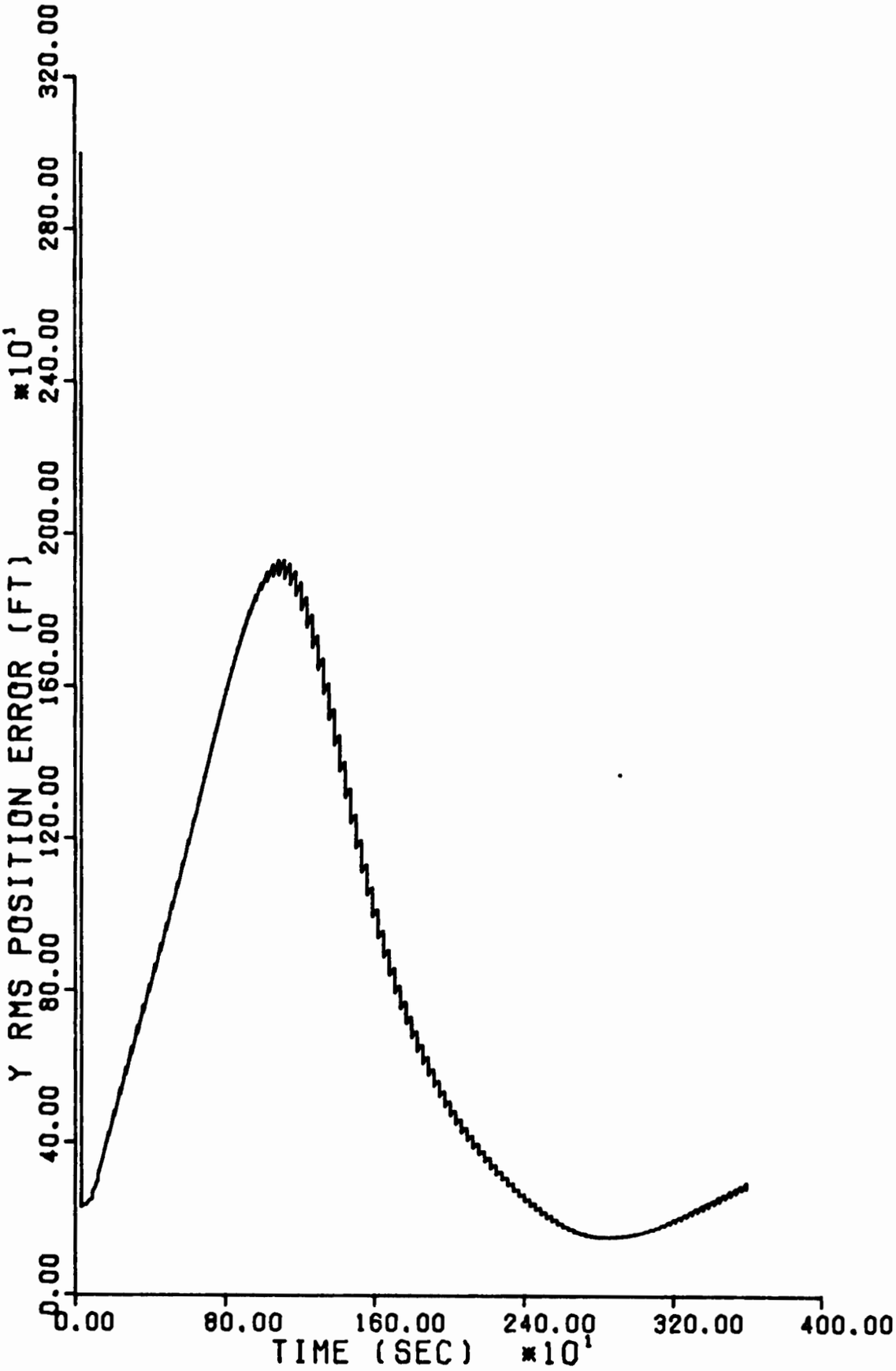

Fig. 52. 10 State Filter, y Position Error

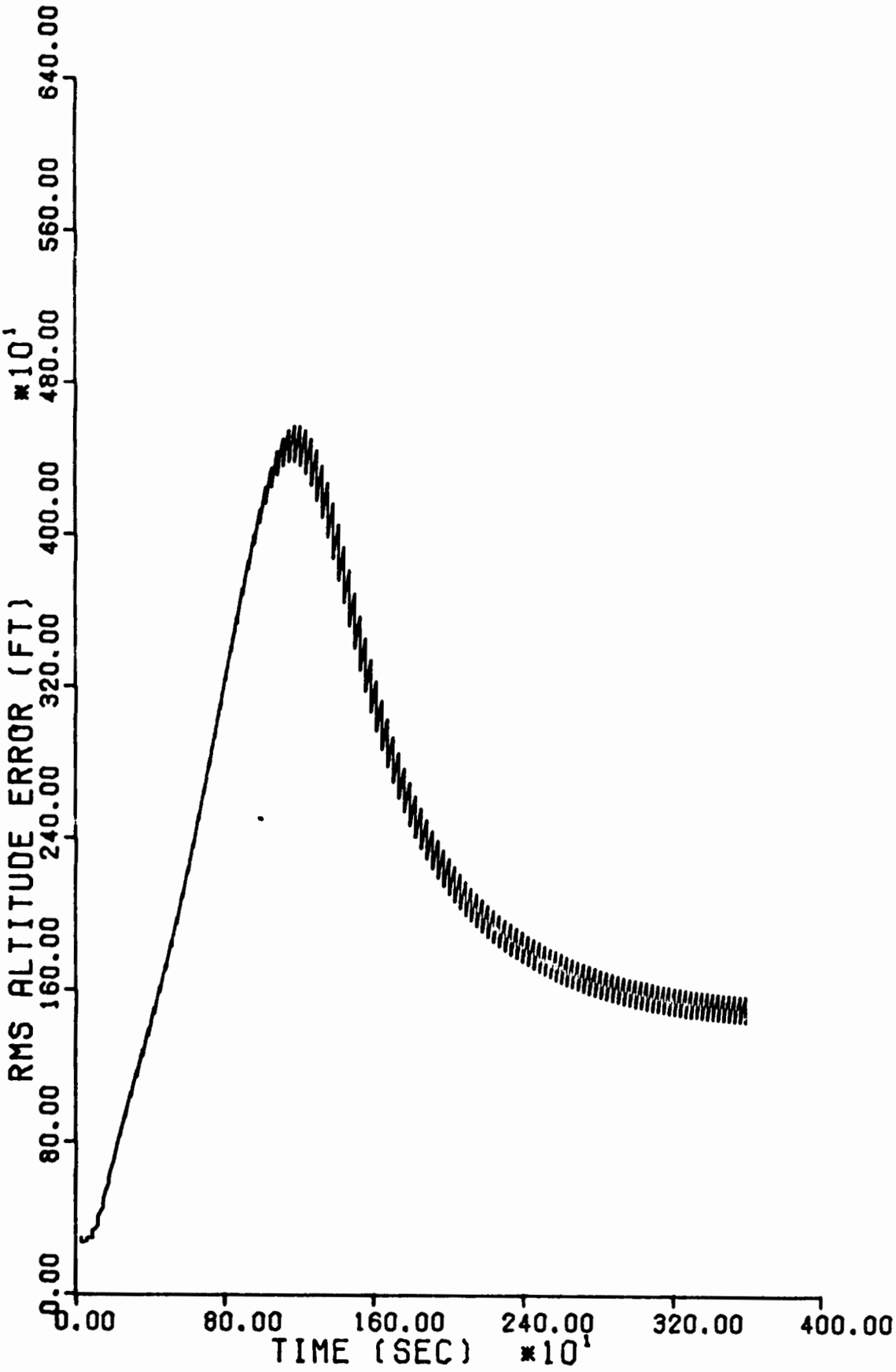

Fig. 53. 10 State Filter, Altitude Error

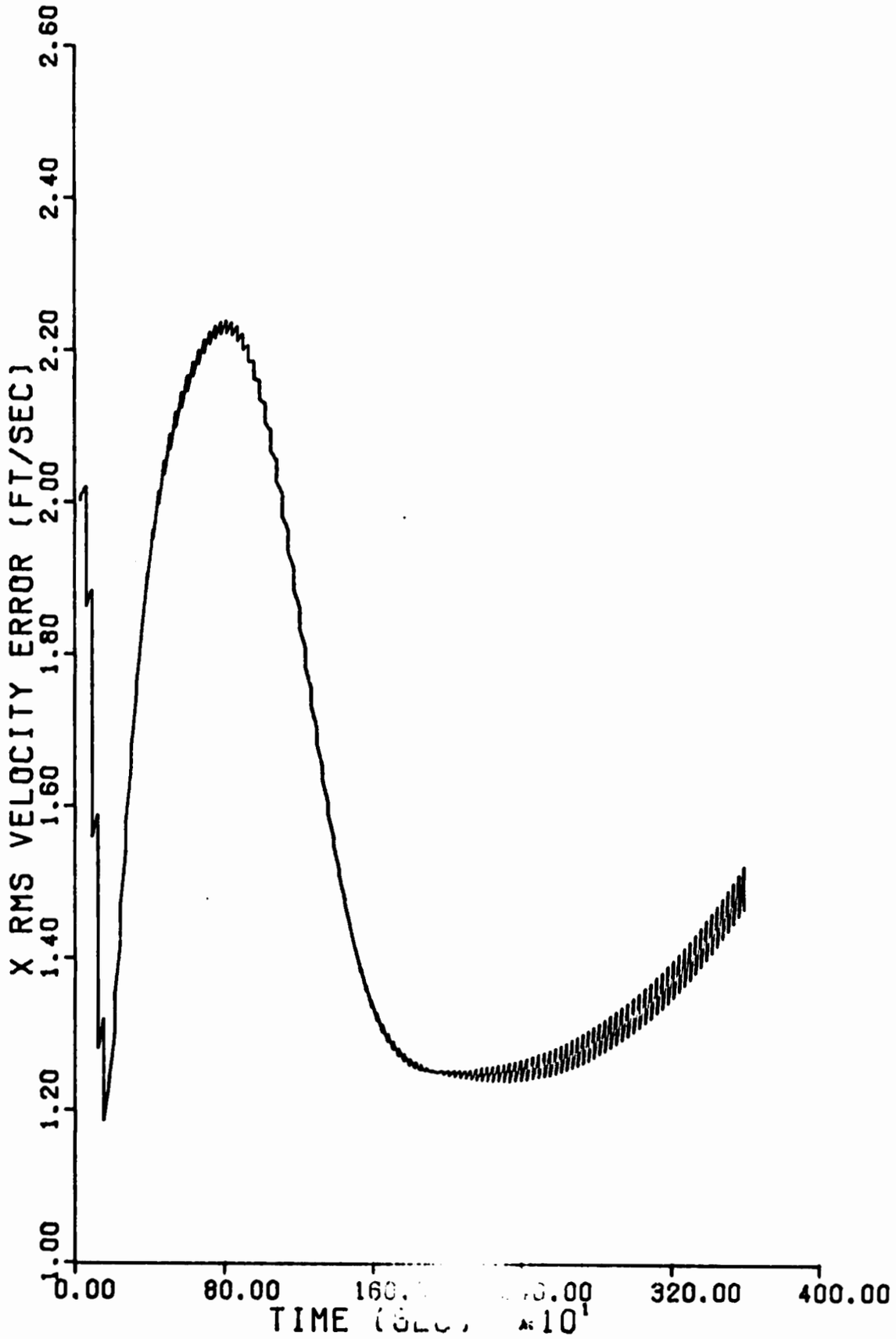

Fig. 54. 10 State Filter, x Velocity Error

Fig. 55. 10 State Filter, y Velocity Error

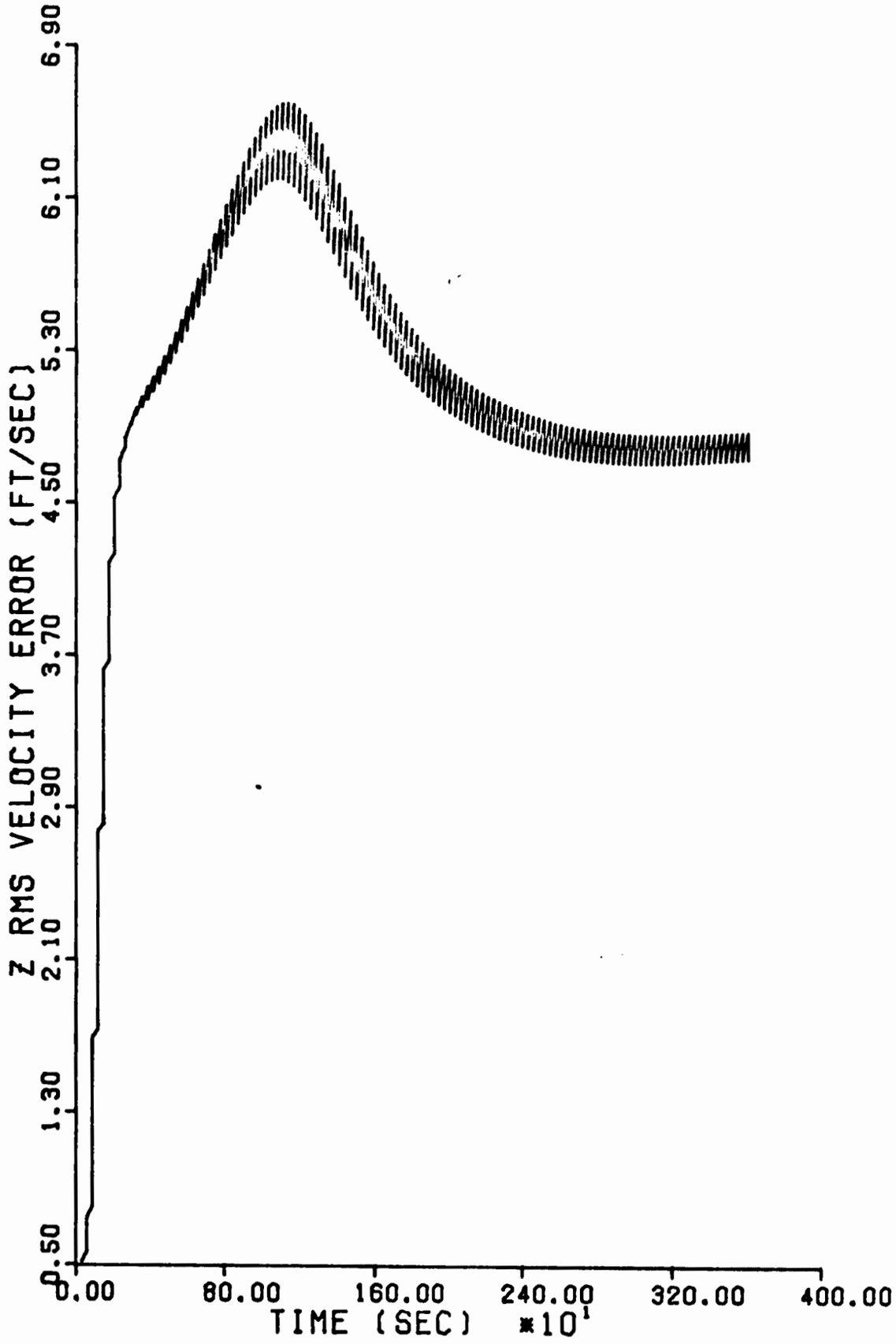

Fig. 56. 10 State Filter, z Velocity Error

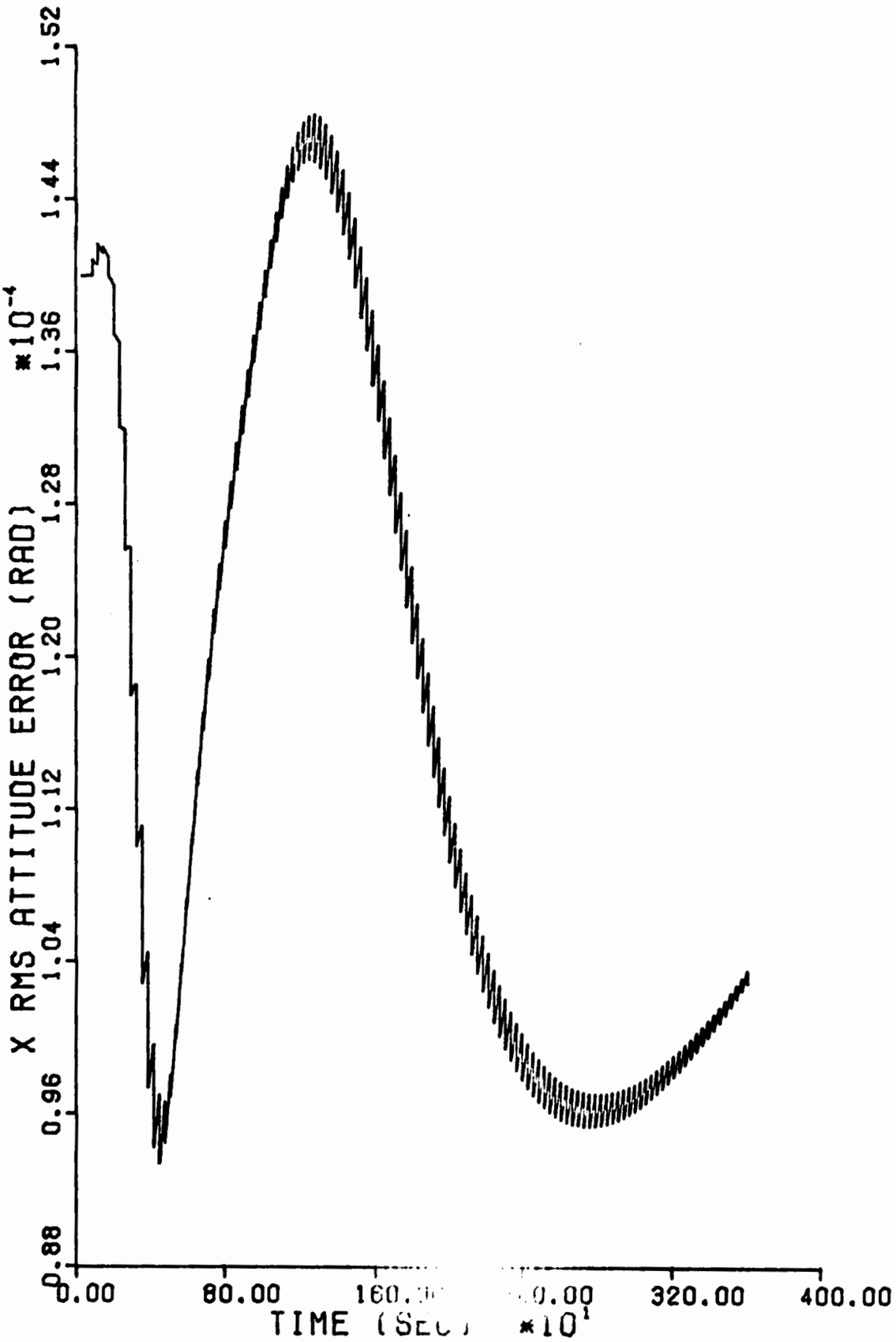

Fig. 57. 10 State Filter, x Attitude Error

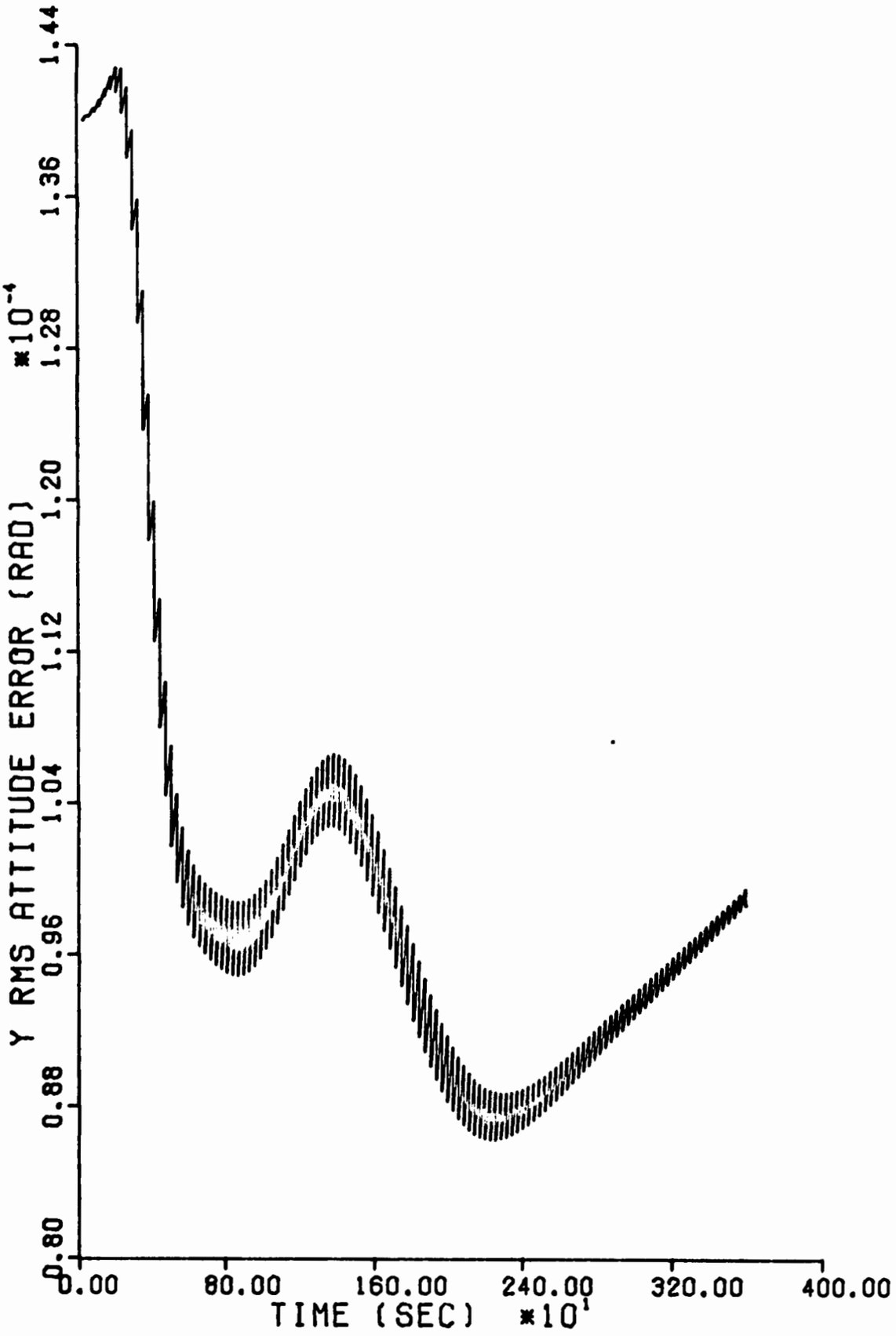

Fig. 58. 10 State Filter, y Attitude Error

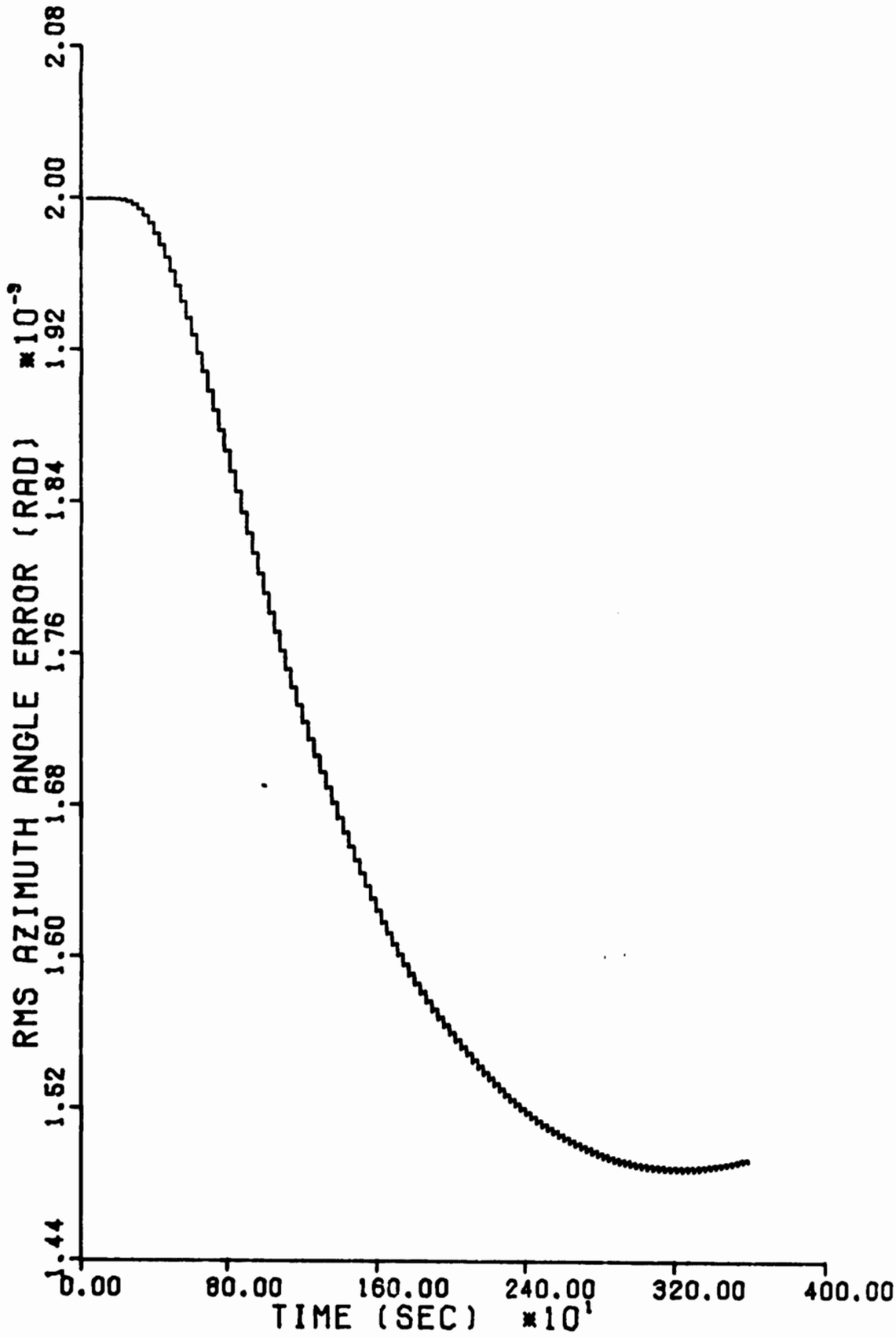

Fig. 59. 10 State Filter, Azimuth Error

Appendix B

Plots of the Plant Error States at Specified Update Rates

The plots contained in this appendix are the remaining six plant error states at the various update rates from Chapter VII. The plots on the following pages are as follows: y position error with update rates of 5 seconds, 15 seconds, 60 seconds, and 90 seconds are shown in Figures 60 through 63, Altitude error with the same rates are shown in Figures 64 through 67, x and y velocity error in Figures 68 through 75, x attitude error in Figures 76 through 79, and azimuth error in Figures 80 through 83.

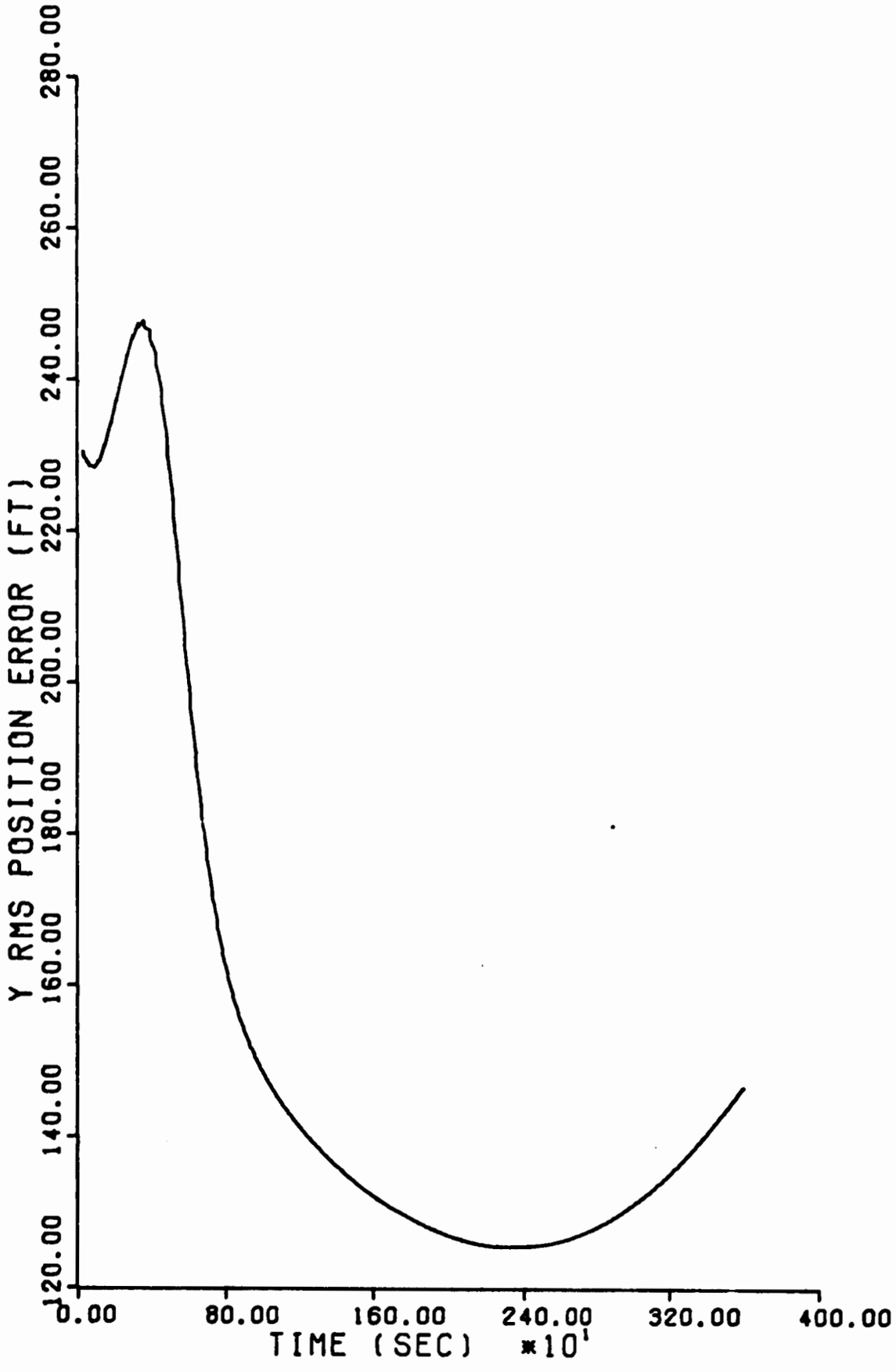

Fig. 60. y Position Error, 5 Second Update Rate

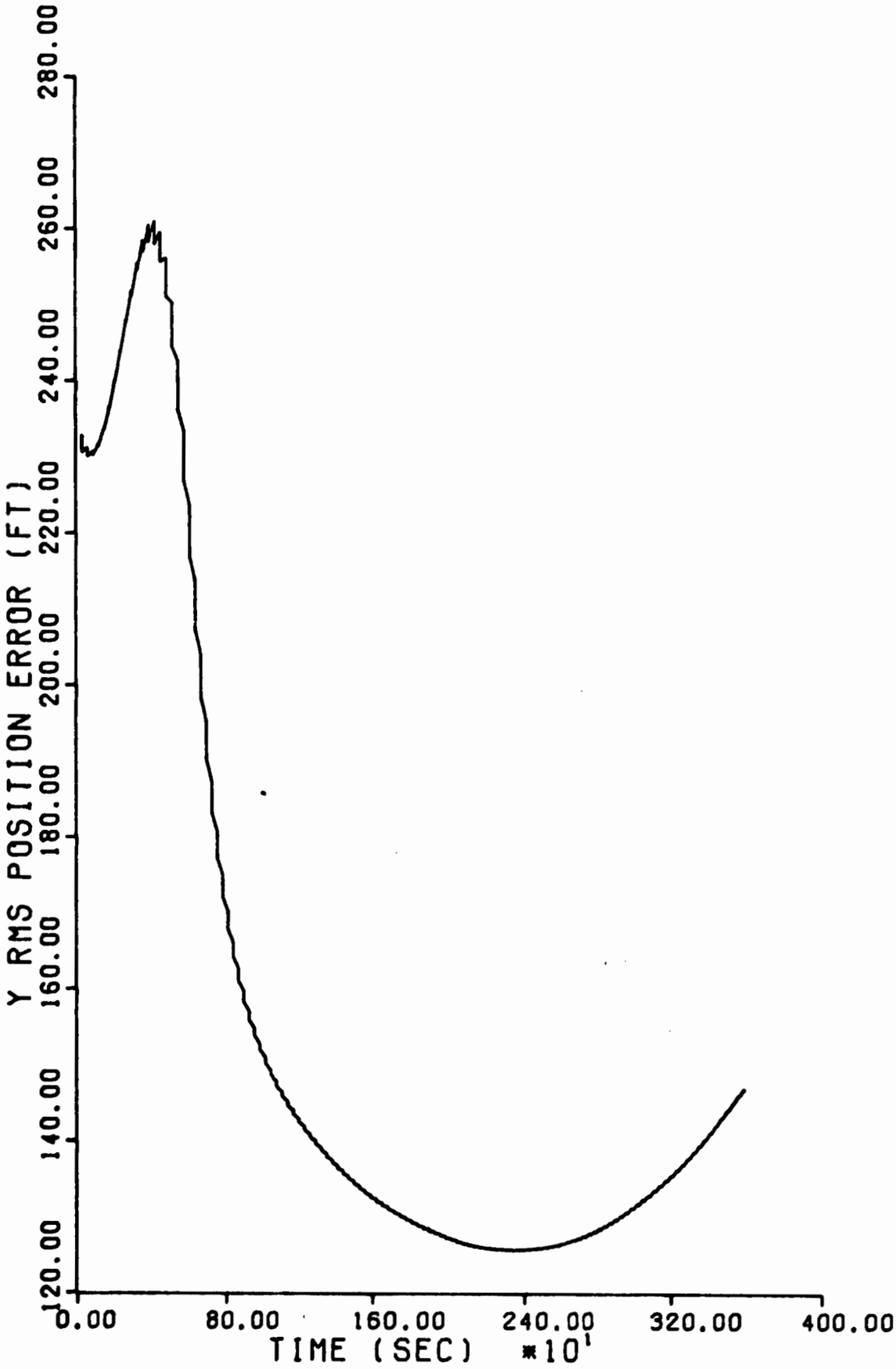

Fig. 61. y Position Error, 15 Second Update Rate

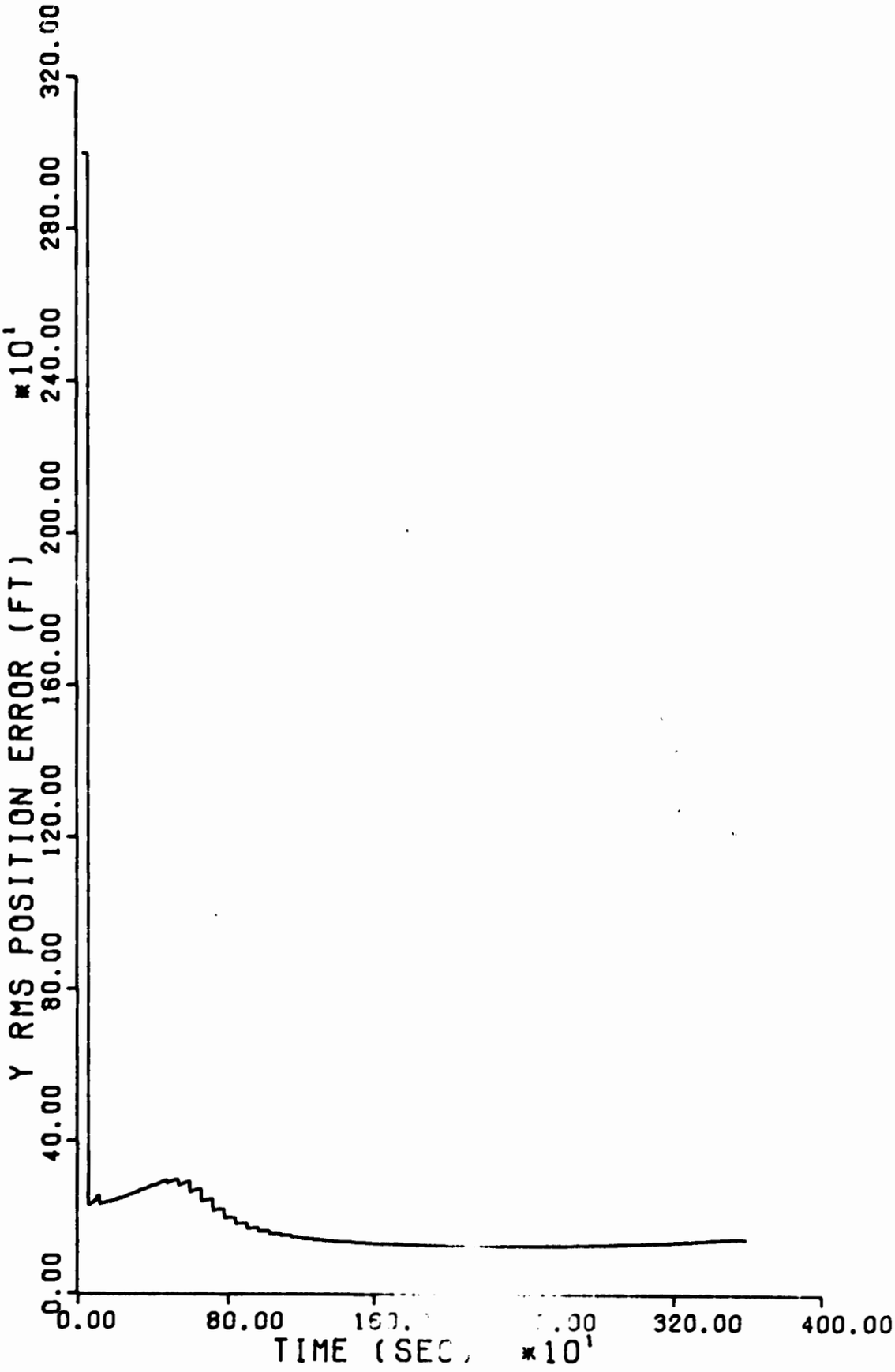

Fig. 62. y Position Error, 60 Second Update Rate

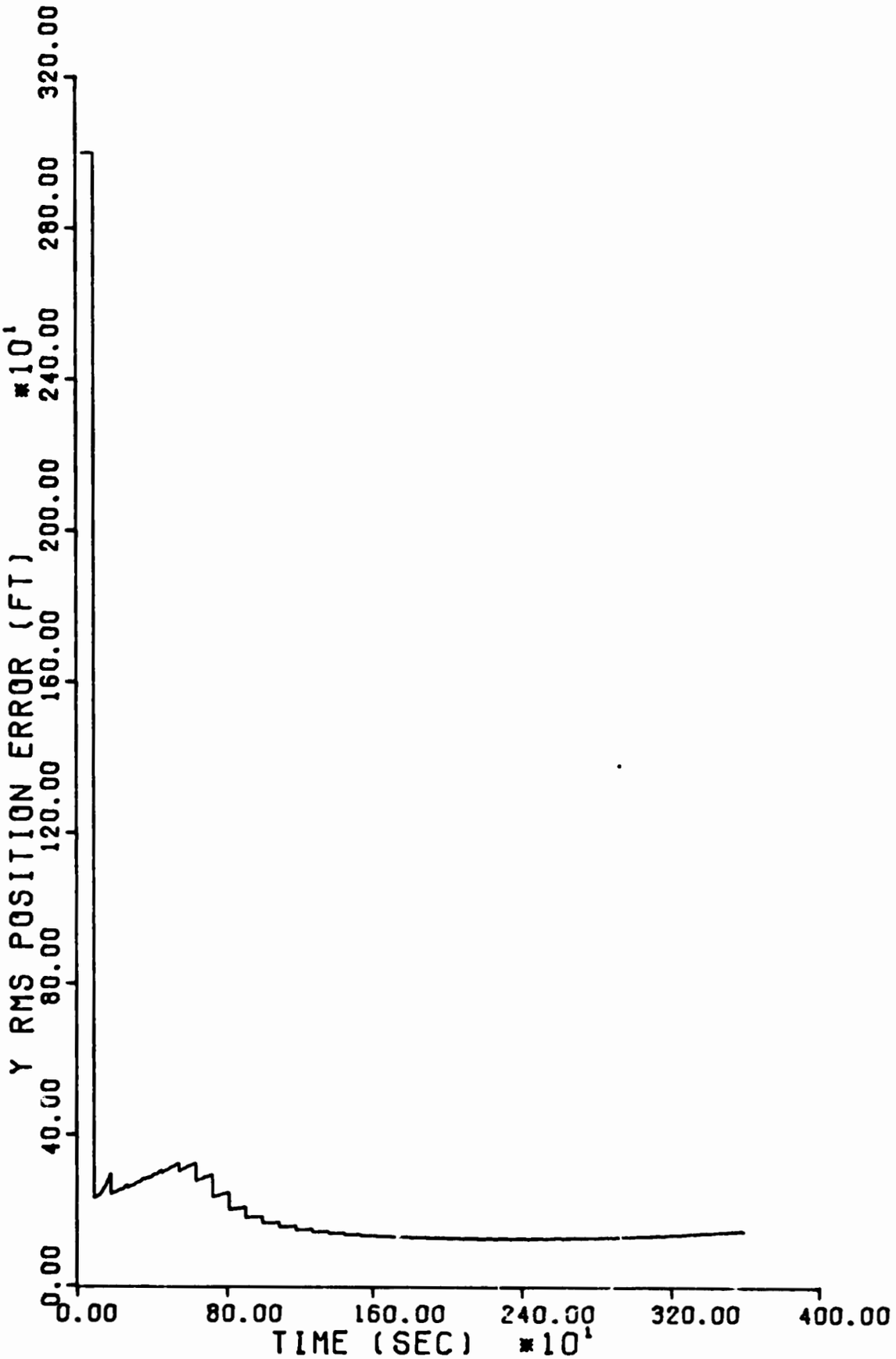

Fig. 63. y Position Error, 90 Second Update Rate

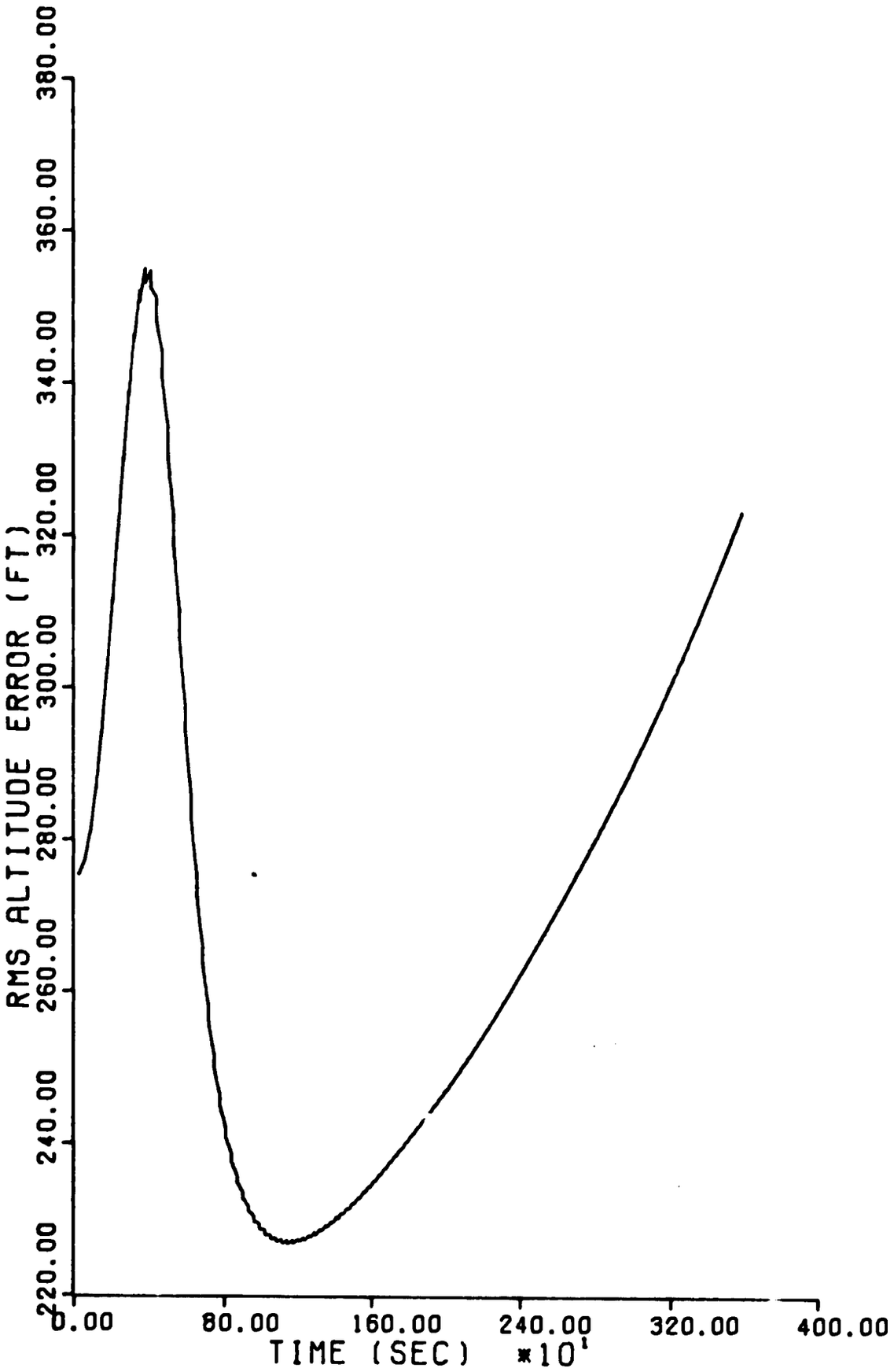

Fig. 64. Altitude Error, 5 Second Update Rate

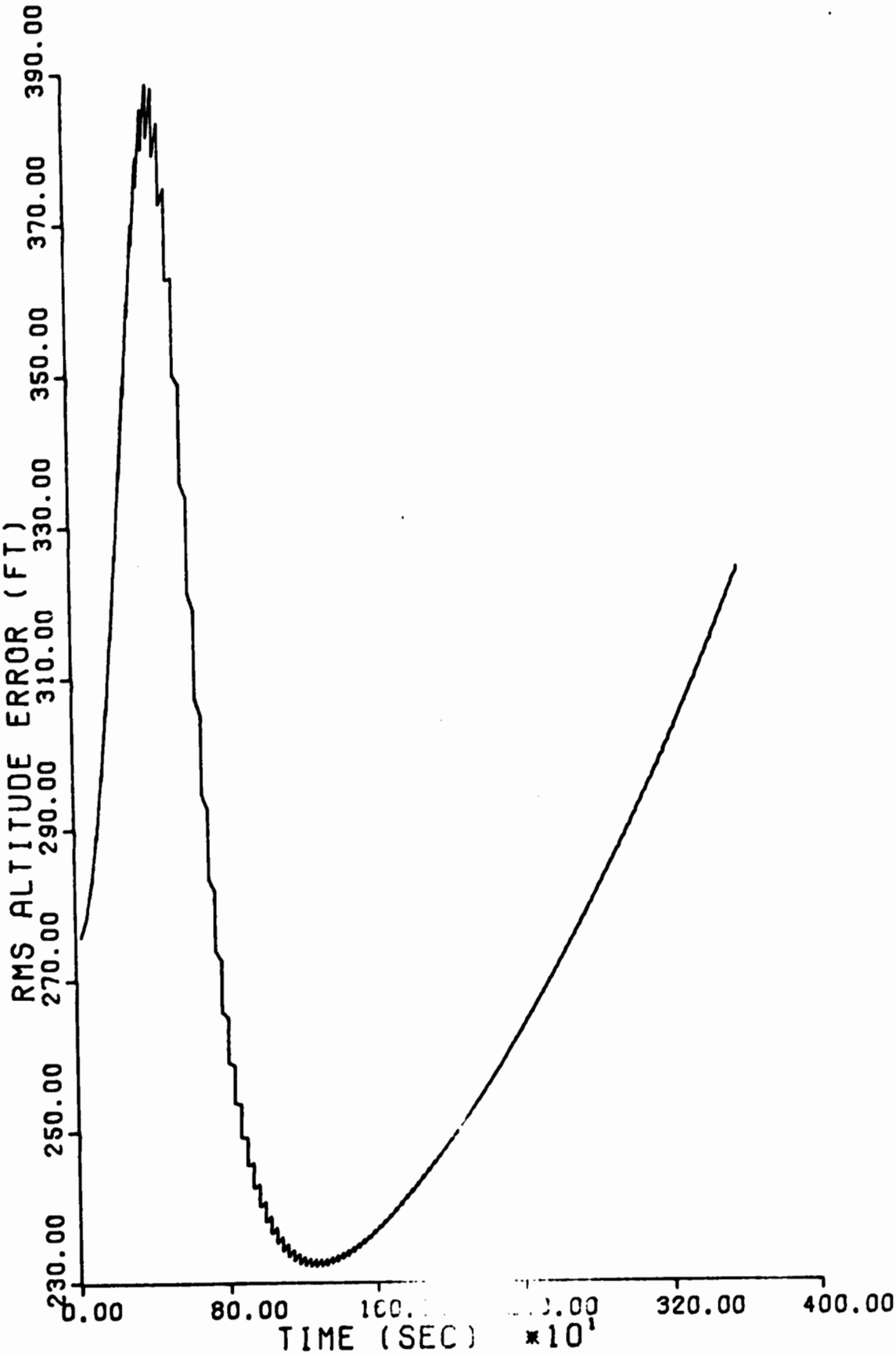

Fig. 65. Altitude Error, 15 Second Update Rate

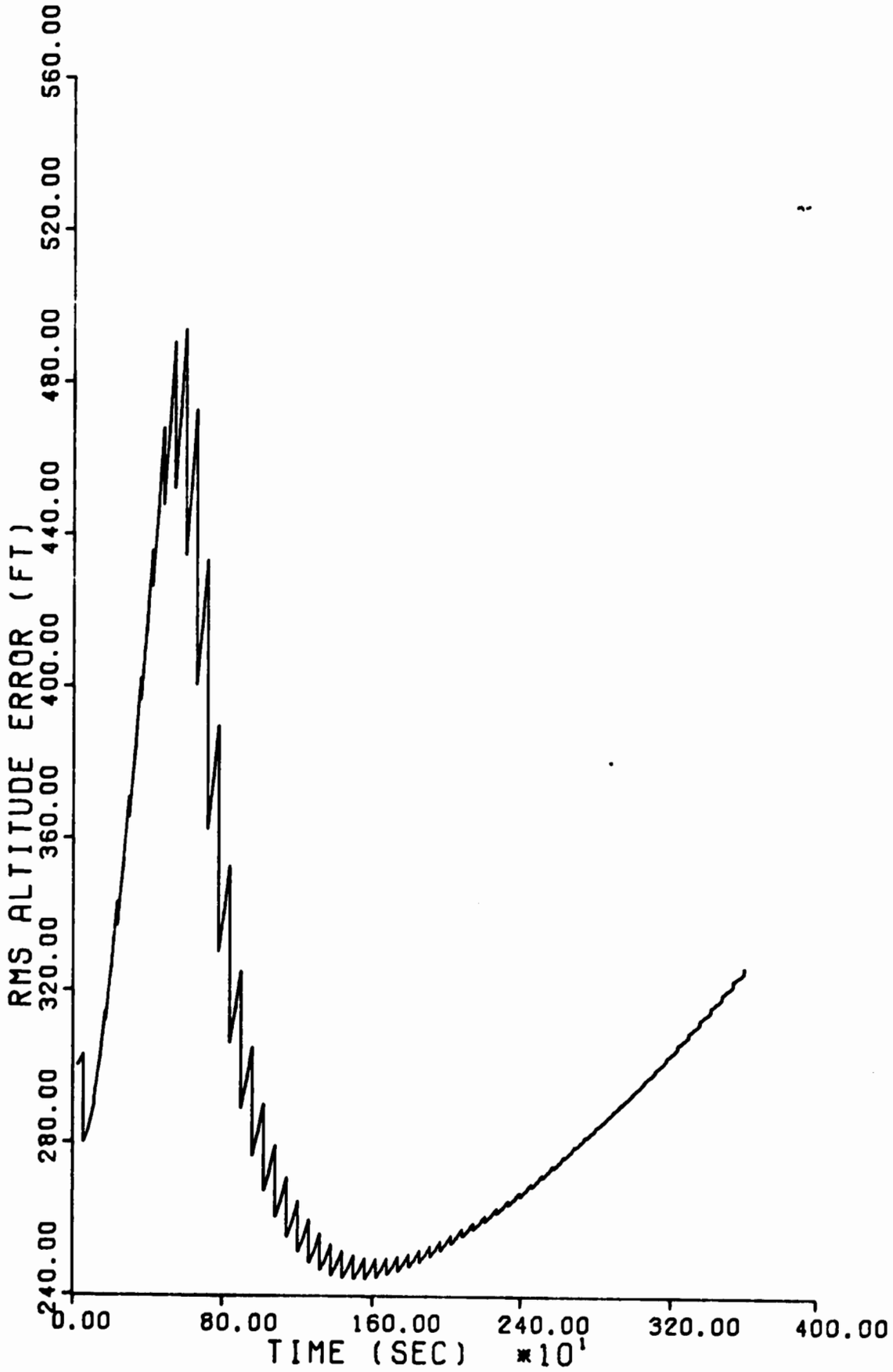

Fig. 66. Altitude Error, 60 Second Update Rate

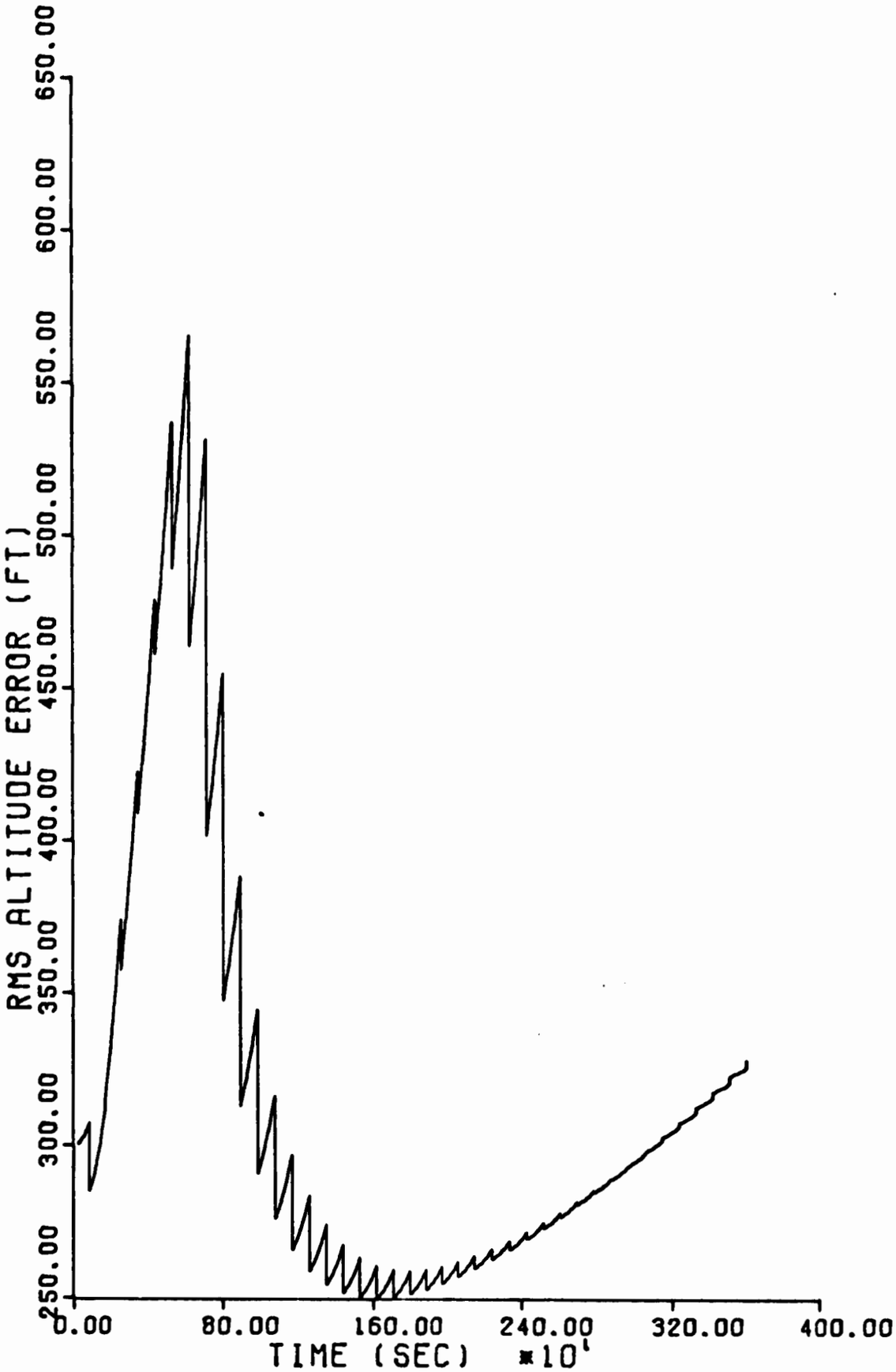

Fig. 67. Altitude Error, 90 Second Update Rate

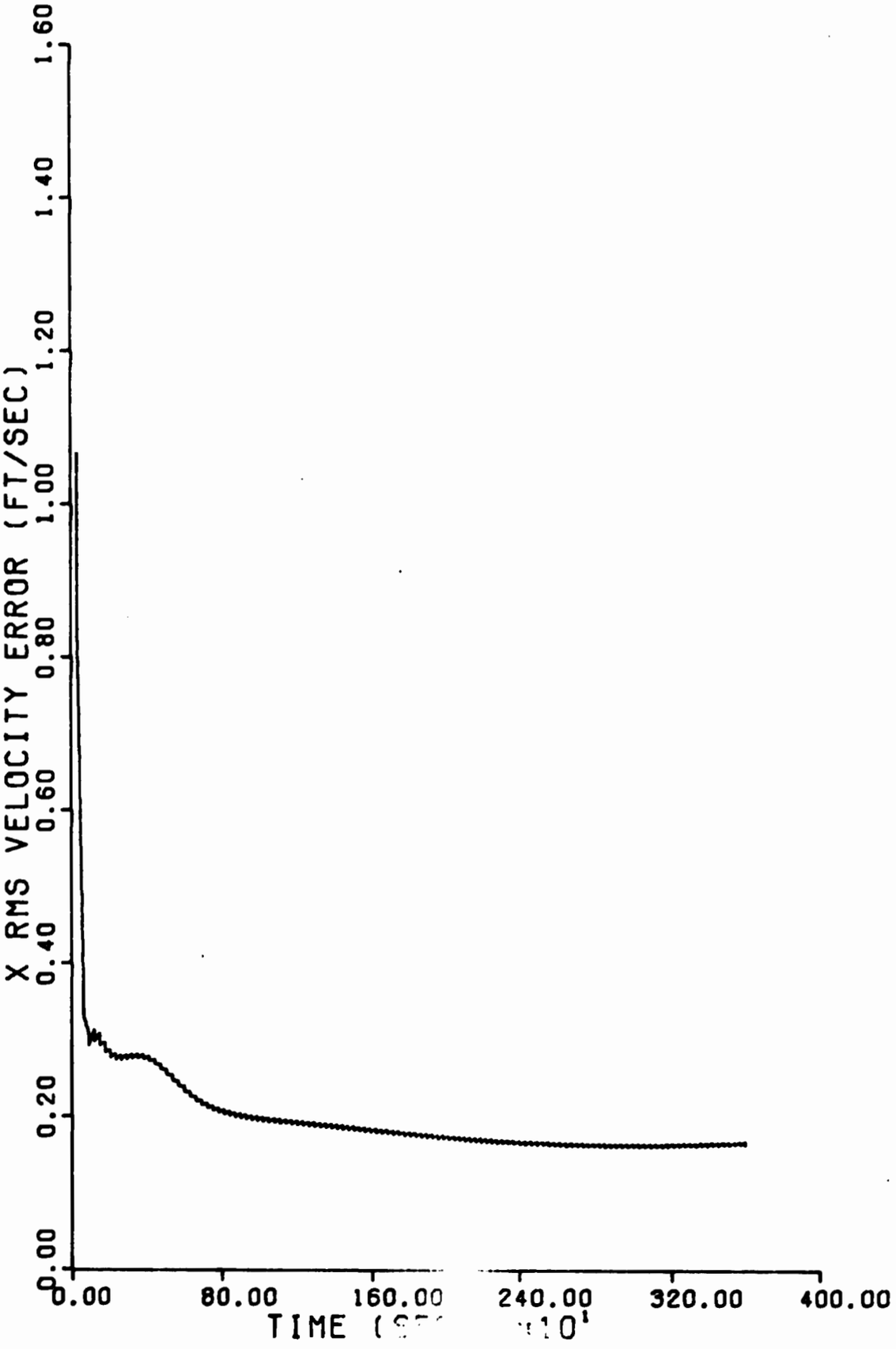

Fig. 68. x Velocity ..or, 5 Second Update Rate

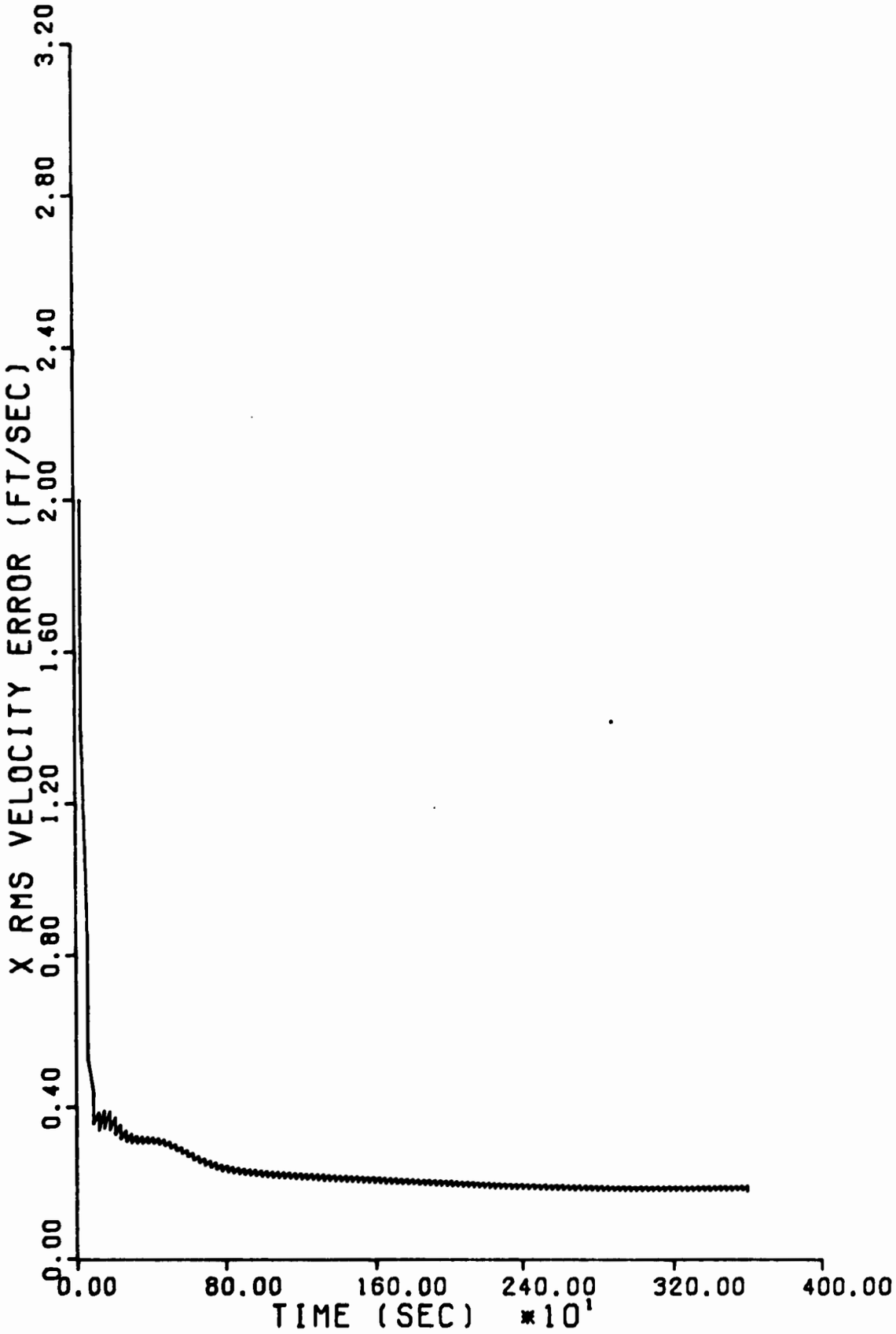

Fig. 69. x Velocity Error, 15 Second Update Rate

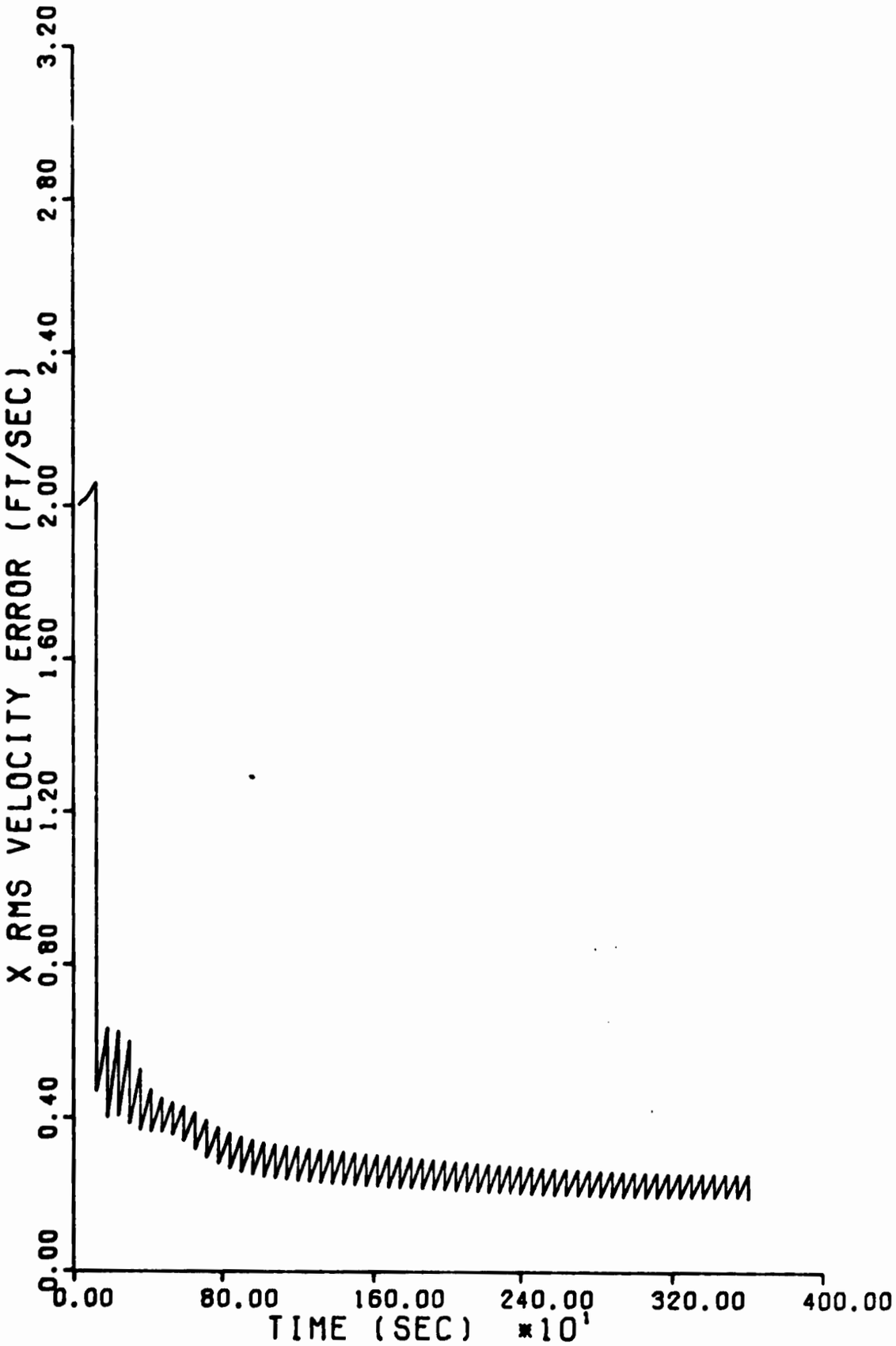

Fig. 70. x Velocity Error, 60 Second Update Rate

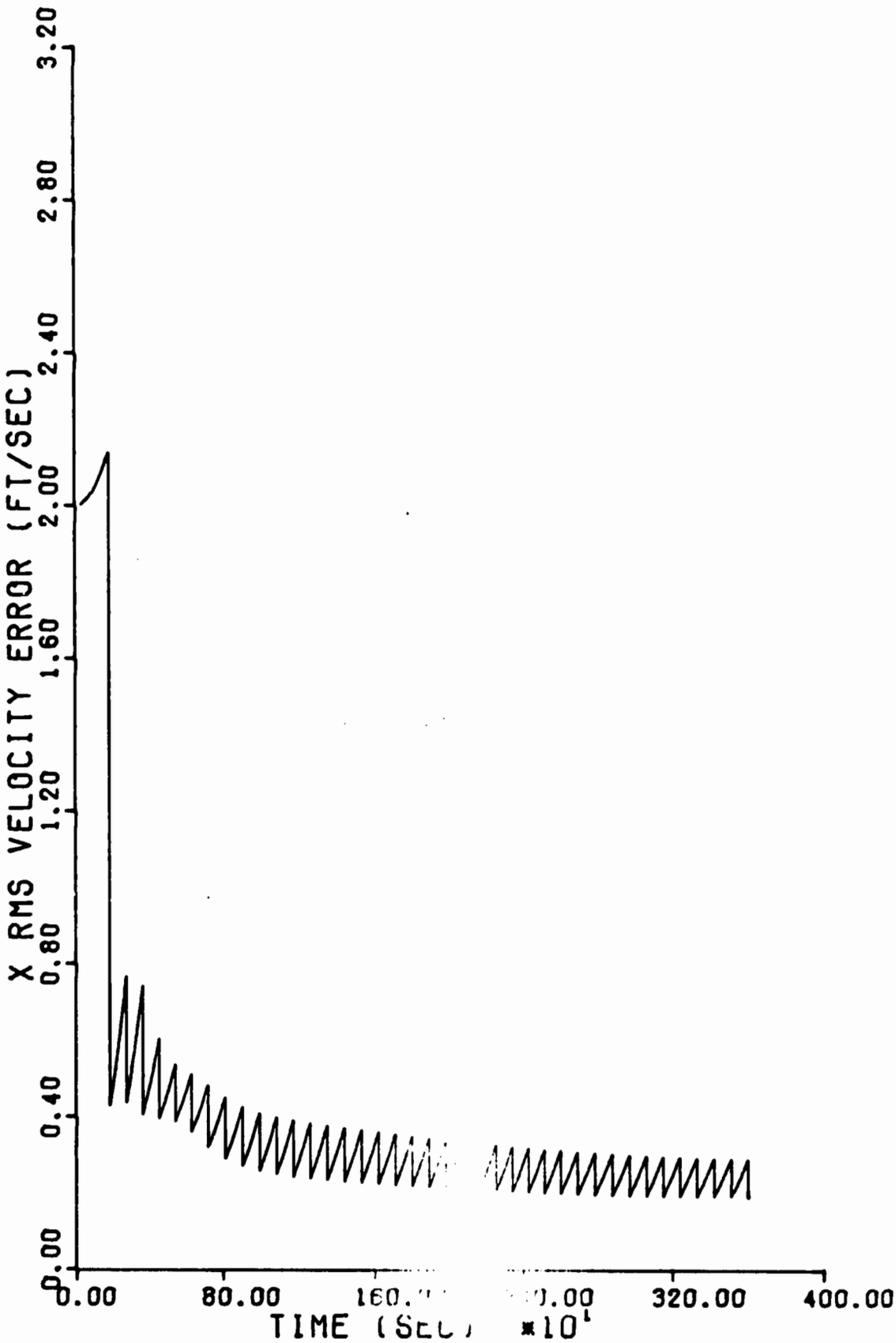

Fig. 71. x Velocity Error, 90 Second Update Rate

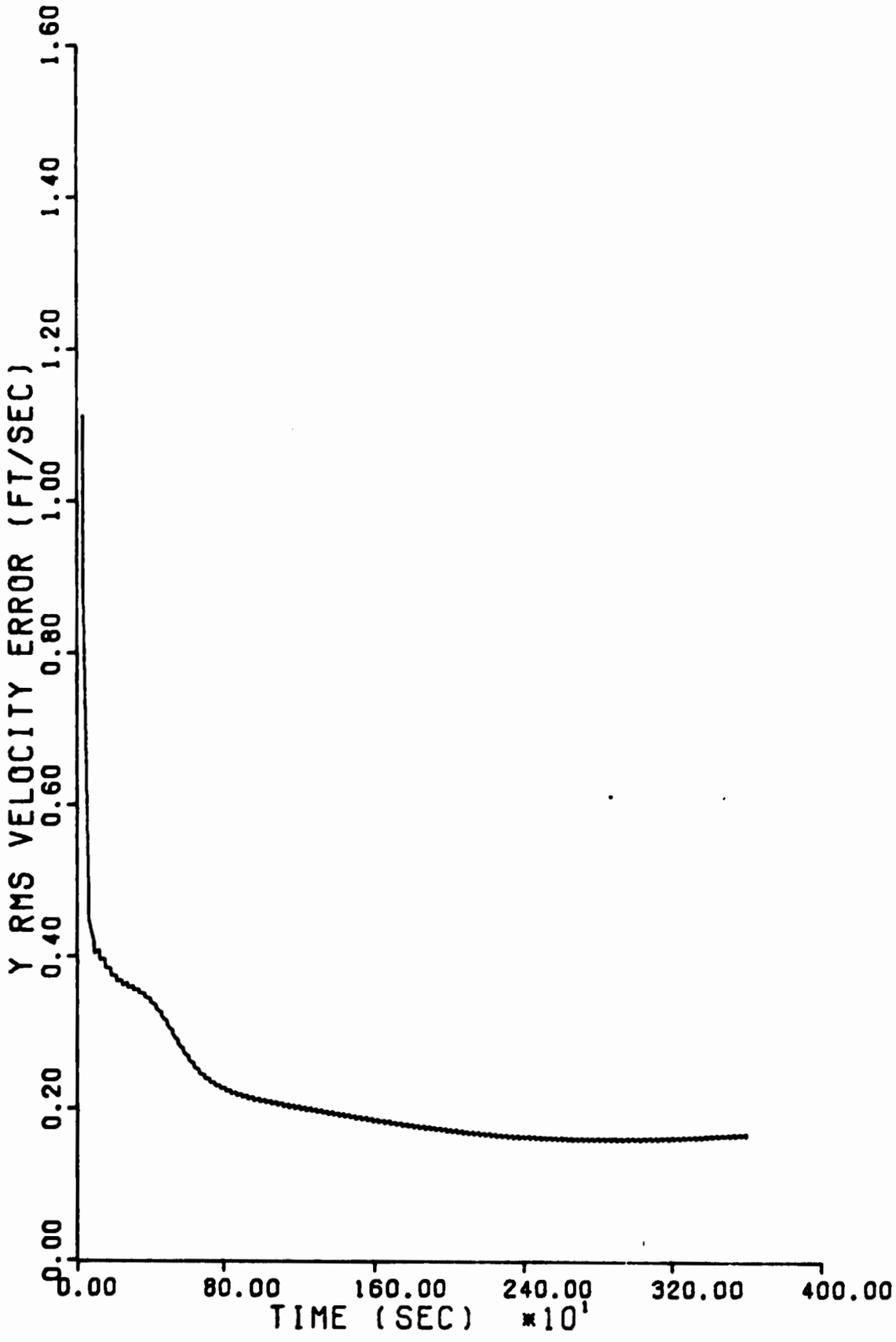

Fig. 72. y Velocity Error, 5 Second Update Rate

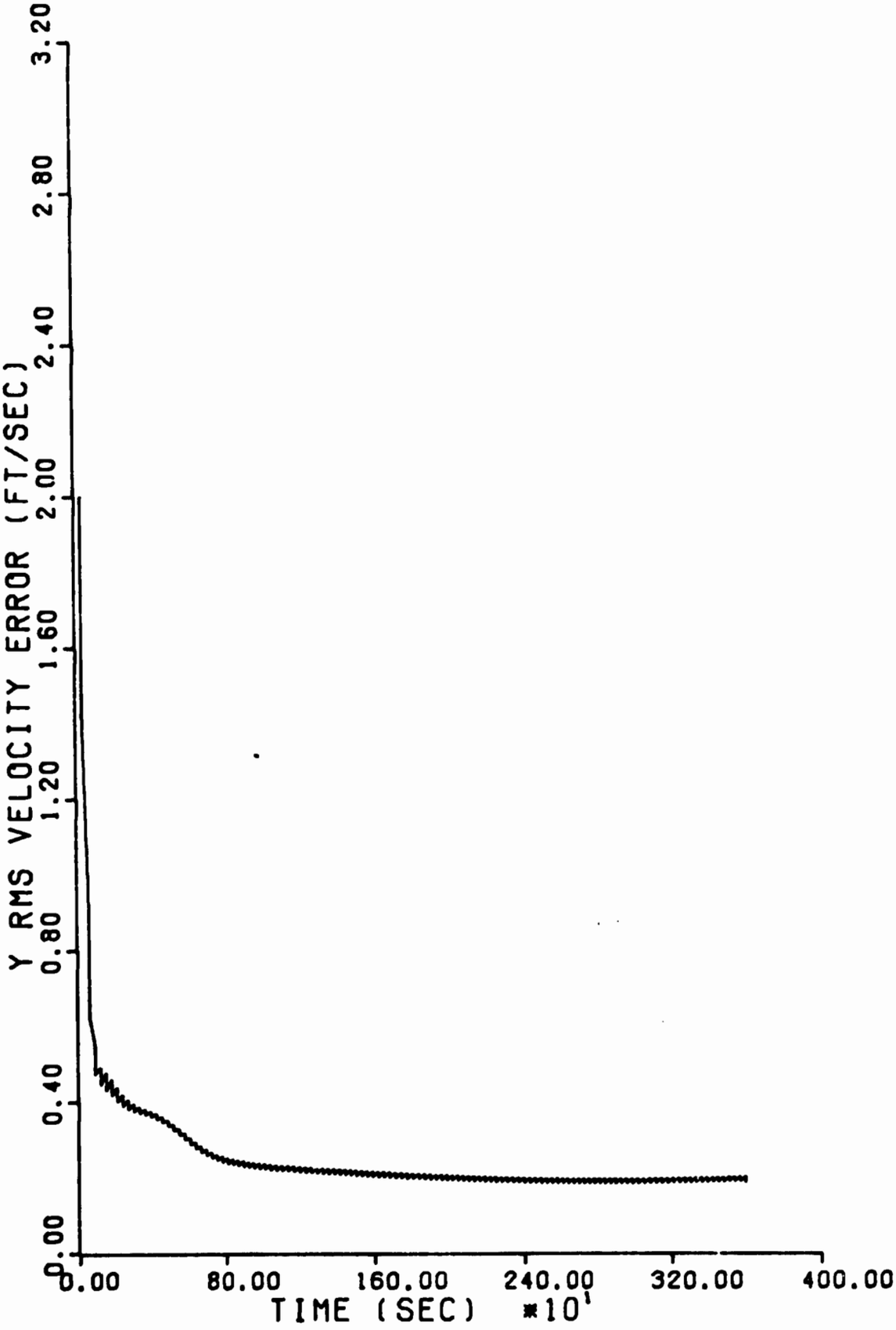

Fig. 73. y Velocity Error, 15 Second Update Rate

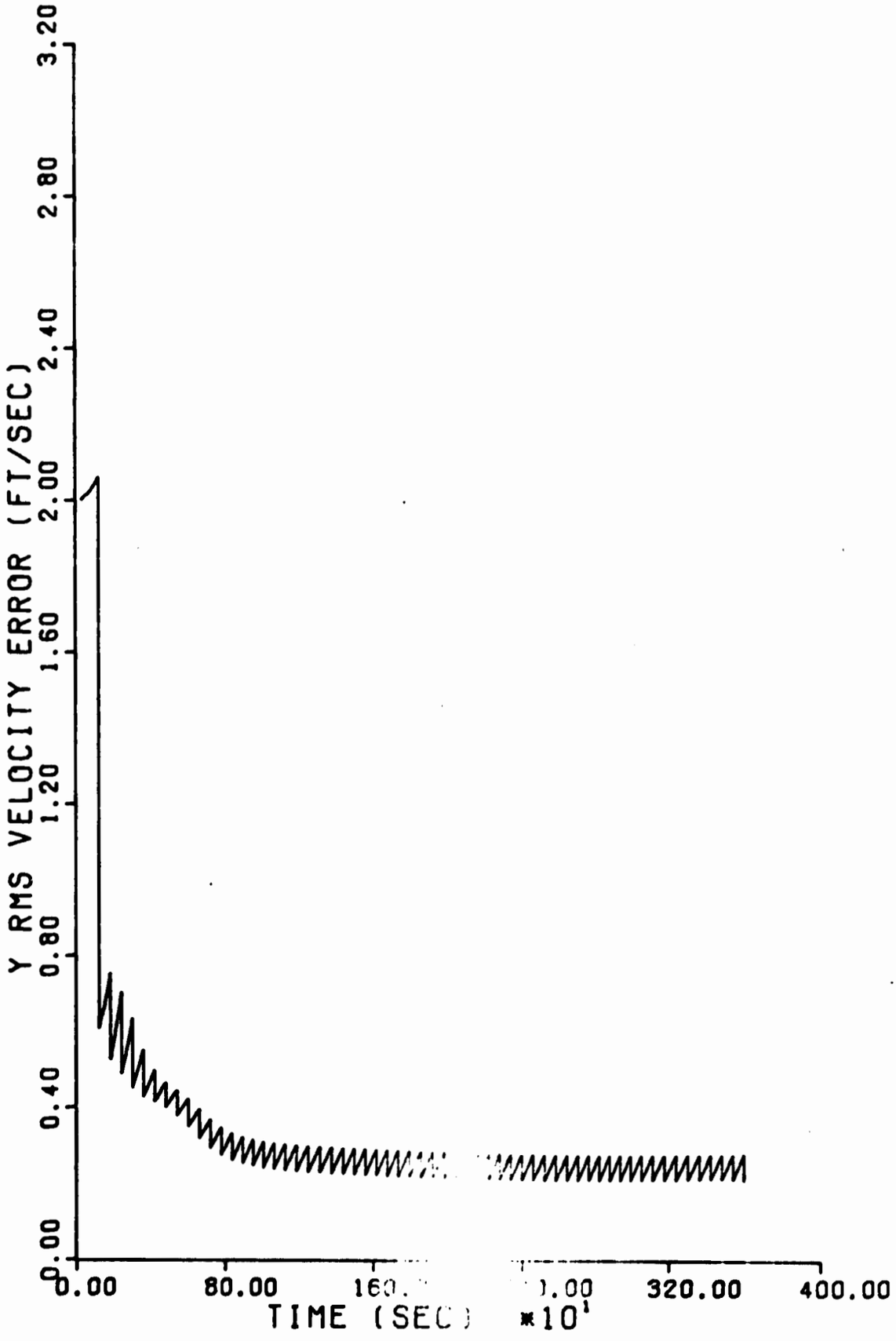

Fig. 74. y Velocity Error, 60 Second Update Rate

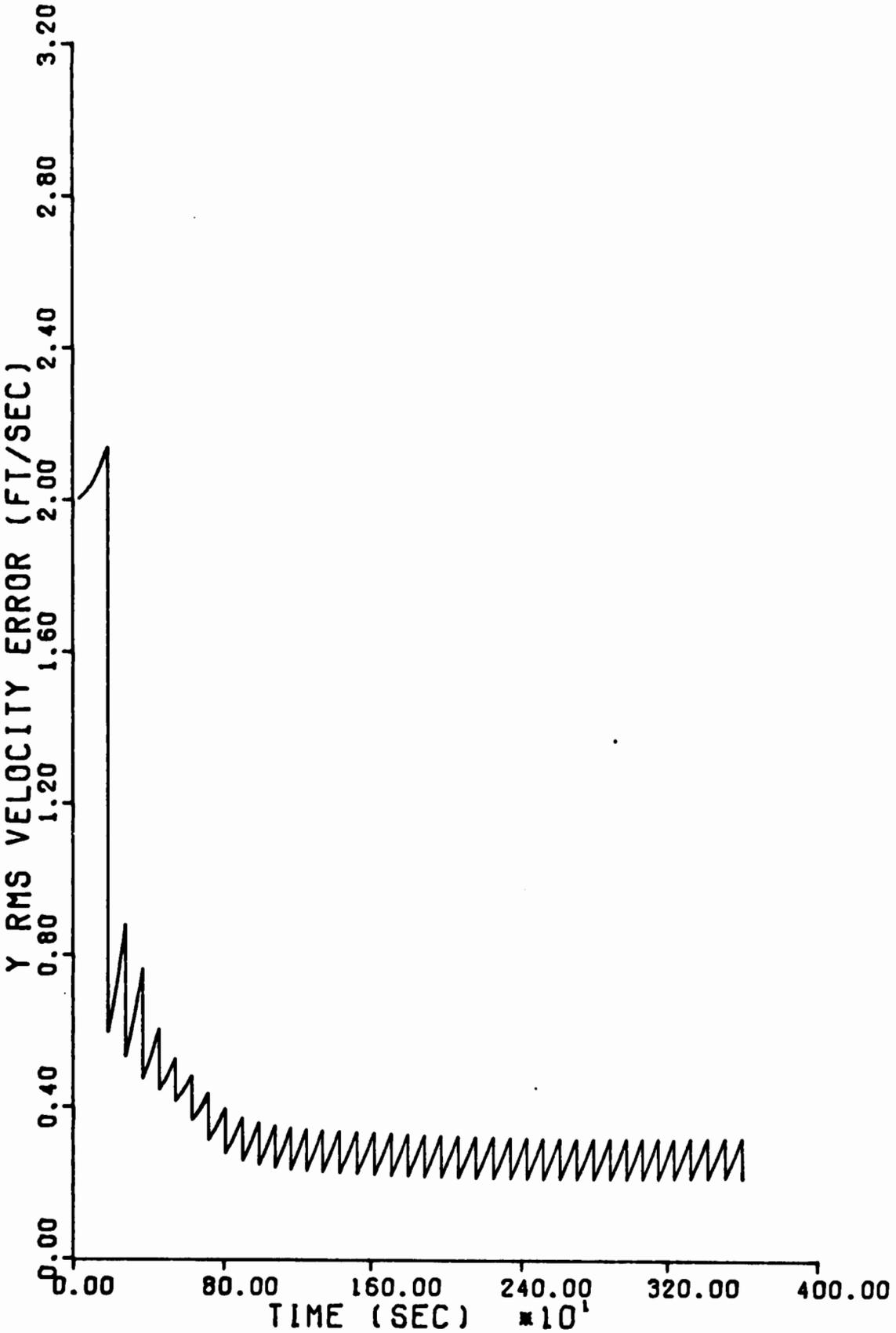

Fig. 75. y Velocity Error, 90 Second Update Rate

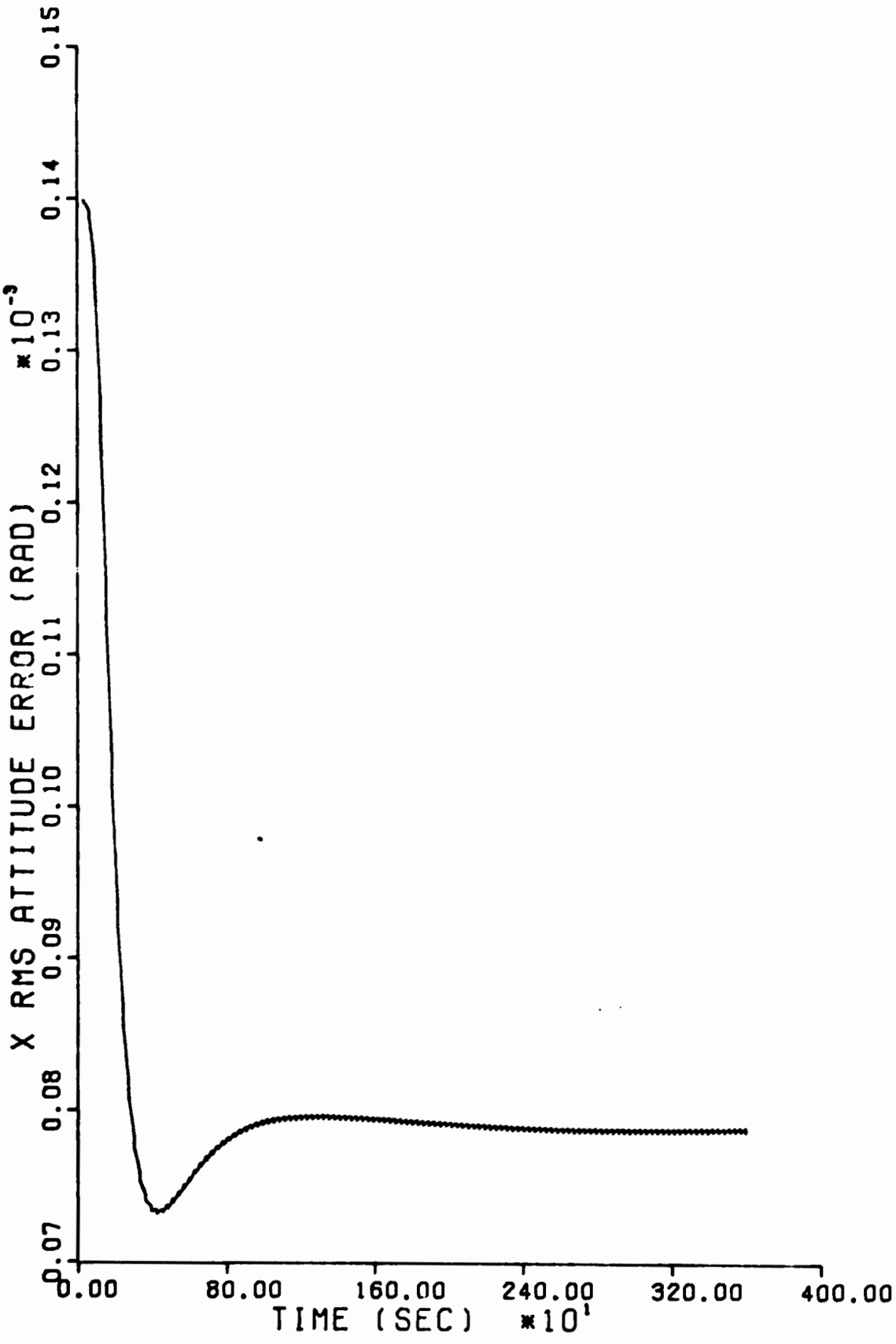

Fig. 76. x Attitude Error, 5 Second Update Rate

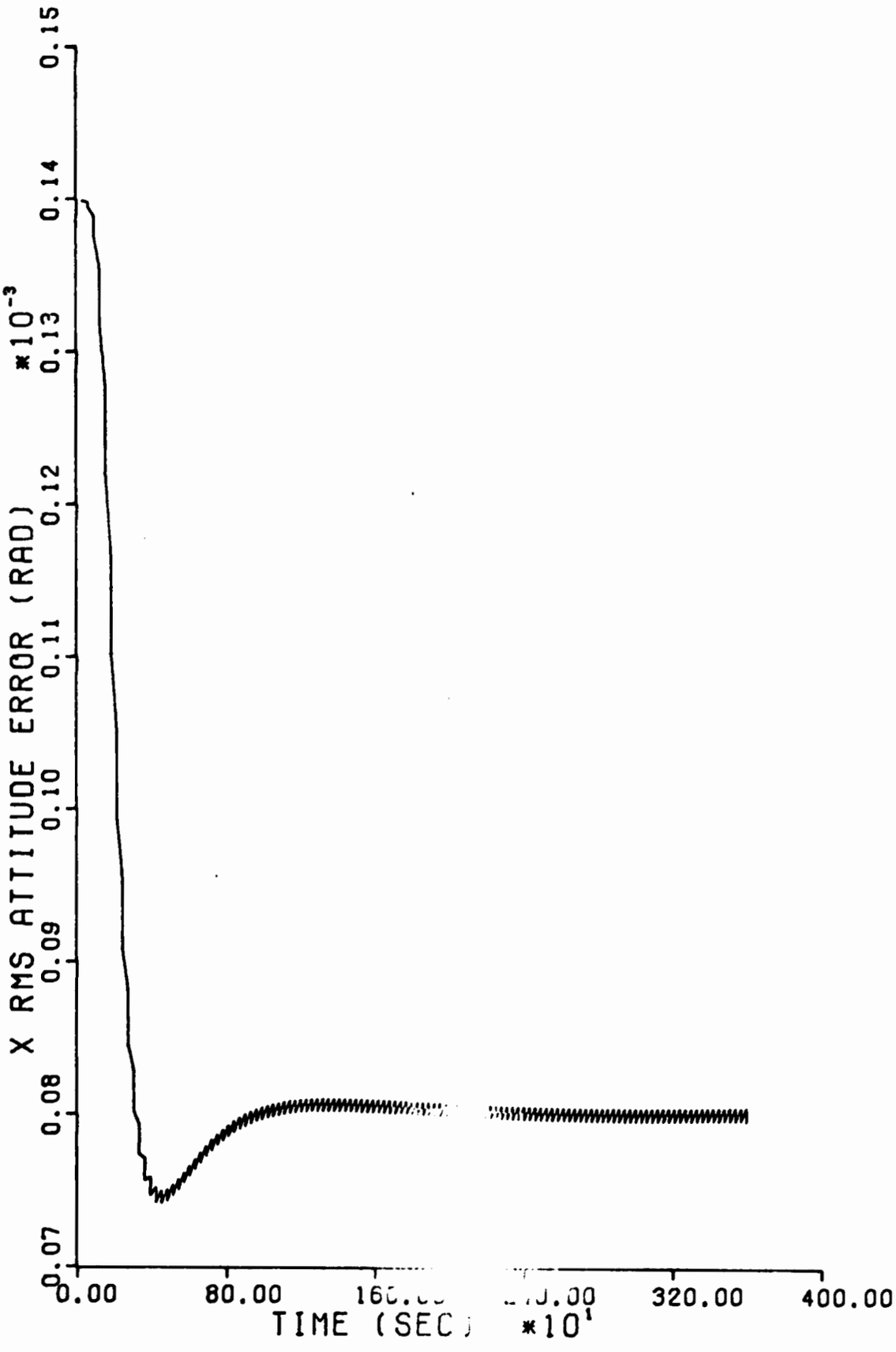

Fig. 77. x Attitude Error, 15 Second Update Rate

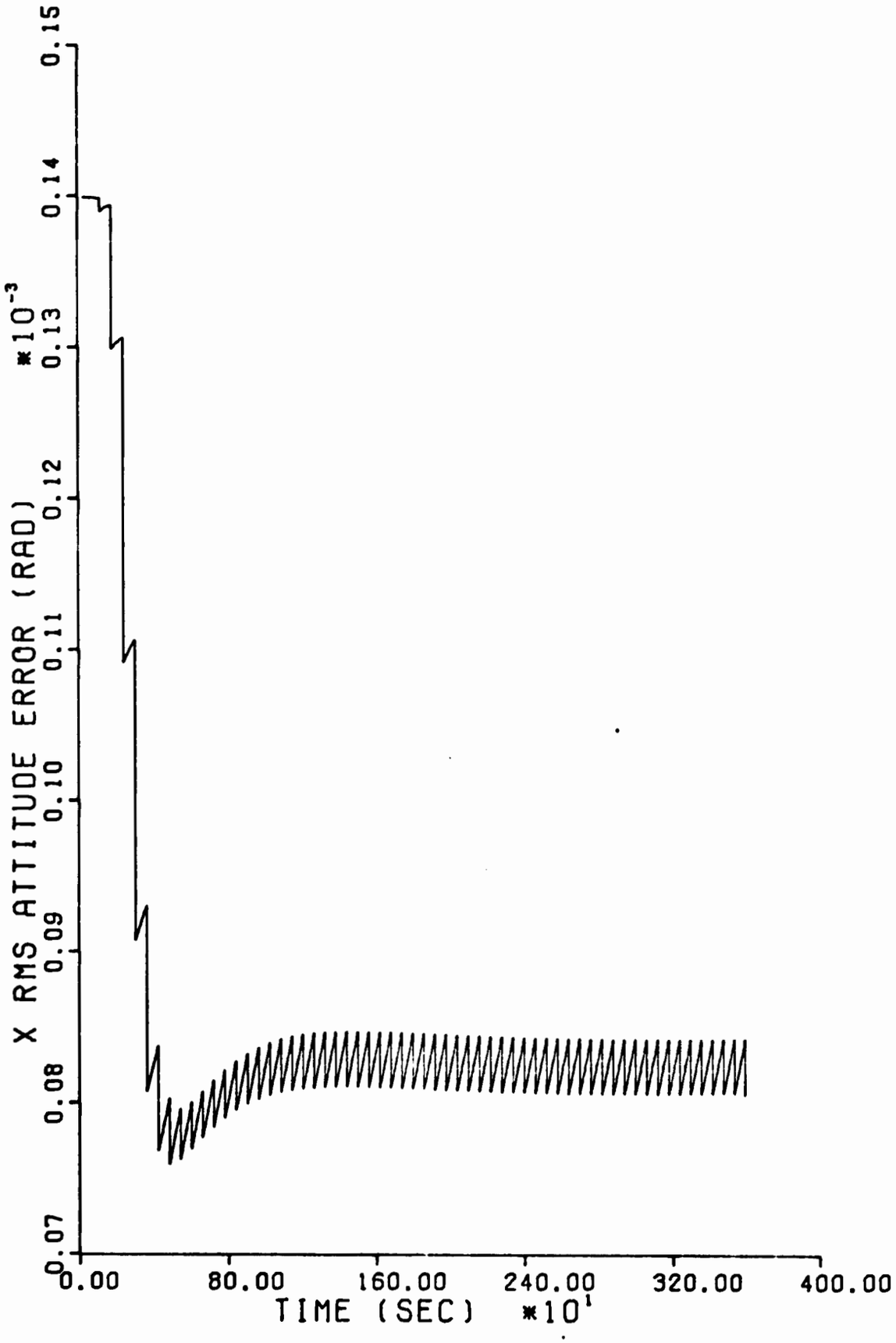

Fig. 78. x Attitude Error, 60 Second Update Rate

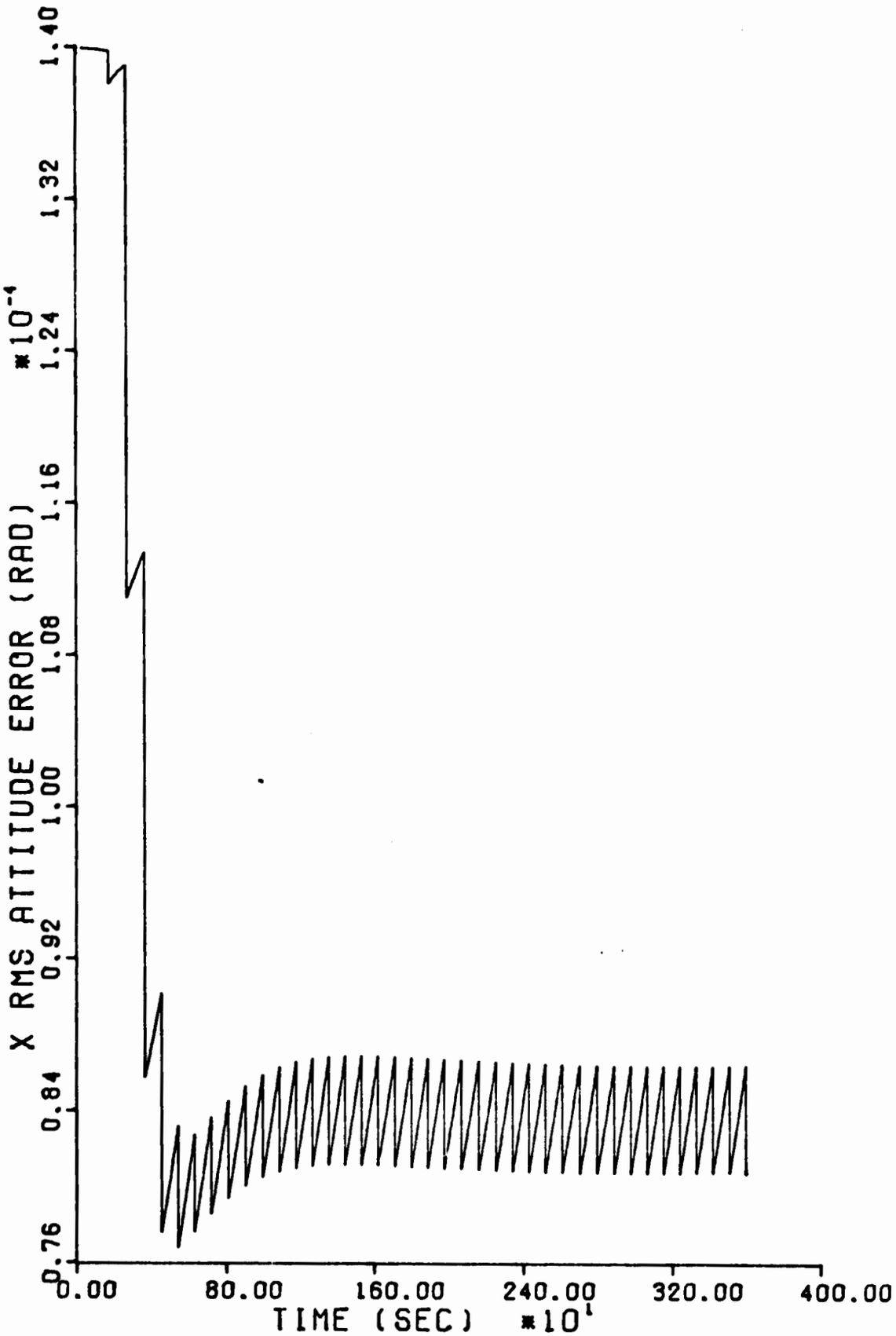

Fig. 79. x Attitude Error, 90 Second Update Rate

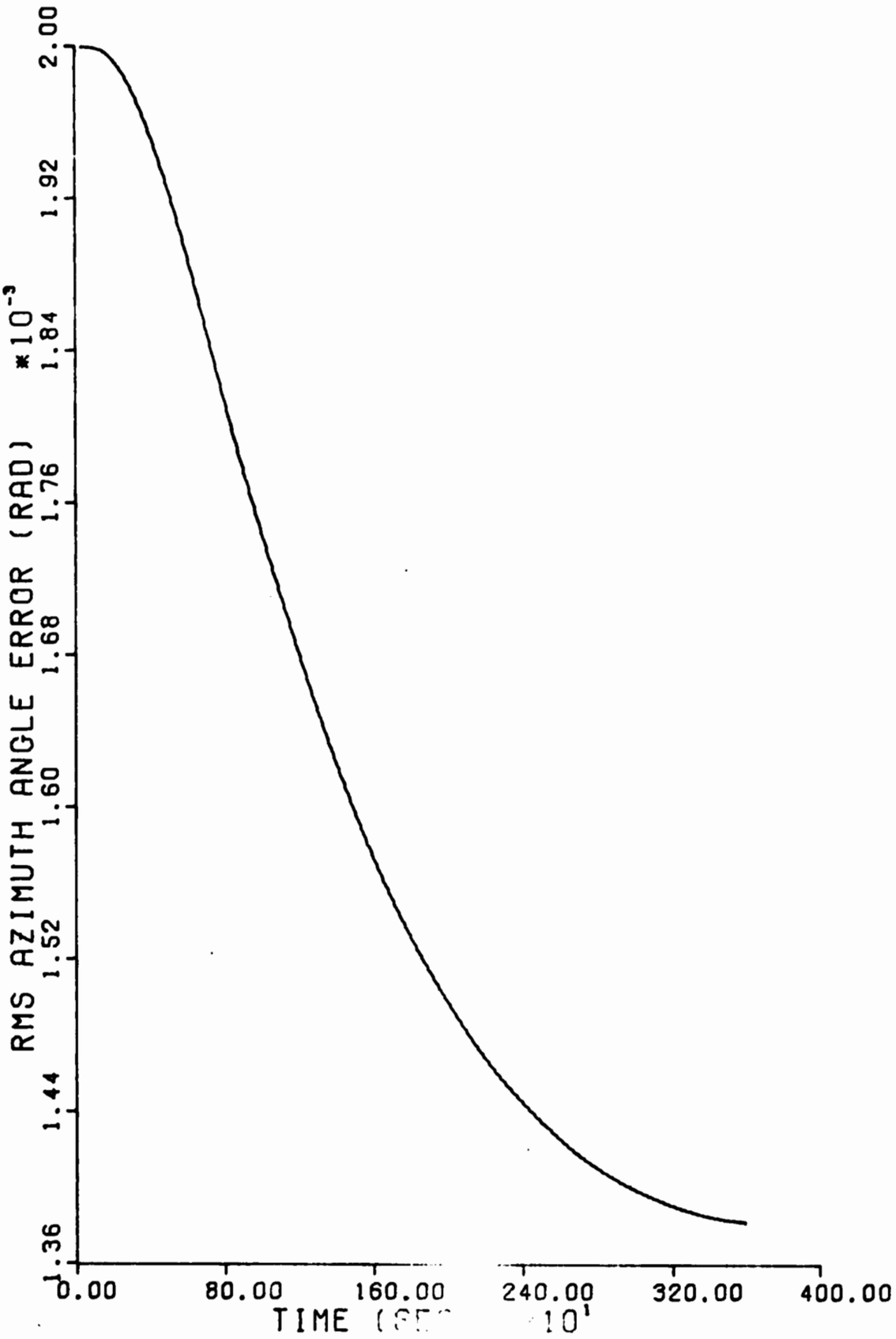

Fig. 80. Azimuth Error, 5 Second Update Rate

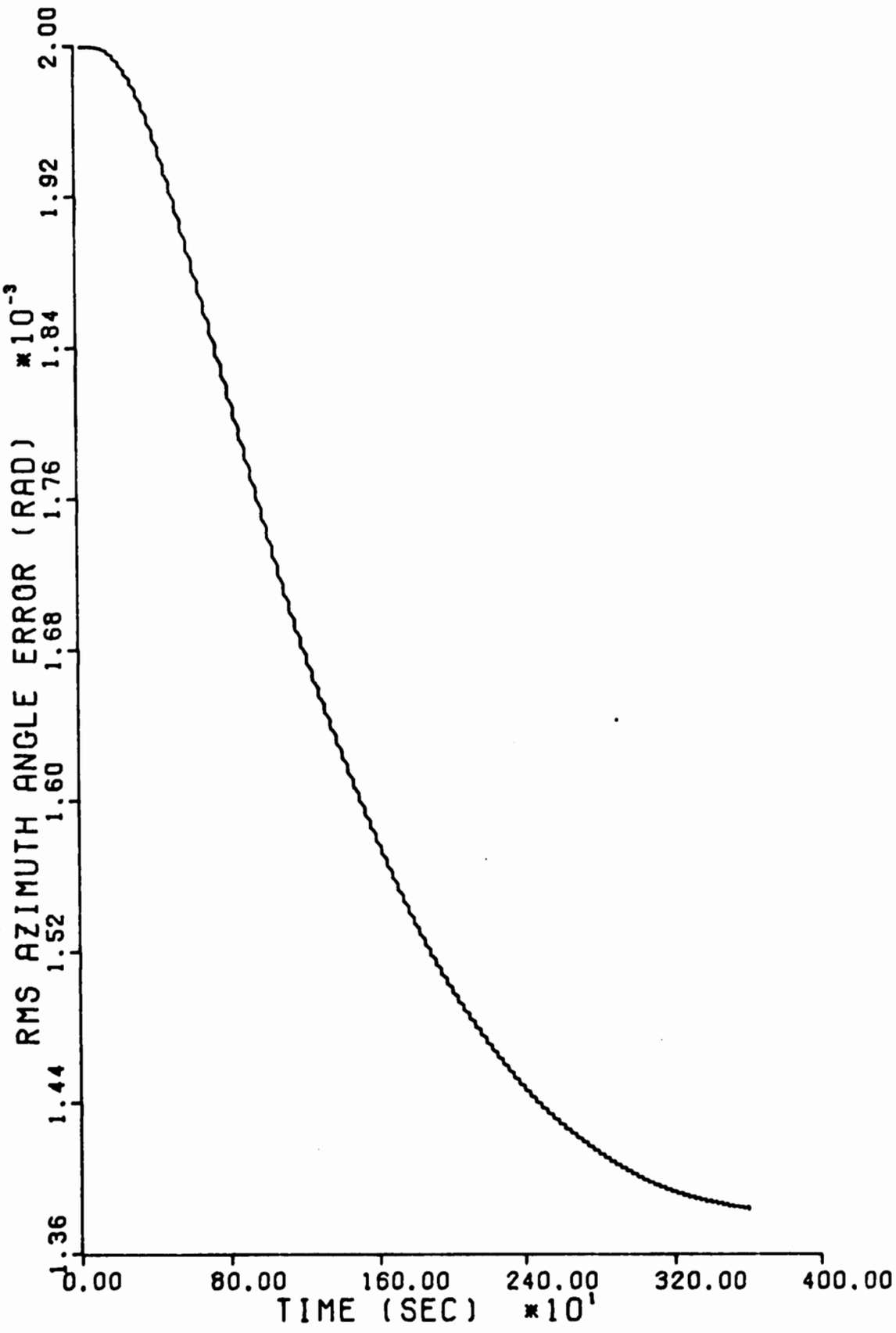

Fig. 81. Azimuth Error, 15 Second Update Rate

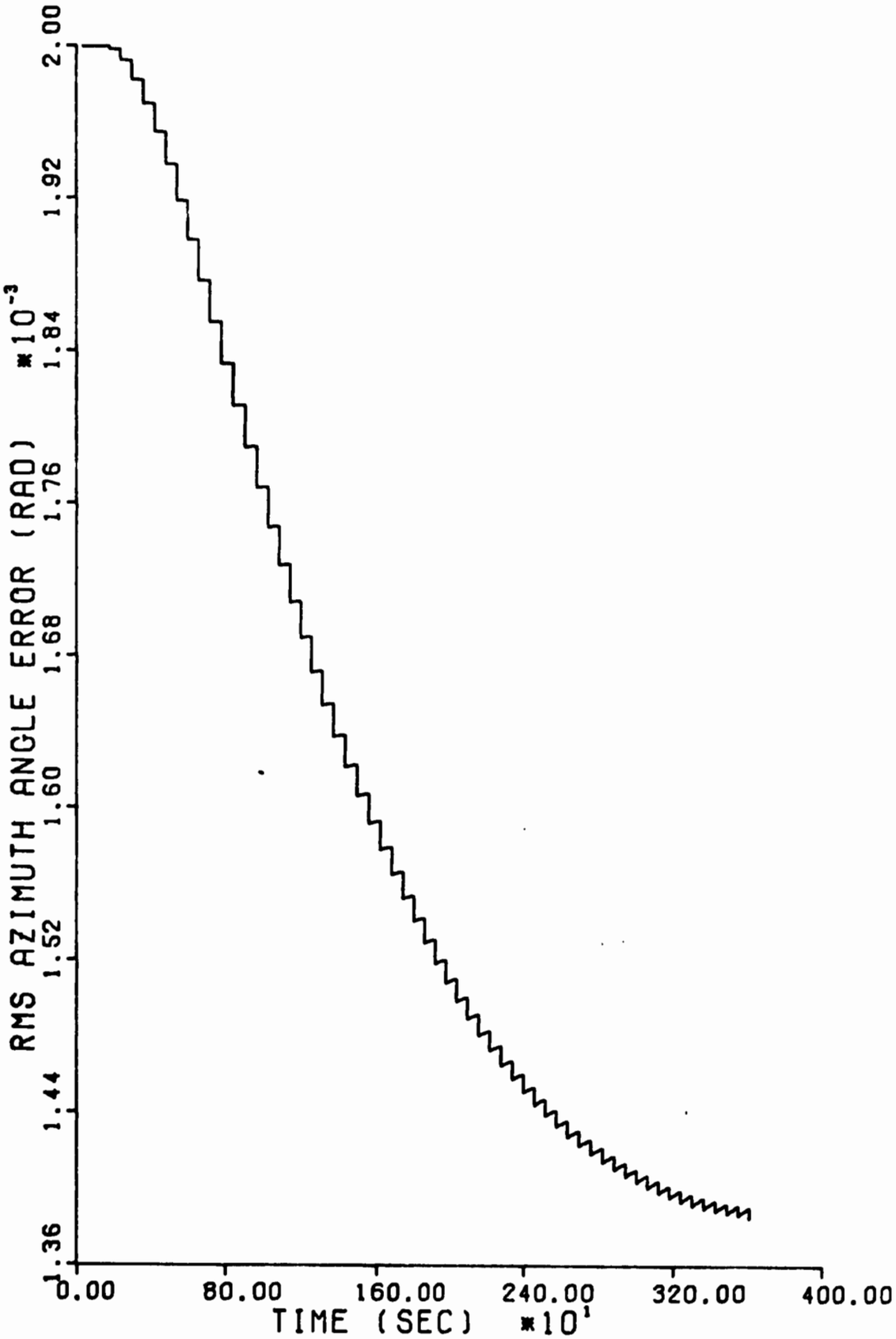

Fig. 82. Azimuth Error, 60 Second Update Rate

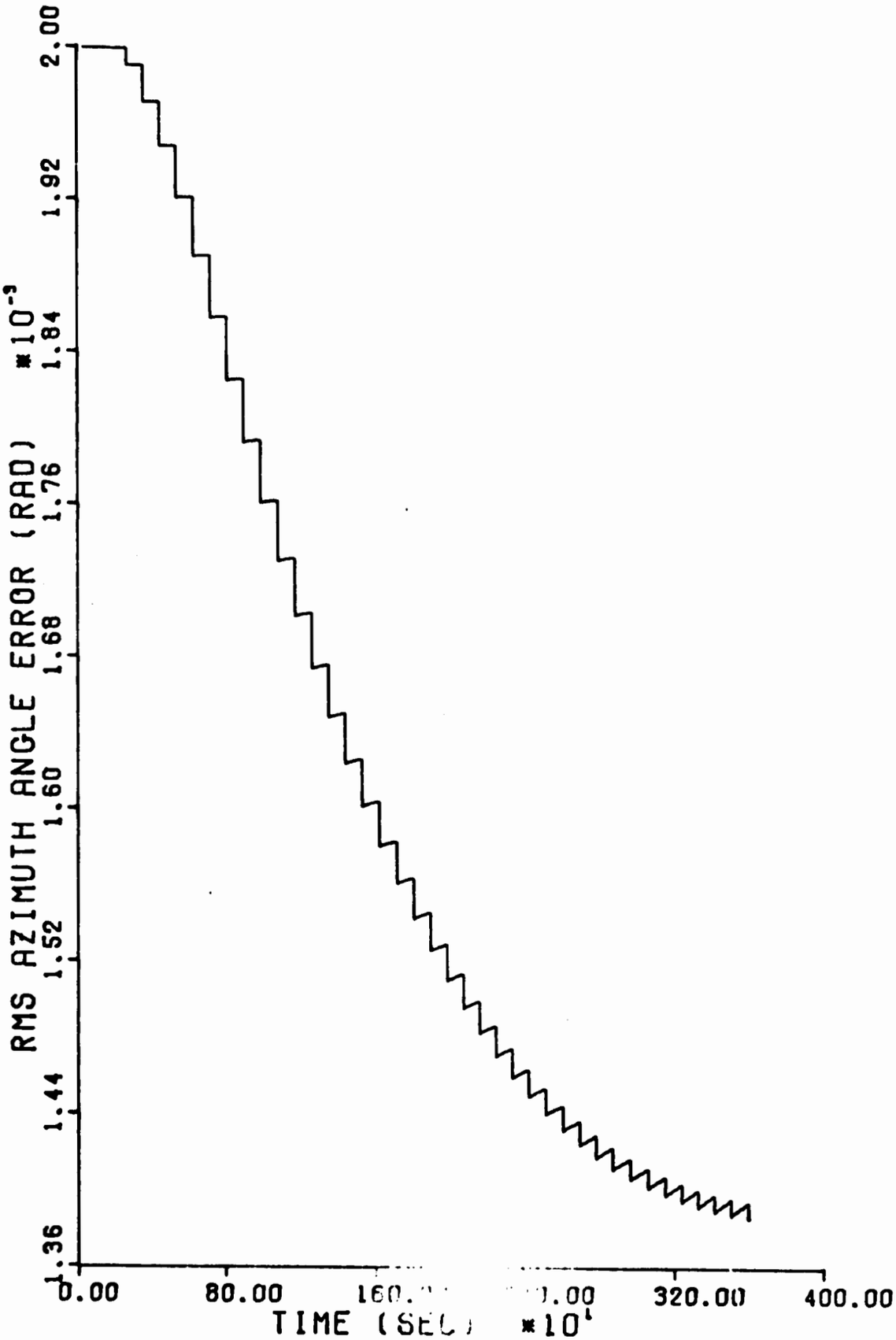

Fig. 83. Azimuth Error, 90 Second Update Rate

Vita

Ronald Ray Butler [redacted] He enlisted in the United States Air Force in January 1966 and received language training in Basic Chinese Mandarin from the Defense Language Institute West Coast at Monterey, California. Following a two year tour with the U.S.A.F. Security Service in Taiwan, he returned to Washington, D.C. to complete the Intermediate Chinese Mandarin course at the Defense Language Institute East Coast. In 1970 he was selected for the Airman Education and Commissioning Program and enrolled at Auburn University. He graduated with a Bachelor's degree in Aerospace Engineering and was elected to membership in the Sigma Gamma Tau and Tau Beta Pi national engineering honor societies. Upon completion of the School of Military Sciences, Officer he was commissioned a 2nd Lieutenant in November 1972. Lt Butler entered the Air Force Institute of Technology Resident School of Engineering in pursuit of a Master's Degree in Astronautical Engineering in January 1973.

[redacted]

Vita

George Truitt Rhue [redacted]

[redacted] He enlisted in the United States Air Force in August 1961 and was trained as a missile maintenance technician at Chanute Air Force Base in Illinois. In 1962 he was stationed with the 46th Air Defence Missile Squadron at McGuire Air Force Base, New Jersey, and in 1967 he was transferred to the 22nd Air Defence missile squadron, Langley Air Force Base, Virginia. In 1970 he was accepted for the Airman Education and Commissioning program and enrolled at Purdue University. Upon graduation with a Bachelor of Science in Aeronautical and Astronautical Engineering degree, he attended Officer's Training School and was commissioned as a 2nd Lieutenant in November 1972. After receiving his commission, Lt Rhue was assigned to the Air Force Institute of Technology to pursue a Master's Degree in Astronautical Engineering, Guidance and Control.

[redacted]

This thesis was typed by Sherry Willman.